BOLT BERANEK AND NEWMAN INC

CONSULTING • DEVELOPMENT • RESEARCH

Job No. 11268

Report No. 1592

EXPERIMENTAL STUDY OF SOUND AND VIBRATION TRANSMISSION TO A SHROUD-ENCLOSED SPACECRAFT

Jerome E. Manning
Nicholas Koronaios

1 August 1968

Submitted to:
National Aeronautics and Space Administration
Goddard Space Flight Center
Greenbelt, Maryland

Contract No. NAS5-10302

ANNUAL REPORT

EXPERIMENTAL STUDY OF SOUND AND VIBRATION TRANSMISSION TO A SHROUD-ENCLOSED SPACECRAFT

(20 January 1967 – 20 January 1968)

Contract No.: NAS5-10302

Goddard Space Flight Center

Contracting Officer: A.L. Essex
Technical Monitor: J.P. Young 321

Prepared by:

Bolt Beranek and Newman Inc
50 Moulton Street
Cambridge, Massachusetts 02138

Project Manager: Jerome E. Manning

for

Goddard Space Flight Center
Greenbelt, Maryland 20771

EXPERIMENTAL STUDY OF SOUND AND VIBRATION TRANSMISSION TO A SHROUD-ENCLOSED SPACECRAFT

by

Jerome E. Manning
Nicholas Koronaios

ABSTRACT

An experimental study of the vibration transmission in a 1/2-scale-model spacecraft-shroud assembly is described. The role of acoustic and mechanical vibration-transmission paths is studied. The individual elements of the assembly are studied as well as the complete assembly in order to better understand the vibration-transmission mechanisms. Data obtained in the program are compared with predictions obtained by using statistical energy analysis. An Appendix describes vibration measurements made on an actual OGO-Nimbus shroud.

TABLE OF CONTENTS

TABLE OF CONTENTS (continued) Page

LIST OF ILLUSTRATIONS AND TABLES

LIST OF ILLUSTRATIONS AND TABLES (continued)

LIST OF ILLUSTRATIONS AND TABLES (continued)

1. INTRODUCTION

This report describes an experimental study of the sound-induced vibration of a shroud-enclosed model spacecraft. A typical spacecraft-shroud assembly, which was the basis of our model, is shown in Fig. 1. The major structural elements of this assembly are identified in Fig. 2. Two paths of vibration transmission from the external acoustic field to the spacecraft exist: first, an acoustic path, involving the external acoustic space, the shroud, and the interior acoustic space; and second a mechanical path, involving the external acoustic space, the shroud, the ring frame, and the mounting trusses. The purpose of our experimental study is (1) to determine experimentally the relative magnitude of the vibrations transmitted to the model spacecraft by the acoustic path and the mechanical path, and (2) to support the theoretical predictions of the vibration transmission obtained in Ref. 1 by using statistical energy analysis.

The spectra of the experimentally measured vibration transmitted to the spacecraft by the two paths are shown in Fig. 46. Vibrations transmitted by the paths are comparable in amplitude. The statistical-energy-analysis predictions are compared with the experimental measurements in Figs. 33-45. Agreement between the predictions and the measurement for acoustic path transmission is acceptable, which indicates that statistical energy analysis is a useful means of estimating high-frequency vibration transmission in the acoustic path. Agreement for mechanical path transmission, however, is not acceptable; differences greater than 5 dB occur for many frequency bands. We have concluded that the assumptions made in obtaining the theoretical predictions are not valid.

The experimental program which we conducted is described in the next section.

1.1 Description of the Program

Members of the staff at Bolt Beranek and Newman Inc. (BBN) have designed, fabricated, and conducted experiments on a 1/2-scale model of a spacecraft-shroud assembly. Section 2 describes this model. Theoretical estimates of the sound-induced vibrations of the full-scale assembly were obtained in Ref. 1 by using statistical energy analysis. Experimental data obtained during the present program are compared with estimates for the 1/2-scale model in Section 5.

The experimental program is divided into three phases: model design and construction, conduct of experiments, and comparison of the experimental results with theoretical predictions.

Phase 1, described in Section 2, includes design and fabrication of a 1/2-scale model of a typical spacecraft-shroud assembly. The OGO spacecraft-shroud assembly was chosen as the basis for our model. Properties of our model that determine its sound-induced vibrations only *approximate* those of the OGO assembly. We do not intend that the vibration levels measured for this model be indicative of vibration levels in the actual assembly. The shroud model is a ribbed cylindrical shell. The spacecraft model is an array of honeycomb panels. The model spacecraft is connected to the model shroud by four channel trusses and a ring frame.

Phase 2 of the study, described in Sections 3 and 4, consists of several experiments to investigate the flow of vibratory energy in individual structural elements of the model and in combinations of the elements coupled together. The experiments are divided into two types: (1) experiments to investigate the flow of energy in the acoustic path—this path consists of the external sound field, the shroud, the internal sound field, and the spacecraft; (2) experiments to investigate the flow of energy in the

mechanical path—this path consists of the external field, the shroud, the ring frame, the mounting trusses, and the spacecraft.

In phase 3 of the program, described in Section 5, we compare our experimental results with theoretical predictions obtained in Ref. 1. Specifically, the measured vibratory response of the individual assembly elements is compared with the theoretical predictions, and the experimentally determined parameters governing power flow between the elements are compared with the theoretical values. In addition, we measured the spatial variation of the vibration on each element of the assembly.

A fourth phase of the program, described in the Appendix to this report, operates independently of the first three phases. This phase consists of conducting experiments at Goddard Space Flight Center on a Nimbus-OGO type shroud. The experiments included measurement of the acoustic-induced response of the shroud and the reduction of sound-pressure level (SPL) from the outside to the inside of the shroud, and measurement of the damping of the shroud and the absorption of the internal acoustic space. The experimental results are compared with theoretical predictions and other experimental results.

2. DESIGN AND CONSTRUCTION OF THE MODEL

2.1 Description of the OGO Assembly

The assembly, sketched in Fig. 1, is composed of four structural elements as follows: (1) a ribbed cylindrical shroud, (2) a ring frame, (3) four wishbone mounting trusses, and (4) the spacecraft.

The OGO Shroud, shown in Fig. 3, is a Nimbus-type shroud. It is a ribbed cylindrical shell capped by a conical nose. The shell is made of a glass-reinforced plastic laminate whose thickness varies, both along the length of the shell and around its circumference, from 0.1 to 0.14 in. The ribs are aluminum hat-section rings spaced at various intervals within the shroud. The entire shroud is split axially (Fig. 4) to permit shroud separation. Approximate structural properties of the shroud are summarized in Table I.

The lining of the shroud is a microquartz/felt thermal blanket. Since this blanket controls the absorption of acoustic energy inside the shroud, it had to be considered in designing a model. The blanket thickness varies from 1/2 to 1 in. Its acoustic properties are not known and must be found experimentally.

The ring frame in the OGO assembly is shown in Fig. 5. The shroud is clamped around the ring frame. The important structural properties of the ring frame are given in Table I.

The mounting trusses for the OGO spacecraft are wishbone legs consisting of aluminum channel beams, as shown in Fig. 6. The geometric and structural properties of these trusses are given in Table I.

The OGO spacecraft is shown in Figs. 6 and 7. Basically, it is a box of four corrugated-core sandwich panels. The structural properties of these panels are given in Table I. Two opposite panels of the box are hinged and can be opened to allow access to the spacecraft. The top and bottom of the spacecraft are closed by thin panels. The spacecraft instruments are mounted on the sandwich panels, as shown in Fig. 7. The base of the spacecraft is supported by a large X frame as shown in Fig. 6. The spacecraft connects to the mounting trusses by a clamp arrangement.

2.2 Design of the Model

In order to obtain data relevant to our theoretical predictions, we have made several idealizations in designing a model. For example, the model shroud is a ribbed cylindrical shell with constant skin thickness. We have not included the conical section of the OGO shroud for the following reasons: we do not feel that it has great effect on vibration transmission characteristics of the shroud; and it was not included in the theoretical predictions. In modeling the OGO shroud, we did not preserve the exact spacing between the ribs.

It is important for the experiments that the material properties of the OGO shroud be preserved in the model. Therefore, we selected a fiberglass/epoxy laminate for the shell. The density and elastic modulus of this material are similar to those of the OGO-shroud material.

We selected a 1-in.-thick porous fiberglass blanket to line the model shroud. The surface density and absorptive properties of this blanket approximate those of the microquartz/felt lining used in the OGO shroud.

Our model does not preserve the exact geometry of the OGO ring frame. In the analysis of Ref. 1, the assumption was made that only bending around a vertical axis that is parallel to the axis of revolution of the shroud will transmit vibratory energy to the spacecraft. This assumption was made because the spacecraft vibration induced by such moments is greater than that induced by other forces and moments. Since only moments around the vertical axis are important, our model preserves only the linear density and bending stiffness around the vertical axis of the ring frame. Bending stiffnesses around the other two axes and torsional stiffness are preserved only within 50% of the actual values.

The wishbone trusses of the OGO spacecraft are replaced in the model by four channel beams. This substitution allows simplification of the theoretical calculations without altering the transmission characteristics at high frequencies to any great extent. The structural properties of the single beams are designed to be similar to those of one leg of the wishbone.

The actual dimensions of the model elements were determined by using a dimensional analysis.[2] According to this analysis, the following dimensionless groups must be held constant:

$$\frac{S_p \Delta}{\rho_o^2 c_o^4}, \frac{\ell f}{c_o}, \frac{c_\ell}{c_o}, \frac{\rho_s f}{\rho_o c_o}, \frac{\rho_\ell f^2}{\rho_o c_o^2}, \eta_{loss}, \frac{\Delta}{f}, \text{ and } \frac{c_b}{c_o} \quad , \tag{1}$$

where ℓ is a typical length, f is the test frequency, c_o is the speed of sound in the acoustic media, c_ℓ is the longitudinal wavespeed in the structural material, ρ_s is the surface density of a typical panel, ρ_ℓ is the lineal density of a typical beam, ρ_o is the volume density of the acoustic medium, η_{loss} is the dissipation

loss factor of a typical element, Δ is the test bandwidth, and c_b is the bending wavespeed of a typical structural element.

If we use air as the acoustic medium, the test frequencies for the 1/2-scale model are double those for the full-scale assembly. The longitudinal wavespeed—a material property—remains constant so that the same materials can be used for the model as were used for the full-scale assembly. The properties of the 1/2-scale model, according to the above dimensionless groups, are given in Table I.

2.3 Construction of the Model

The 1/2-scale-model shroud and spacecraft have been constructed. Details of the model design are shown in Figs. 8-11. The parameters of the constructed model do not agree exactly with the design parameters. Changes were dictated by availability of construction materials. A list of the design parameters and the constructed-model parameters is given in Table I.

Figure 8 shows the outside view of the shroud. The shroud consists of a 3/32-in.-thick NEMA Grade G-11 fiberglass/epoxy laminate. Ribs of aluminum channel have been epoxied in position at the locations shown. The ends are sealed off with 0.75-in. plywood baffles.

Details of the ring frame are shown in Fig. 9. The ring frame was constructed from an aluminum channel and two aluminum angles connected by a rigid epoxy and screws.

Details of the model spacecraft and mounting trusses are shown in Figs. 10 and 11. The spacecraft is a rectilinear box, composed of four honeycomb panels, approximately 3/8 in. thick. The panels are an aluminum honeycomb structure, with a cell size

of 0.25 in. and a foil thickness of 0.0005 in. The skin thickness is 0.010 in. The panel edges terminate in solid-aluminum-bar stock of 0.5-in. width that provides a region of high compressive strength near the attachment point. The spacecraft box has been assembled on a frame of 0.5x0.5x0.125-in. aluminum angle.

The model spacecraft is supported on the ring frame by four mounting trusses. These trusses are made from 1.5x1.5x0.063-in. aluminum channel. The trusses have been stiffened by introducing gussets in the middle in addition to the mounting plates on each end.

3. MEASUREMENT TECHNIQUES

Three types of measurement are made in the experimental program: (1) the vibratory response of the structural elements to acoustic excitation is measured, (2) the damping of the structural and acoustical elements is measured, and (3) the sound power radiated by the structural elements when they are excited with mechanical shakers is measured. Techniques for these measurements are described in the following sections.

3.1 Response Measurements

The experimental setup for measuring response consists of a set of instruments that produce the sound field in the test room and a set of instruments that pick up and analyze the vibrations of the structure under excitation. The experimental setup is shown in Fig. 12.

The system for producing the sound field is as follows: the output signal of a Grason-Stadler white-noise generator model 90A is filtered by a Brüel and Kjaer (B&K) 1/3-oct-band filter model 1609; and is amplified by a McIntosh model K170 power amplifier. The signal is then converted to a sound field in the test room by either of two loudspeaker systems. For low-frequency, 1/3-oct-bands (250-3150 Hz center frequency), a large horn loudspeaker is used. Twelve drivers, arranged around a pipe manifold, exhaust into the throat of the horn. For high-frequency 1/3-oct-bands (4000-12 500 Hz center frequency), the signal from the power amplifier is fed to three, small, horn loudspeakers, each of which is driven by a University model T50 horn driver. The overall system is capable of producing 1/3-oct-band SPL of 90-100 dB in the test room.

A diffuse field was established in the center of the test room by carefully positioning the speakers. The large horn speaker is directed into a solid angle made up of two walls and the room floor. Hence, the sound produced by the horn is scattered into the room by the walls. The three high-frequency horns are placed apart from each other and are directed toward different walls.

Before response measurements were made, the uniformity of the sound field—a practical measure of diffuseness in a reverberant room—was determined. The spacecraft model was hung in the center of the room. For each 1/3-oct band, the loudspeaker output was adjusted so that the SPL at a chosen reference point in the room had a fixed value (90 dB). A B&K type 4135 microphone with a B&K type 2630 cathode follower and a B&K type 2801 power supply were used to measure the SPL at eight locations in a circle at a distance of 3 ft from the model. Variation in SPL between positions did not exceed ±3 dB. The SPL's at these eight points were averaged and the difference of this average from the SPL at the reference point was recorded. Thereafter, whenever response measurements were made on the spacecraft, the SPL at the reference point was recorded.

The same procedure was followed for determining the average value of the SPL around the shroud. In this case, the shroud was hung in the center of the room and the SPL was measured at 10 locations around the shroud while the SPL at the reference microphone was maintained at 90 dB. The results of this measurement are shown in Fig. 14; the scatter was found to be less than ±3 dB.

The vibratory response of the structure was measured with six accelerometers, as shown in Fig. 12. Three of the accelerometers used were of an experimental design not commercially

available, and the other three were B&K type 4336, 2-gram accelerometers. All six accelerometer outputs were led to a switchbox. The reference-microphone output was also led to this same switchbox.

The switchbox output was connected to a General Radio type 1551C preamplifier, and then to a General Radio type 1564 sound and vibration analyzer. The latter instrument is a 1/3-oct-band filter. The response signal was filtered in the same 1/3-oct band as the excitation signal, and the root-mean-square value of the filtered signal was read on the instrument's meter. In low-frequency 1/3-oct bands, the meter fluctuated too widely for accurate reading, a B&K random-noise voltmeter type 2471 was used; this is an active averaging instrument that provides adjustable averaging time. This instrument was connected to the output of the General Radio sound and vibration analyzer. Accuracy of the acoustic and vibration measurements is ±1 dB.

3.2 Damping Measurement

The decay-rate technique was used for the determination of damping. This technique can be applied to measure the damping loss factor of either an acoustic space or a structure. Using this method, one measures the reverberation time—the time for the vibration to decay 60 dB after all external excitation is stopped. A measurement setup is shown in Fig. 13. The structure, or the acoustic space, is excited until a steady response level is reached. The excitation is then switched off and the decay rate of either the acceleration or the SPL is observed.

The decay-rate measurements were made with a Krohn-Hite decay-rate meter, which automatically switches the excitation signal on and off. The response signal, whose decay is to be measured, is

also led to this instrument. The instrument displays the logarithm of the response signal and allows an operator to compare the vibration decay with an RC-circuit decay. The operator can adjust the RC-circuit decay and make it fit the envelope of the response signal. The time that it takes for the response signal to decay 60 dB is read directly from the instrument.

Matching the RC-circuit decay with the envelope of the decaying signal is, to a degree, subjective. Our measurements were taken by two or three operators and the results averaged.

The decay-rate method of determining damping loss factors has some inherent shortcomings, which have made it impossible to determine the model-spacecraft damping loss factor with this technique. One of the limitations of the decay-rate technique is quite general and is discussed here. The particular problems encountered with the determination of the spacecraft damping loss factor will be described later. The major limitation arises when one measures the damping of a structure that has two groups of modes with significantly different values of damping. The modes with low damping values decay more slowly than those modes with high damping values. If the modes are excited equally, the vibration decay will have a double slope. The initial slope results from decay of modes with high damping, and the final slope results from decay of modes with low damping. In this case, it is possible to determine the damping values of each group of modes. If, however, modes with low values of damping are excited more strongly, the decay rate of the total vibration will be dominated by these modes; hence, the decay rate of modes with high damping will not be measured.

3.3 Radiation Measurement

Measurements of sound radiation were made by measuring the sound field that is established in response to excitation of the structure by a mechanical shaker. For these measurements, the radiating structure was hung in the center of the room and excited using a Goodman V47 shaker. The signal applied to the shaker was generated by a Grason-Stadler 96A white-noise source and filtered into 1/3-oct bands by a B&K 1609 filter. The exciting signal was amplified by a McIntosh 300 power amplifier.

The SPL in the test room was determined by averaging results from 10 microphones surrounding the structure. The instrumentation used for measuring SPL was the same as that used for response measurements.

3.4 Calibration

All microphones and accelerometers were calibrated five times during the course of the measurement program. Microphones were calibrated with a B&K pistonphone. Calibrating with this pistonphone is accurate to within 0.5 dB.

The procedure employed for calibrating accelerometers was more complicated. Initially, a General Radio type 1557 vibration calibrator was used. This calibrator is equipped with two platforms, to which accelerometers can be attached. The platforms vibrate with a 1-g acceleration at 100 Hz. A complication arises, however, if the accelerometer capacitance is small. This capacitance with the input impedance of the amplifier forms an RC circuit. The response of such a circuit falls at low frequencies. Thus, calibration at low frequency can lead to error.

To offset this complication, the following procedure was used for all calibrations. The accelerometer of a Wilcoxon impedance head was calibrated carefully by using the General Radio vibration calibrator. Also, the impedance-head force-gauge was used to detect the force exerted on the impedance head by a known mass and hence to infer the acceleration. Both methods of calibration were found to be in agreement with the manufacturers specifications. The impedance head was attached to a shaker, and all accelerometers were mounted on the impedance head and calibrated at six frequencies: 100, 250, 500, 1000, 5000, and 10 000 Hz.

All microphones and accelerometers were calibrated in the complete instrument setup in which they were used. The majority of measurements were made to determine either acceleration per unit SPL of excitation or the inverse—SPL per unit acceleration. The same instrument system was used to measure both the SPL and the acceleration. In this way, the final result of the measurement was independent of the gain of the measuring instruments.

4. PRESENTATION OF DATA

4.1 Classification by Experiment

Data obtained in the experimental study are presented in Figs. 14-32. The procedures used to obtain these data are described below.

We define acceleration level (AL) as

$$AL_{re\ 1g} \equiv 10 \log_{10} \langle a^2 \rangle_t \quad , \tag{2}$$

where $\langle a^2 \rangle$ is the mean-square acceleration in g's^2. SPL is defined as

$$SPL_{re\ 0.0002\mu bar} = 10 \log_{10} \frac{\langle p^2 \rangle_t}{(0.0002)^2} \quad , \tag{3}$$

where $\langle p^2 \rangle_t$ is the mean-square acceleration in dynes^2/centimeters^4.

4.1.1 Test-room acoustic field. Our first measurements were conducted to determine whether the field established in the test room is diffuse. In a diffuse field, the sound intensity incident from one direction is equal to and uncorrelated with the intensity incident from other directions. A requirement for diffuseness of a reverberant field is that many modes contribute independently to the sound field. To determine the extent to which the sound field in the test room is reverberant, we measured the dissipation loss factor of the test room by using the decay-rate method described in Section 3.2. The measured loss factors are shown in Fig. 15. These are related to the absorption coefficient by Eq. (4).

$$\bar{\alpha} = (8\pi fV/c_o A)\eta \quad , \tag{4}$$

where $\bar{\alpha}$ is the statistical absorption coefficient, c_o is the speed of sound, A is the surface area of the room, f is the frequency, V is the volume of the room, and η is the dissipation loss factor. The dissipation loss factors shown in Fig. 15 indicate an approximately constant value of $\bar{\alpha}$=0.15. The acoustic field in the test room will be reverberant everywhere, except within 6 ft of the acoustic source. In our experiments, the test objects were located approximately 12 ft from the source.

The number of modes in the test room is given statistically by Eq. (5).

$$n(f) = 4\pi f^2 V/c_o^3 \quad , \tag{5}$$

where n(f) is the average number of modes per unit frequency. The volume of the test room is 3000 ft^3 so that there are 450 modes in the lowest 1/3-oct band used in the experiments, (centered at 400 Hz).

The extent to which the modal responses are independent is determined by the uniformity of the sound field. Measurements taken at 10 locations in the test room are plotted in Fig. 14. These show a maximum variation of ±4 dB. No quantitative result exists that relates uniformity of the sound field to diffuseness. We feel, however, that the measured variations are sufficiently small that the sound field can be considered diffuse.

Before conducting experiments on the model, we placed each test object in the middle of the test room and measured SPL at a number of points surrounding the object. The average value

of these measurements was taken as the SPL of the diffuse-field excitation. To simplify the tests, the average SPL surrounding the spacecraft was referred to the SPL at a reference location. Similarly, the average SPL surrounding the model shroud was also referred to the SPL at the reference location.

4.1.2 Model-spacecraft response. To determine the response of the model spacecraft to diffuse-sound-field excitation, we hung the model in the center of the test room by using flexible string. Following the procedure described in Section 3.1, we excited the room acoustically, and measured the resulting SPL and AL. Three accelerometers were located without any particular pattern on each panel of the model; no accelerometer was within 4 in. of the panel boundaries. The measured data are shown in Fig. 16. The response level of each panel of the model was within ±2 dB of the average.

4.1.3 Model-spacecraft radiation. We measured the radiation by the model spacecraft by using the same experimental setup as described in the previous section. A point-drive mechanical shaker was used to excite the frame of the model. We measured the AL at six locations on the two opposite panels; no accelerometer was located within 9 in. of the shaker. The SPL's in the test room were measured at eight locations around the spacecraft. These locations were approximately 3 ft from the structure. The AL of each panel was approximately equal, ±2 dB. Measured data are shown in Fig. 17.

4.1.4 Model-spacecraft dissipation. We conducted the measurements to determine the total loss factor* of the model spacecraft.

*The total loss factor is the sum of the dissipation loss factor and the radiation loss factor.

Many difficulties were encountered during these measurements. Our conclusion is that the decay-rate method is not satisfactory for this structure.

Our first decay-rate measurements were conducted by using the setup described in the previous section. We excited the spacecraft frame mechanically, and observed the decay of the response at several points on the panels. The measurements were performed in the reverberant test room. The observed decay rate was not constant; hence, a unique value for the reverberation time could not be obtained. The reason for the nonconstant decay rate is given in the following paragraph.

In the decay-rate procedure, the spacecraft is excited by intermittent bands of noise. During excitation, a sound field is generated in the test room owing to radiation by the model spacecraft. Because the dissipation loss factor of the test room is less than that of the model spacecraft, the sound field decays more slowly than the vibration of the spacecraft. The initial slope of the vibration decay is a measure of the spacecraft dissipation. The subsequent slope is a result of excitation of the structure by the slowly decaying sound field. This slope is controlled by losses in the acoustic space and not by losses in the structure. It soon became evident that the spacecraft was so well coupled to the acoustic field that the initial slope could not be determined with accuracy. Measurements in the reverberant test room were abandoned.

In a second set of experiments, we conducted decay-rate measurements in an anechoic chamber. Although the loss factor of the chamber is known to be greater than that of the spacecraft, the vibration decay continued to show a double slope. As discussed in Section 3.2, the cause of this double slope is the

occurrence of two classes of modes with different values of damping. The lightly damped modes predominantly involve motion of the spacecraft frame. In an attempt to keep the frame from being excited, we performed decay-rate measurements by striking the panels with an impulsive load. Decay-rate measurements were taken both on the panel being excited and on the opposite panel. Loss factors measured in this way were larger then those measured using a shaker. Subsequent calculations have shown, however, that these measured loss factors are still less than the radiation loss factors. We attribute this discrepancy to the occurrence of modes which predominantly involve motion of the frame.

As a final measurement, we determined the loss factor of a single panel without the frame. Measured values of the dissipation loss factor are shown in Figs. 18 and 19. Above the critical frequency of the panels (800 Hz) the measured loss factors are greater for the single panel than for the model spacecraft. We would expect that addition of the frame would increase the mechanical damping. The frame surely could not decrease the damping as indicated by our measurements. We conclude that the decay-rate method cannot be used when two classes of modes that have significantly different values of damping exist. Further discussion of this point is given in Section 4.3.

4.1.5 Model-shroud response. To measure the response of the model shroud to acoustic excitation, we removed the model spacecraft from the test room and hung the model shroud in its place. The ends of the shroud were baffled with 3/4-in. plywood panels. The baffles were sealed to the edges of the shroud to prevent acoustic transmission, but they were mechanically isolated from the shroud. Using the procedure described in Section 3.1, we excited the test room and measured the resulting SPL and AL. Measurements were taken at 12 random locations on the shroud. None

of these locations was within 4 in. of either a support ring or of the shroud edge. The measured response data are shown in Fig. 20.

4.1.6 Model-shroud radiation. We used the experimental set-up described above to measure the radiation from the model shroud. The edge of the shroud was excited by a point-drive mechanical shaker. The resulting AL and SPL were measured according to the procedure described in Section 3.3. Accelerometer locations were the same as for the previous experiment. Microphones were located in the reverberant field at 10 positions surrounding the shroud. Each microphone was 2-3 ft from the shroud. The measured radiation data are shown in Fig. 21.

4.1.7 Model-shroud dissipation. The model shroud does not fit in our anechoic chamber. Therefore, all measurements were performed in the reverberant test room. Since the shroud is not well coupled to the sound field, measurements in the reverberant room are satisfactory. We used the same experimental setup as was used for the previous measurement. Three observers measured the decay rates at 20 locations on the shroud. A double slope was evident in the decay, but we were able to determine the initial slope, which is controlled by the dissipation of the shroud. The measured, total dissipation loss factors are shown in Fig. 22.

4.1.8 Model-shroud noise reduction (NR). NR was measured by using the same setup as discussed above. The test room was excited acoustically and the SPL's inside and outside the shroud were measured. Measurements at 6 random locations within the shroud were taken. None of the 6 locations were within 6 in. of the shroud wall. The SPL outside the shroud was found through the SPL at a reference location. The measured NR is shown in Fig. 23.

4.1.9 Internal acoustic-space dissipation. To measure the internal-space dissipation, we used a small electromagnetic loudspeaker to excite the internal space. We measured the decay rate at 8 locations with a microphone in the shroud. The measured, total dissipation loss factors are shown in Fig. 24.

4.1.10 Model-spacecraft response from acoustic-path transmission. To measure the response from acoustic-path transmission, we hung the model spacecraft within the shroud from the top baffle. The mounting trusses were removed from the assembly. Six accelerometers were located randomly on opposite panels of the spacecraft. The shroud was baffled. Using the procedure described in Section 3.1, the test room was excited acoustically and the AL on the spacecraft and the SPL in the test room was measured. The measured-response data are shown in Fig. 25.

4.1.11 Model ring-frame response. For this experiment, the shroud was supported by resilient foam rubber on the floor of the test room. The spacecraft and mounting trusses were removed from the assembly. The test room was excited acoustically and the resulting AL on the ring frame and SPL in the test room were measured. Measurement locations on the ring frame are shown in Fig. 26. Measurements were taken at a number of points around the shroud. The measured ring-frame AL relative to the shroud AL are shown in Fig. 26. The AL's of the shroud have been corrected for accelerometer loading according to the procedure described in Section 4.2. The ring-frame response measurements were performed both with and without the baffle in place. The data show only a slight effect by the baffle. This indicates that the vibration transmitted through the ring frame is not affected by the baffle. Measurements were repeated with the mounting trusses and spacecraft connected. The data are shown in Fig. 27. Connection of the mounting trusses and spacecraft has only a small effect on the vibration levels of the ring frame.

4.1.12 Model-mounting-truss response. The response of two mounting trusses was measured by using the setup of the previous experiment. The test room was excited acoustically and the resulting SPL in the test room and AL on the mounting trusses were measured. Accelerometers were located on the trusses at the points shown in Fig. 28. Measurements could only be taken where the channel beam was supported by a crossmember. Measurements at other points along the truss showed that the truss cross section was not rigid at the measurement frequencies. The AL's of the mounting trusses relative to the AL's of the shroud corrected for accelerometer loading are plotted in Figs. 28 and 29. In both cases, the spacecraft was connected to the mounting trusses.

4.1.13 Model-spacecraft response from mechanical-path transmission. For this measurement we eliminated the acoustic-path transmission by enclosing the spacecraft in a soundproof box. The box was constructed with double walls of 1/2-in. gypsum board. Both sides of the box were covered with acoustically absorbent material. The spacecraft was placed within the soundproof box, which in turn was located inside the shroud.* Holes were cut to allow the mounting trusses to pass through the box without contact. The trusses were connected to the ring frame. Accelerometers were located at 5 random positions on opposite spacecraft panels. Using the procedure of Section 3.1, the test room was excited acoustically and the resulting SPL's in the test room and AL's on the spacecraft panels were measured. The response data from this experiment are shown in Fig. 30.

To verify that no acoustic excitation was present, we repeated this experiment with the mounting trusses disconnected. Short

*The assembly was turned upside-down for this particular experiment.

strings were used to hang the base of the mounting trusses from the ring frame; the soundproof box was not altered. Measured data are shown in Fig. 31. Comparison of these data with data taken when the mounting trusses were connected indicate that all transmission is along the mechanical path.

4.1.14 Model-spacecraft response from combined-path transmission. Our final experiment was to support the spacecraft inside the shroud using the mounting trusses. Thereby, both acoustic-path and mechnical-path transmission contributes to the model spacecraft response. Six accelerometers were located on 2 opposite panels of the spacecraft. Using the procedure of Section 3.1, the test room was excited acoustically and the resulting SPL's in the test room and AL's on the spacecraft panels were measured. Data are shown in Fig. 32.

4.2 Accelerometer Loading

At high frequencies the mass of an accelerometer impedes the structural motion that it is measuring. For very lightweight structures, this accelerometer loading can appreciably reduce the local vibration level near the accelerometer. When the impedance of the accelerometer equals the driving-point impedance of the structure, the loading reduces the local acceleration by 3 dB. The frequency at which the impedances are equal is given by

$$f_\ell = \frac{8\rho_s \kappa c_\ell}{2\pi M} \quad , \tag{6}$$

where ρ_s is the surface density, κ is the bending radius of gyration, c_ℓ is the longitudinal wavespeed, and M is the accelerometer mass. Above f_ℓ, loading reduces the acceleration 6 dB/octave.

The accelerometer loading frequency for the model-spacecraft panels is f_{ℓ}=12 000 Hz. Therefore, no correction of the data is necessary. The loading frequency for the model shroud is 4500 Hz. Vibration data for the shroud, Figs. 20 and 21, have been corrected for accelerometer loading according to this frequency. The corrected AL's will be used in comparing theoretical predictions with the experimental data.

4.3 Parameter Determination

The parameters governing vibration transmission are the modal densities and dissipation loss factors of each element and the coupling loss factors between elements.

The modal densities of the individual elements can be determined by sweeping a sine-wave excitation and counting resonances. The technique is useful as long as the spacing between modes exceeds the modal bandwidth. The modal density of the elements in our model is sufficiently high that this technique of mode counting is possible only below 400 Hz. Since this frequency range is below the frequency range of interest, mode counting has not been performed in our experiments. We have not attempted to develop other techniques for verifying the theoretical predictions, because our confidence in these predictions is high.

The dissipation and coupling loss factors are determined by combining the decay-rate and radiation measurements. The reverberation times from the decay-rate measurements are related to a total dissipation loss factor by the equation

$$\eta_{tot} = \frac{2.2}{f T_{rev}} \quad , \tag{7}$$

where η_{tot} is the total dissipation loss factor, T_{rev} is the reverberation time, and f is the frequency.

The structural elements in the acoustic path cannot be separated from the acoustic media without a large vacuum chamber. Rather than resort to the use of a vacuum chamber, we performed decay-rate measurements in the acoustic media. The total loss factor is, then, a measure of the mechanical damping internal to the structure and its boundaries and of the radiation losses to the surrounding medium. The mechanical damping is inferred from the total dissipation loss factor measurement and a determination of the radiation loss factor which we obtain from a radiation measurement. When the structure is excited with a shaker, the ratio of the reverberant, mean-square sound pressure radiated into the test room to the mean-square acceleration is related to the radiation coupling loss factor by Eq. (8)

$$\frac{\langle p^2 \rangle_{t,x}}{\langle a^2 \rangle_{t,x}} = \frac{\rho_o c_o^2}{\omega^2} \frac{M}{V} \frac{\eta_{S,A}}{\eta_A + (n_S/n_A)\,\eta_{S,A}} \quad , \tag{8}$$

where $\langle p^2 \rangle_{t,x}$ is the time/space, mean-square sound pressure in the test room, $\langle a^2 \rangle_{t,x}$ is the time/space, mean-square acceleration of the structure, ρ_o is the acoustic-medium volume density, c_o is the speed of sound, ω is the radian frequency, M is the total mass of the structure, V is the volume of the test room, $\eta_{S,A}$ is the radiation coupling loss factor of the structure, η_A is the dissipation loss factor of the test room, n_S is the modal density of the structure, and n_A is the modal density of the test room.

The parameters of our test room are such that

$$\eta_A >> \frac{n_S}{n_A} \eta_{S,A} \quad . \tag{9}$$

Thus, a measurement of η_A and the radiated sound field gives the radiation coupling loss factor for the structure.

4.3.1 Model-spacecraft parameters. Radiation and decay-rate measurements were made for the model spacecraft and the model shroud. The measured, total dissipation loss factor for the spacecraft is plotted in Fig. 18. This total loss factor is the sum of the mechanical dissipation loss factor η_{diss} and the radiation coupling loss factor $\eta_{sc,ac}$:

$$\eta_{tot} = \eta_{diss} + \eta_{sc,ac} \quad . \tag{10}$$

The measured SPL of the radiated sound field is plotted in Fig. 17. These data and the measured loss factor of the test room give an experimental estimate of $\eta_{sc,ac}$. In Fig. 33, this estimate is compared with a theoretical estimate.[3]

The experimentally obtained values of $\eta_{sc,ac}$ exceed η_{tot}. This is physically impossible and indicates that one of the measurements is in error. As explained earlier in this report, we have concluded that the decay-rate measurements do not give a valid estimate of the total loss factor for the model spacecraft.

4.3.2 Model-shroud parameters. The measured, total dissipation loss factor for the model shroud is plotted in Fig. 22. This total loss factor is determined by the mechanical damping of the shroud and the radiation to the test room and to the internal acoustic space. The total loss factor is

$$\eta_{tot} = \eta_{diss} + 2\eta_{sh,ac} \quad , \tag{11}$$

where $\eta_{sh,ac}$ is the coupling loss factor between the shroud and an acoustic space.

The SPL of the sound field radiated by the shroud is plotted in Fig. 21. These data can be used in Eq. (8) to obtain an experimental determination of the coupling loss factor $\eta_{sh,ac}$. This experimentally determined value is compared with a theoretically predicted value[4] in Fig. 35.

The theoretical value of $\eta_{sh,ac}$ is consistently low. A calibration error was suspected but not found. We conclude that the material properties used in the theoretical prediction are inaccurate. We determined these properties by experiments on a sample taken from the edge of the shell. Properties at the edge are perhaps not representative of those in the remainder of the shell. A second possible conclusion is that the theoretical estimates are consistently low by 1 or 2 dB.

The dissipation loss factor of the model shroud was inferred from the measured, total loss factor and the measured, radiation coupling loss factor. The experimentally determined values are compared with an empirical prediction of the dissipation loss factor in Fig. 36. The agreement between values is satisfactory. We conclude that the decay-rate technique is valid for the model shroud.

4.3.3 Internal-acoustic-space parameters. The measured, total dissipation loss factor for the internal acoustic space is plotted in Fig. 24. This total loss factor is determined by absorption in the space and losses to the external acoustic space through the shroud. Because of the absorptive liner in the model, the absorption will dominate the total loss factor so that

$$\eta_{tot} \approx \eta_{diss} \quad . \tag{12}$$

The measured, dissipation loss factors for the internal acoustic

space are compared with lines of constant absorption coefficient in Fig. 37. Measured data lie between a value of $\bar{\alpha}$=0.2 and $\bar{\alpha}$=0.6 which indicates that the liner is more effective at high frequencies.

The dissipation loss factor of the internal acoustic space of an actual shroud is shown in Fig. A-9. Loss factors for the model and the actual shroud are comparable over only a small frequency range. For this reason, our experimental results should only be used to support the theory and not to predict vibration levels in the actual OGO assembly.

4.3.4 Discussion. Our conclusion that the decay-rate technique is valid for the model shroud but not for the model spacecraft is not fully understood. Apparently, two classes of modes with greatly different radiation properties exist in the spacecraft. The dissipation of one class of modes—those that will be strongly excited by an acoustic field—is very great and is dominated by radiation. The dissipation of the second class of modes is significantly less. Decay-rate measurements cannot be used to determine the dissipation of the first class of modes. We do not completely understand the reasons for this limitation.

The dissipation of all modes of the model shroud is dominated by mechanical damping. The decay-rate technique appears to be valid for this situation.

Initially, the experimental program included decay-rate measurements on the elements of the mechanical path. In view of our lack of understanding of this technique, we did not conduct these experiments. Therefore, experimental determination of the remaining coupling parameters is not possible.

In the following section, we compare the measured response of the assembly elements with theoretical predictions.

5. COMPARISON OF DATA WITH THEORETICAL PREDICTIONS

The major purpose of our experimental study is to obtain data that can be compared with the theoretical predictions developed in Ref. 1. These predictions were developed through a statistical energy analysis. We will not discuss this type of analysis. Instead, we refer the reader to Refs. 1, 5, 6, and 7.

Reference 1 gives numerical evaluations of the theoretical predictions for a full-scale model of the OGO-spacecraft assembly. The structural parameters used in these evaluations are not correct for the actual assembly or for the 1/2-scale model described in Section 2. For this reason, we have reevaluated the predictions by using the correct parameters for the 1/2-scale model that are given in Table I.

In our evaluation, we use an empirical value for the dissipation loss factor of the model shroud and the model spacecraft,

$$\eta_{diss} = 0.01 \quad , \tag{13}$$

where η_{diss} is the dissipation loss factor. Agreement between this empirical value and the value measured for the shroud is shown in Fig. 36. We cannot obtain an estimate of the dissipation loss factor for the spacecraft by using the decay-rate technique.

We use the measured value for the dissipation loss factor of the internal acoustic space in our evaluation of the theoretical predictions. This measured value is plotted in Fig. 37, where it can be compared with lines of constant absorption coefficient. Our reason for using the measured value is that we do not feel that our ability to estimate this parameter correctly should effect our comparison of theory with experiment. Of course, correct

evaluation of the dissipation loss factor of the internal acoustic space is necessary for correct prediction of the vibration transmitted by the acoustic path.

The dissipation loss factors of the model mounting trusses and the model ring frame were assumed, in our evaluation, to be less than the coupling loss factors. The same assumption is made in Ref. 1. An experimental verification of this assumption was not obtained because of the limitations of the decay-rate method.

5.1 Comparison for Acoustic Path

The resonant response of the spacecraft to diffuse acoustic-field excitation is calculated in Section 3.8.1 of Ref. 1. The critical frequency for the model spacecraft panels is 800 Hz. The resonant response calculated by using two values of mechanical dissipation is shown in Fig. 38 and can be compared with the measured data. The nonresonant, mass-law response is calculated in Section 3.8.2 of Ref. 1. This nonresonant response is also plotted in Fig. 38. The measured response is greater than the theoretical prediction for most frequency bands. The deviations are between 0 and 5 dB. Such deviations are within the expected accuracy of the theory.

The resonant and nonresonant response of the shroud to diffuse-acoustic-field excitation is calculated in Section 3.7 of Ref. 1. The ring frequency of the model shroud is 1160 Hz. The critical frequency is 10 000 Hz. The response calculated from the theoretical equations is plotted in Fig. 39, where it can be compared with the measured data. As for the model spacecraft, the measured response of the model shroud above the ring frequency is 1-6 dB greater than the theoretical prediction. This consistent deviation is not expected; although, random deviations up to

5 dB commonly occur when comparing predictions found by using statistical energy analysis with measured data. Below the ring frequency the measured response is consistently less than the theoretical prediction. But again, the deviations are within the expected accuracy of the theoretical predictions. We conclude that the deviations between theory and measured data are, in part, due to errors in our estimation of the material properties of the model shroud.

The NR by the shroud is predicted in Section 3.6 of Ref. 1. In this prediction the transmission by both resonant and nonresonant modes is considered. To evaluate the NR, we use the measured values of dissipation loss factor for the internal acoustic space. The theoretically predicted NR is plotted in Fig. 40, where it is compared with the measured data. The lack of agreement at the critical frequency again indicates that the material properties of the shroud which are used in the evaluation are incorrect. On the whole, the agreement between theory and experiment is good.

The theoretical predictions of model-spacecraft response to acoustic excitation and of NR by the model shroud can be combined to give the spacecraft response due to vibration transmission by the acoustic path. The comparison between the theoretical prediction and the measured data is shown in Fig. 41. We feel that the agreement between theory and experiment is sufficiently good as to support the use of statistical energy analysis to predict vibration transmission in the acoustic path.

5.2 Comparison for Mechanical Path

The ring-frame response is a combination of bending in the plane of the ring and torsion along the ring. In Ref. 1 we assume that only the bending motion contributes to the spacecraft

response. Therefore, only this motion is calculated in Section 4.6 of Ref. 1. The bending response of the model ring frame is plotted in Fig. 42.

The measured data at Locations B and C, shown in Fig. 26, indicate that bending and torsion of the ring are approximately equal. Measured response at Location A is greater than that at Locations B and C because of resonant deformation of the ring. We take the measured vibration data at Location B as representative of the bending-vibration level. These data are compared with the theoretical predictions in Fig. 42. The agreement is within 5 dB for most frequency bands and shows no systematic deviation. This agreement is considered to be within the expected accuracy of the theory.

The response of the spacecraft panels owing to vibration transmission from the ring frame is calculated in Section 4.7 of Ref. 1. The theoretical prediction of the model spacecraft response is shown in Fig. 43, where it is compared with the measured data. Agreement between theory and data is not as close as expected. Deviations greater than 5 dB occur in many frequency bands. These deviations, which show greater response, are possibly due to vibration transmission by torsion of the ring frame. We have not considered the magnitude of this transmission.

The predicted response of the ring frame and the transmission from the ring frame to the spacecraft can be combined to give the spacecraft response due to transmission by the mechanical path. The theoretical prediction is plotted in Fig. 44 along with the measured data. The measured response due to mechanical-path vibration transmission is considerably greater than that predicted theoretically for many frequency bands. As stated above, part of this increased transmission may be due to transmission by torsional

motion of the ring frame. In the lower frequency bands, the measured data is considerably below the theoretical prediction. These deviations are probably a result of the relatively small number of modes in each 1/3-oct band in the mechanical-path elements. Statistical energy analysis treats the modes statistically and requires that many modes participate in the vibration. No quantitative results exist for the minimum number of modes required for the analysis to be valid.

5.3 Comparison for Combined Path

The theoretical predictions from Sections 5.1 and 5.2 can simply be added in order to obtain a prediction for vibration transmission by the combined path. The theoretical prediction for the model-spacecraft response to transmission by the combined path is plotted in Fig. 45, where it is compared with the measured data. Deviations between theory and experiment are a result of the inaccuracy in the prediction of mechanical-path transmission. We conclude that predictions of the mechanical-path transmission require further investigation.

6. CONCLUSIONS AND RECOMMENDATIONS FOR FUTURE WORK

Data from the experimental program are summarized in Fig. 46. Vibration transmission by the acoustic and mechanical path are comparable. Acoustic-path transmission dominates at low frequencies, whereas mechanical-path transmission dominates at high frequencies. This conclusion is somewhat unique to our model because of the large amount of absorption in the internal acoustic space. Also, the results are unique to the particular configuration that we selected.

We conclude from the program that statistical energy analysis can be used to predict, within 5 dB, vibration transmission by the acoustic path. Accuracy of the predictions for mechanical-path transmission is ±10 dB. A number of problems were encountered in the program. These are discussed below.

6.1 Difficulty in Measuring Damping

The most formidable difficulty that we encountered was that of measuring damping. We found that the decay-rate method cannot be used to determine the damping of the model spacecraft. A general conclusion is that the decay-rate measurements cannot be used to measure the damping of a class of resonant modes in a frequency band when a second set of modes, with significantly less damping, are also resonant in that band. For such a case one must directly measure the power input required to excite the structure to a given steady vibration level.

6.2 Need for Lightweight Accelerometers

The design of scale models requires the use of small, lightweight structures and high test frequencies. Loading by the measuring accelerometer often becomes a problem. In our study we used a 2-gram accelerometer; therefore, we had to correct the

shroud-response data above 4600 Hz for accelerometer loading. The accuracy of the correction is somewhat questionable. Lighter-weight accelerometers are available but, at this time, are not sufficiently reliable or convenient to use.

6.3 Desirability of Other Similar Experiments

The experimental program described in this report was conducted on one particular structural assembly. The results of the study cannot, unfortunately, be taken as sufficient support for the use of statistical energy analysis. Further studies are required in which vibration transmission in other typical configurations is studied.

For our particular model assembly, it would be worthwhile to study the vibration transmitted to instruments on the spacecraft panels, to solar panels, to an antenna, and to other structures connected to the mounting trusses.

APPENDIX A

VIBRATION MEASUREMENTS ON A NIMBUS-OGO SHROUD

A1. INTRODUCTION

Bolt Beranek and Newman Inc. (BBN) has conducted Noise-Reduction (NR) experiments on a Nimbus-OGO shroud at Goddard Space Flight Center. In these experiments the shroud was placed in a large reverberant chamber and was subjected to a diffuse acoustic field. The response acceleration level (AL) at several points on the shroud and the sound-pressure levels (SPL) inside the shroud were measured in 1/3-oct frequency bands. The experimental program is described in this section and the measured data are compared with theoretical predictions.

A1.1 Description of the Nimbus-OGO Shroud

The Nimbus-OGO shroud is shown in Figs. 3 and 4. It is a glass-reinforced, plastic-laminate shell. The shroud geometry is that of a ribbed cylindrical shell capped by a conical nose. The shell-wall thickness varies both circumferentially and axially from 0.10 to 0.14 in. A microquartz/felt blanket lines the inside of the shroud. Its density is 3.5 lb/ft^3 and its thickness varies from 1/2 to 1 in. The major structural and geometric properties of the shroud are summarized in Table I.

A1.2 Experimental Setup

The Nimbus-OGO shroud was set up, as shown in Fig. A-1, on a large carrier used for the Launch Phase Simulator (LPS) at Goddard Space Flight Center. The carrier platform served as a baffle that prevented the flow of acoustic energy through the open end of the shroud. Venting holes were sealed so that the complete shroud and

baffle were air tight. Later in the experiment, the vents were opened. No change in the vibration and acoustic measurements was noted.

The carrier and shroud were placed at one side of the LPS room. A large sound source was placed on the other side of the room. The relative positions of the carrier, the shroud, the sound source, and the LPS are shown in Fig. A-2. These objects were located in the room so that the sound field around the shroud was diffuse.* We used the uniformity of the acoustic field SPL as a measure of diffuseness. We consider a field with spatial variations in SPL less than ±3 dB to be effectively diffuse.

A1.3 Instrumentation

The instrumentation for the sound and vibration measurements on the Nimbus-OGO shroud consists of several functional groups: sound source, microphone system, vibration source, acceleration-measuring system, and reverberation-time measuring system.

A1.3.1 Sound source. The sound source used to excite the LPS room consists of a General Radio (GR) 1390-B random-noise generator, a GR 1564-A sound and vibration analyzer used as a 1/3-oct-band filter, two McIntosh M1-200 AB power amplifiers that are each capable of delivering 200 W, and a University B-12 horn loudspeaker with a flare extender to lower the cutoff frequency. The horn is driven by 12 University 1D-40 drivers rated at 40 W each. The loudspeaker was driven by 1/3-oct bands of noise to achieve as high a level as possible in the band where measurements were being made. One-third-oct-band SPL of 110 dB re 2 x 10^{-4} μbar were achieved in the 500 Hz-1 kHz region.

*The intensity in a diffuse field is uniform for all angles of incidence.

A1.3.2 Microphone systems. Three microphones were used. All were Brüel and Kjaer (B&K) capacitor microphones with attached cathode followers. Two were 1 in. in diameter (type 4131) and one was 1/2 in. (type 4134). The cathode follower used inside the shroud was battery-powered for convenience; the others were not. All microphones were calibrated with a B&K type 4220 pistonphone. The frequency response of the microphones and associated electronics is flat ±1 dB in the frequency range 100 Hz – 6 kHz.

A1.3.3 Vibration source. The vibration source used to excite the shroud consisted of a GR 1390-B random-noise generator, a GR 1564-A sound and vibration analyzer (used as a 1/3-oct-band filter), a McIntosh M1-200 AB power amplifier, and a Goodmans V-50A point-drive shaker mounted on a stand so that it could be lined up with the attachment point on the shroud. The system is capable of exerting 50-lb peak forces. The attachment point chosen (one of the holes used to attach handling fixtures) was equipped with a 1/4-in. -28 captive nut. The shaker-output stud was screwed into the captive nut and a locknut was tightened against the outside skin of the shroud. The hole used was about 22 in. above the base of the shroud. No attempt was made to measure the vibration excitation forces. However, shaker current was monitored to avoid destructive operation of the shaker.

A1.3.4 Accelerometer system. Vibration of the shroud was measured by using a Wilcoxon type 111 accelerometer mounted to the skin with clay. The weight of this accelerometer is 2 grams. Its mounted resonance, using clay, is above 10 kHz. This lightweight unit was chosen in order to avoid mass loading of the skin at the measuring point. Adhesive tape was used to support the weight of the lead wire. A GR 1551 B sound-level meter was used as a preamplifier; its output was fed into the 1/3-oct-band filter of the decay-rate meter according to the quantity being measured. The

system was calibrated by attaching the accelerometer to a GR type 1337 vibration calibrator. Frequency response of the accelerometer and associated electronics is flat ±1 dB from 100 Hz to 6 kHz.

A1.3.5 Decay-rate meter. This instrument was used to measure the acoustic and mechanical reverberation times of the shroud. It furnishes a display on an oscilloscope screen of both an internal RC network discharging and of the signal decay in the environment that is being measured. The RC network is adjusted until the decay rates match and the reverberation time (the time for a 60 dB decay in vibration level) is read from the front panel. The instrument was designed by BBN and is manufactured by Spencer-Kennedy Laboratories.

A2. TEST CONDUCT AND DATA PRESENTATION

Three basic measurement tests were conducted:

(1) shroud response and internal SPL's during acoustic excitation;

(2) reverberation time of the shroud to determine its damping; and

(3) reverberation time of the internal acoustic space to determine its acoustic absorption.

In Test 1 an acoustic field was created in the LPS room by using 1/3-oct bands of noise. The resulting SPL's were measured by using a hand-carried roving microphone. The levels were fairly uniform throughout the LPS room, so that only measurements near the shroud were recorded. The SPL's varied randomly around the shroud for all frequency bands. In the high-frequency bands, there was, in addition, a small amount of shadowing by the carrier. The average SPL's are shown in Fig. A-4. SPL variations were less than ±3 dB, so that the field can be accurately approximated by a diffuse

field. The average level and the spatial variation of the level in each 1/3-oct band were read from the GR vibration analyzer.

During the acoustic excitation, we measured the shroud AL at 7 points. The points were selected at random, but were all on the cylindrical part of the shroud. One of the 7 accelerometers was located near a rib. The accelerometer locations are shown in Fig. A-3.

The average shroud AL and the maximum variation for the 6 measurement locations* are plotted in Fig. A-5 relative to the average exciting SPL.

The SPL's inside the shroud were also measured during the acoustic excitation. The measuring microphone was suspended from a traverse that ran diagonally from one side of the base of the shroud to the nose of the shroud. Measurements were read directly from the GR vibration analyzer as we slowly moved the microphone along the traverse. Figure A-6 shows the average and the spatial variation of the measured internal SPL relative to the average external SPL. The difference between the SPL's outside and inside the shroud is commonly referred to as NR.

The NR measurement was repeated by using the broadband LPS acoustic source. Because of the intense SPL produced by this source, electronic measurement equipment and personnel were stationed outside the LPS room. Two external and one internal measurement locations were monitored and recorded.

The measured SPL in 1/3-oct bands are plotted in Fig. A-7. The NR calculated from these measurements is plotted in Fig. A-6

*The location near the rib is not included. AL's at this location are significantly less than the skin levels in most 1/3-oct bands.

and can be compared with the NR obtained from the low-level 1/3-oct-band test. The agreement is good except for the high-frequency bands in which the NR during the LPS test is significantly less than that recorded in the low-level 1/3-oct test.

The spectrum of the LPS-produced sound field falls off sharply at high frequencies. One percent third-harmonic distortion of the shroud vibration induced by this field produces internal SPL's in the high-frequency bands that exceed the levels produced by acoustic excitation in the bands. It follows that the NR measured at high frequencies in the LPS test is influenced by a small amount of nonlinearity because of the particular shape of the exciting acoustic spectrum.

Test 2 is required in order to estimate the shroud damping loss factor. The damping loss factor is necessary in order to make theoretical predictions of the shroud response and NR. It cannot be accurately estimated without experimental data.

We excited the shroud in 1/3-oct bands with a shaker and measured the reverberation time—the time for the vibration level to decay 60 dB after the exciting source has been stopped. The total dissipation loss factor of the shroud η_d is related to the reverberation time T by Eq. (A1)

$$\eta_d = \frac{2.2}{fT} \quad , \tag{A1}$$

where f is the band center frequency. The measured dissipation loss factor for the shroud is plotted in Fig. A-8.

Test 3 is required in order to estimate the absorption in the internal acoustic space. This parameter is necessary to make a theoretical prediction of shroud NR and cannot be accurately estimated without experimental data.

We excited the internal space with a small loudspeaker that was placed inside the shroud, and we measured the reverberation time. The total dissipation loss factor is related to the reverberation time by Eq. (A1). The measured internal-absorption loss factor is plotted in Fig. A-9.

A3. COMPARISON OF DATA WITH THEORETICAL PREDICTIONS

We have predicted the response and NR of the Nimbus-OGO shroud in Ref. 1. In these predictions we used empirically estimated values for the dissipation loss factor of the shroud and the internal acoustic space. To compare the theoretical predictions with the experimental results, we will use the experimentally measured values of the dissipation loss factors.

The predictions in Ref. 1 did not include the axial split in the shroud. The effect of this split is to add twice the length of the split to the radiating perimeter. The theoretical predictions used in this section are based on the correct radiating perimeter, which includes ribs, the end of the shroud, and the axial split.

Figures A-5 and A-6 present a comparison of the theoretical predictions with the experimentally measured shroud response and NR. The agreement between theory and experiment is within the expected accuracy of the theory.

Other experimental NR-measurement programs have been conducted on the Nimbus-OGO shroud.[8] The data from these programs were analyzed in octave bands. We have combined the data from our measurement program to give octave-band results. These are compared with the results of other programs in Fig. A-10. The comparison is satisfactory, considering that the NR obtained in the other programs is based on only a few measurement locations.

NOTES AND REFERENCES

1. J.E. Manning, R.H. Lyon, and T.D. Scharton, "Transmission of Sound and Vibration to a Shroud-Enclosed Spacecraft," BBN Rept. 1431 (Oct. 1966).

2. See Ref. 1, Appendix A.

3. The spacecraft/acoustic space coupling loss factor is calculated in Ref. 1, Sec. 3.4.

4. The shroud-acoustic-space coupling loss factor is calculated in Ref. 1, Sec. 3.4.

5. J.E. Manning, and G. Maidanik, "Radiation Properties of Cylindrical Shells," J. Acoust. Soc. Am. 36:1691-1698 (1964).

6. P.A. Franken, and R.H. Lyon, "Estimation of Sound-Induced Vibrations by Energy Methods, with Application to the Titan Missile," Shock Vib. Bull. 31:12-26, Pt. III (1963).

7. R.H. Lyon, "Noise Reduction of Rectangular Enclosures with One Flexible Wall," J. Acoust. Soc. Am. 35:1791-1797 (1963).

8. P.J. Alfonsi, "The Response of the OGO Spacecraft Structure to High-Intensity Acoustic Loading," Shock Vib. Bull. 34: 125-140, Pt. 5 (1965).

TABLE I: PHYSICAL PARAMETERS

	OGO Assembly	Designed Model	Constructed Model
Shroud:			
Diameter	65 in.	32.5	32
Length (cylinder section)	137 in.	68.4	73.5
Surface area (cylinder section)	200 ft^2	50	51.2
Rib spacing, base to 1st	24 in.	12	16.2
1st to 2nd	30 in.	15	19.8
2nd to 3rd	34 in.	17	13.0
3rd to 4th	42 in.	21	17.0
Skin thickness	0.1→0.14 in.	0.06	0.087
Material	phenolic fiberglass	phenolic fiberglass	G-11 nema fiberglass
Material density	113 lb/ft^3	113	112
Longitudinal wavespeed	~10 000 ft/sec	10 000	9500
Internal Acoustic Space:			
Volume	374 ft^3	46.8	34.1
Liner material	microquartz felt	same	porous fiberglass
Liner thickness	0.5→1.0 in.	0.75	0.75
Liner density	3.5 lb/ft^3	3.5	?
Ring Frame:			
Lineal density	2 lb/ft	0.5	0.65 lb/ft
Bending radius of gyration around vertical axis	? in.		0.65 in.
Mounting Trusses:			
Length (each leg)	20 in.	10	9.875
Lineal density (each leg)	0.68 lb/ft	0.34	0.337
Bending radius of gyration, axis 1	? in.	0.66	0.66
axis 2	? in.	0.51	0.51
Torsional radius of gyration	1.67 in.	0.83	0.83
Spacecraft:			
Panel material	aluminum with corregated core	same	aluminum with honeycomb core
Panel width	30 in.	15.0	15.0
Panel length	70 in.	35.0	35.0
Panel surface density	0.765 lb/ft^2	0.382	0.38
Bending radius of gyration, axis 1	0.258 in.	0.135	0.161
axis 2	0.284 in.	0.135	0.161

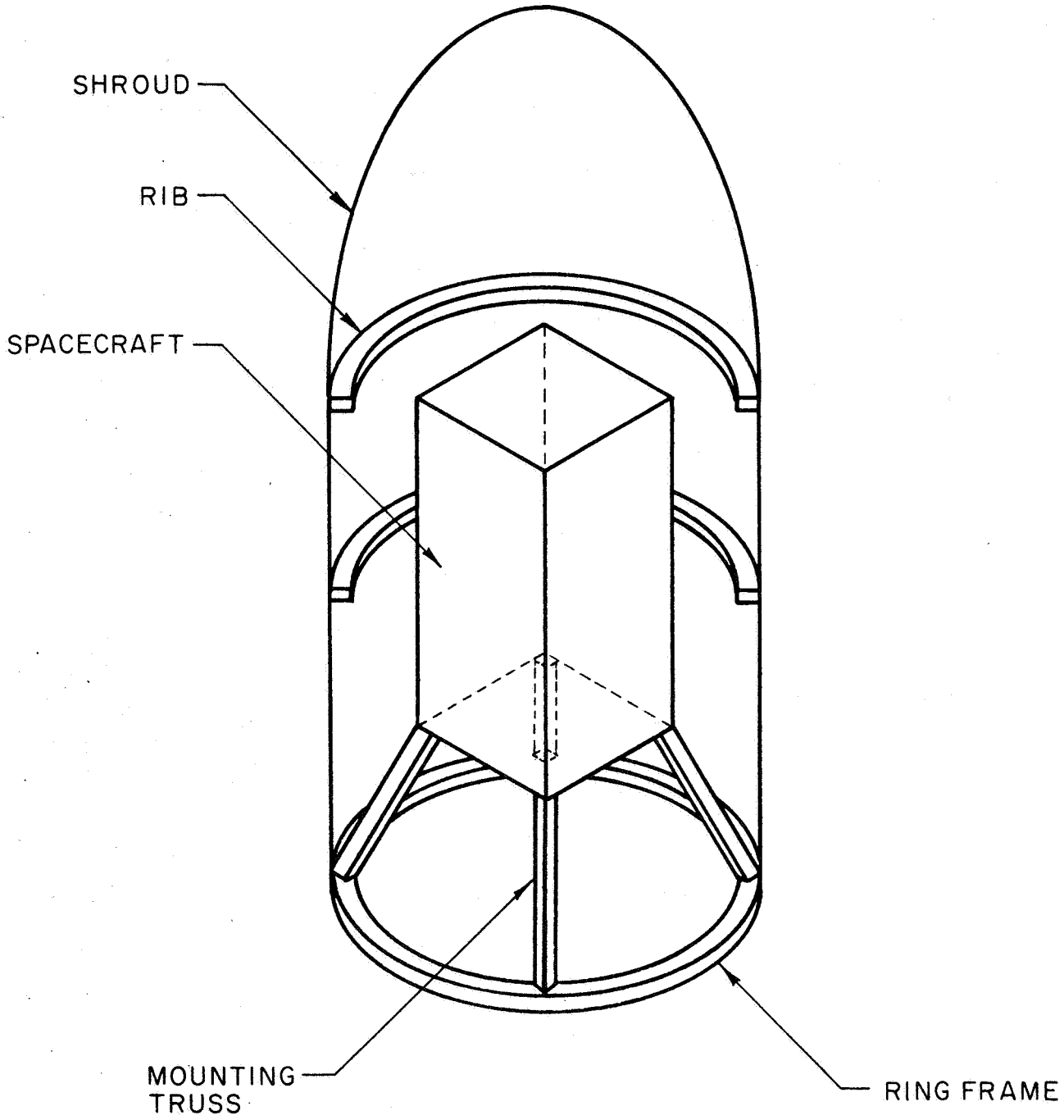

FIG. 1 TYPICAL SPACECRAFT-SHROUD ASSEMBLY

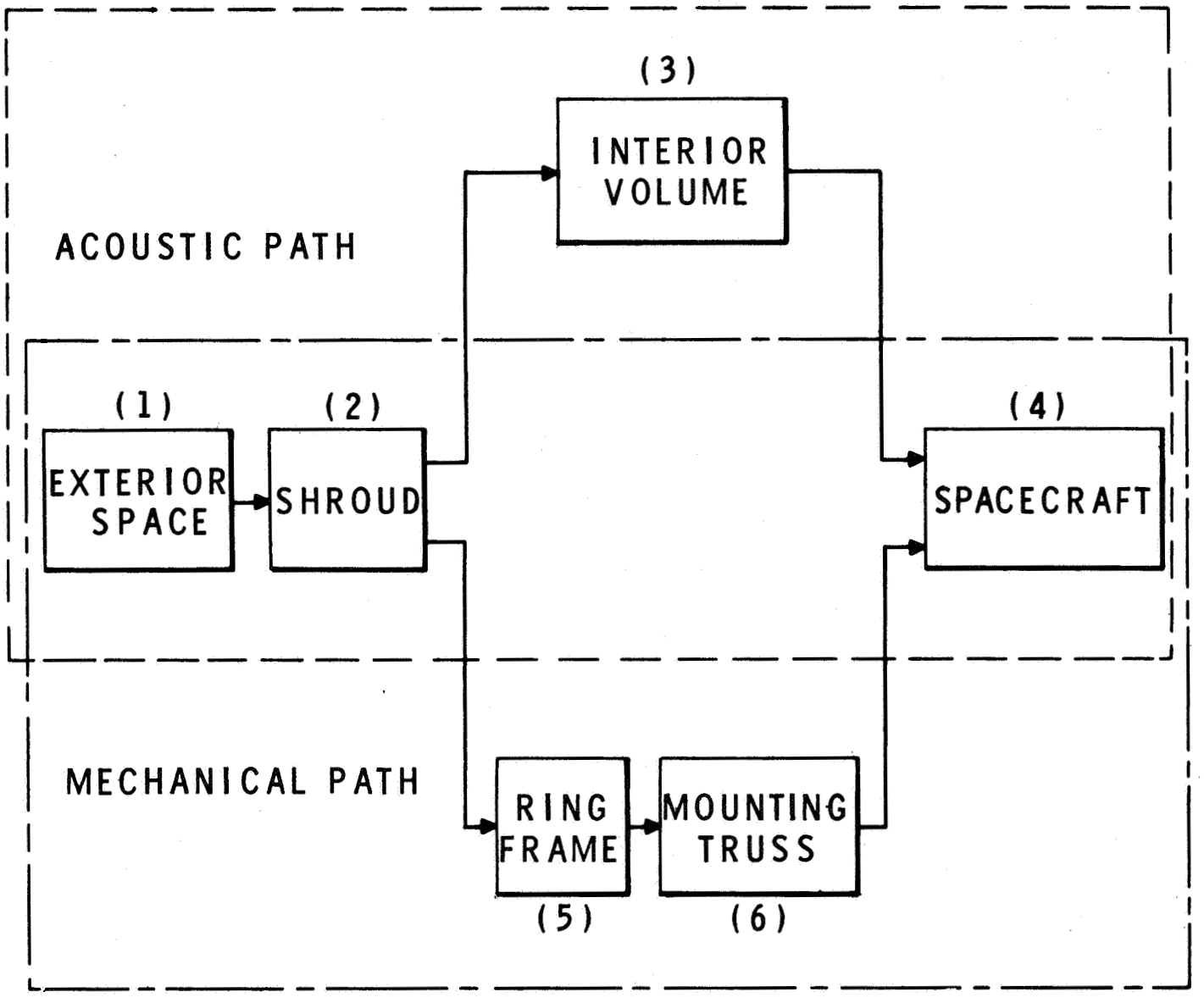

FIG. 2 ELEMENTS OF THE SPACECRAFT-SHROUD

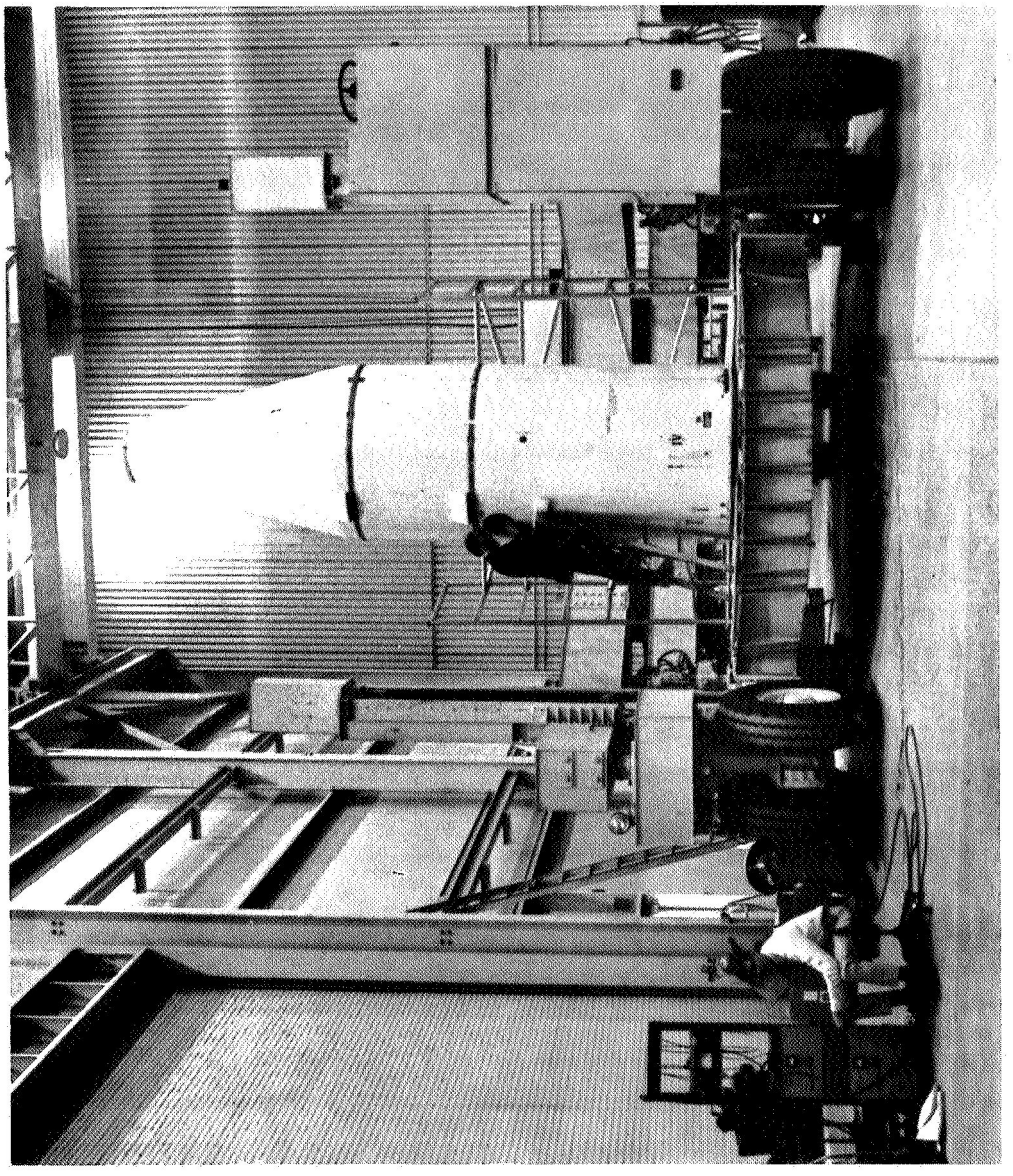

FIG. 3 THE OGO - NIMBUS SHROUD

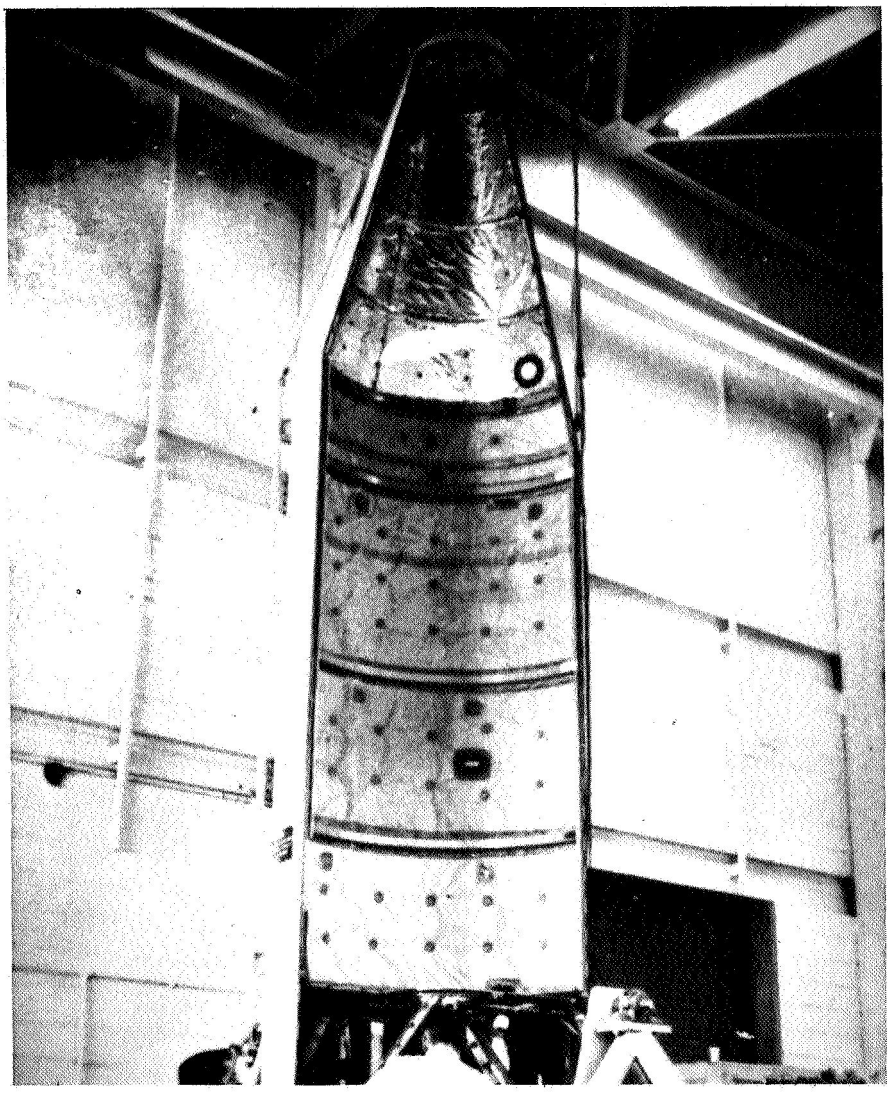

FIG. 4 ONE HALF OF THE OGO-NIMBUS SHROUD

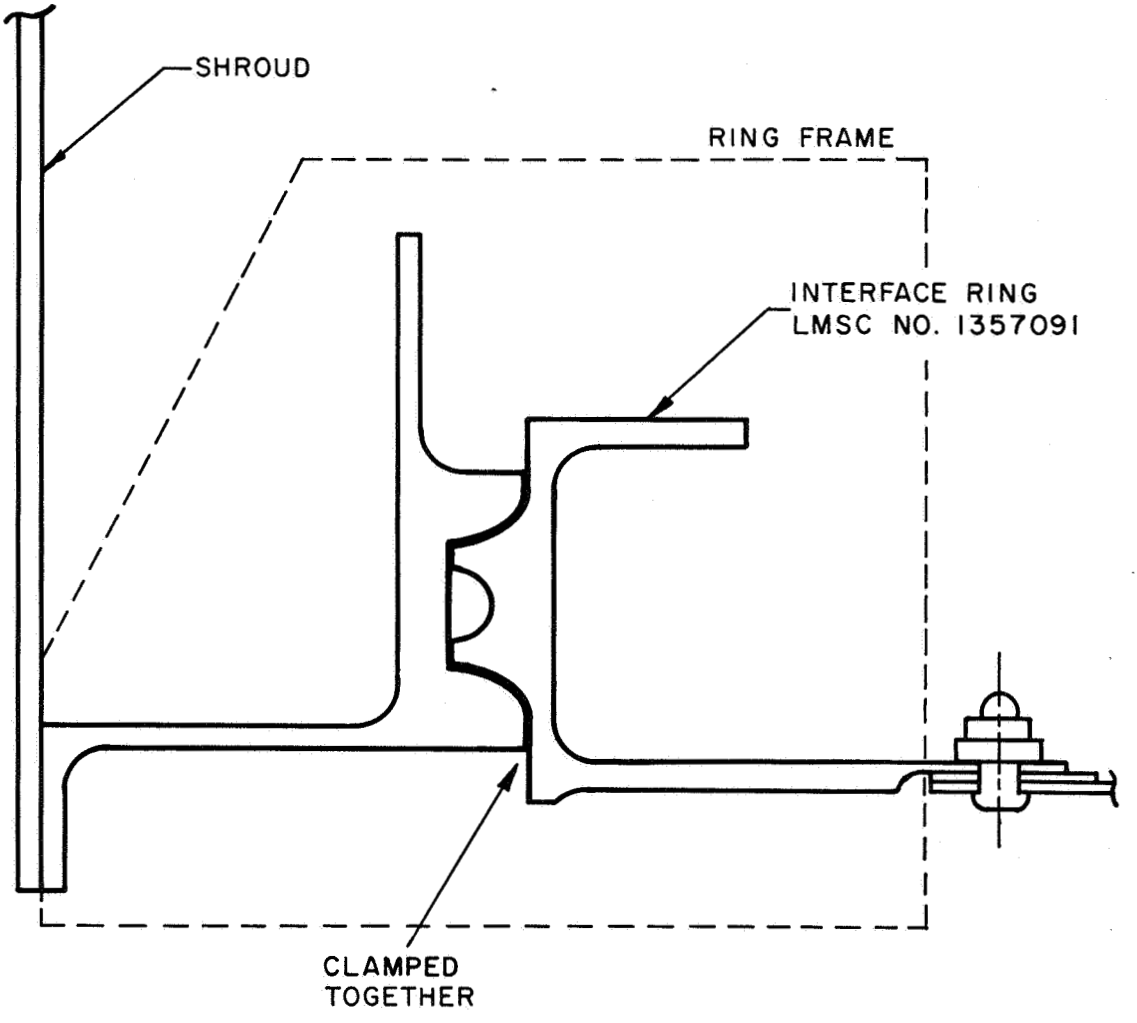

MATERIAL: ALUMINUM
SCALE: 1/1
TAKEN FROM LMSC
DRAWING NO. 1359163
SHEET 3

FIG. 5 DETAILS OF THE OGO RING FRAME

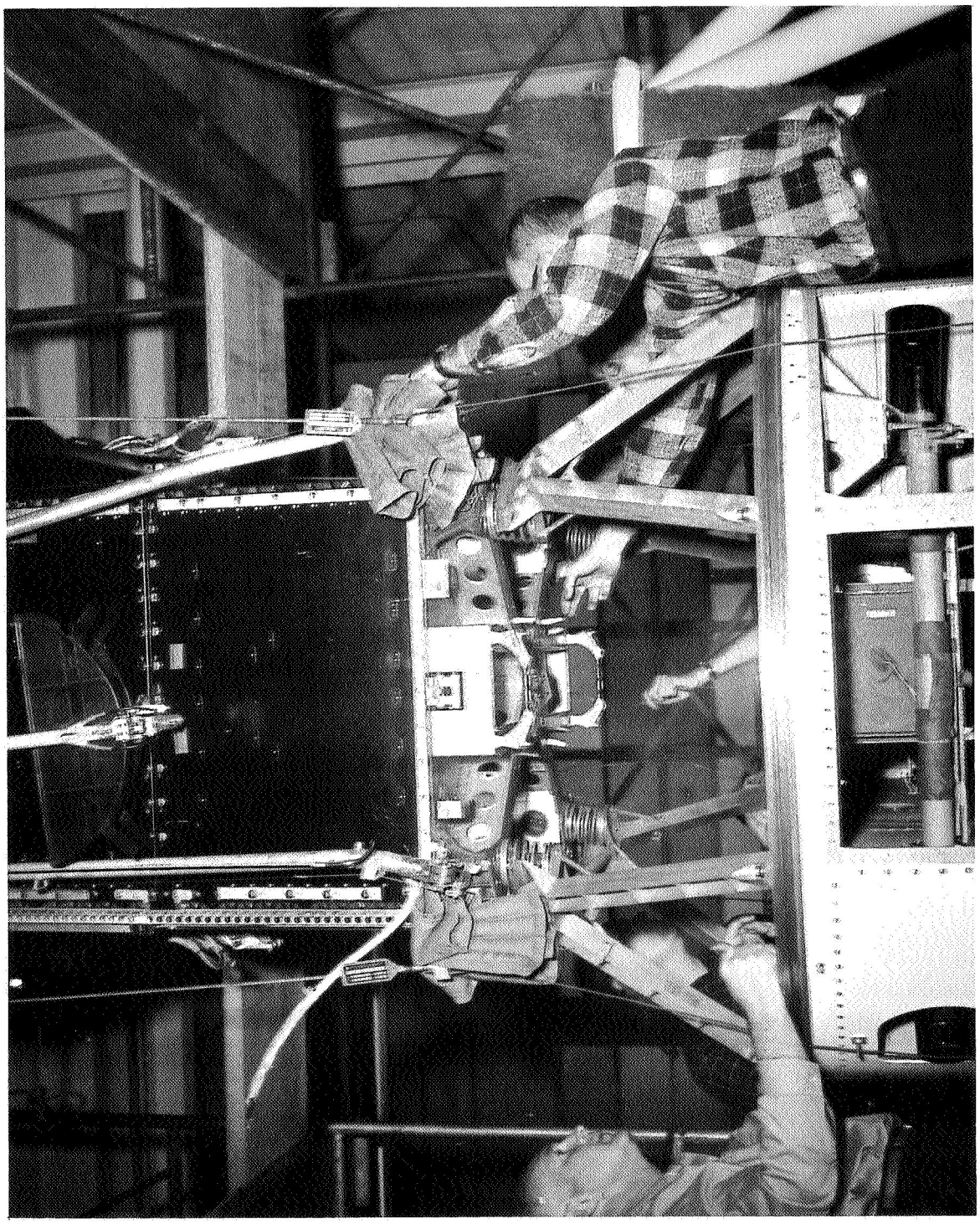

FIG. 6 THE OGO MOUNTING TRUSSES

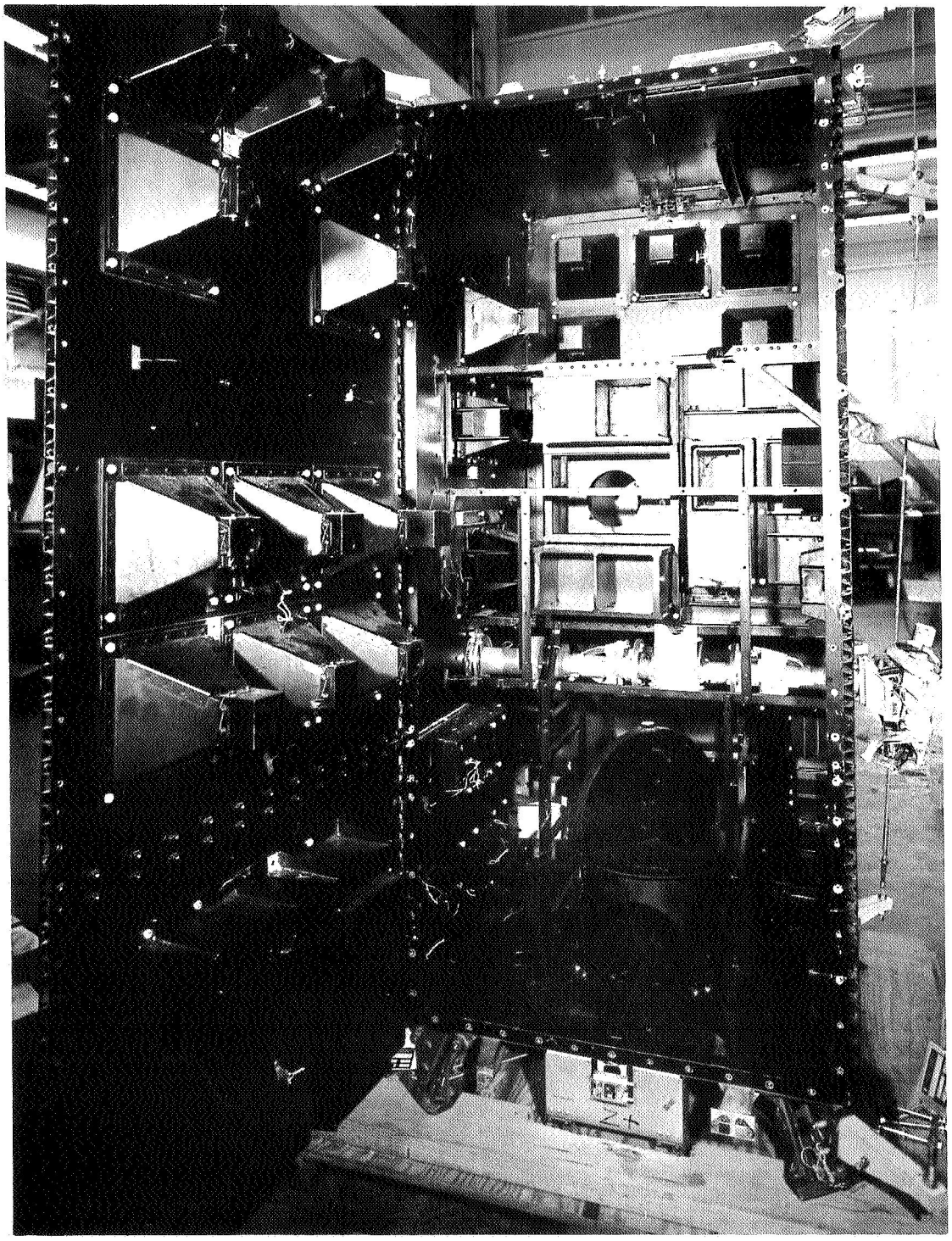

FIG.7 INTERIOR OF THE OGO SPACECRAFT

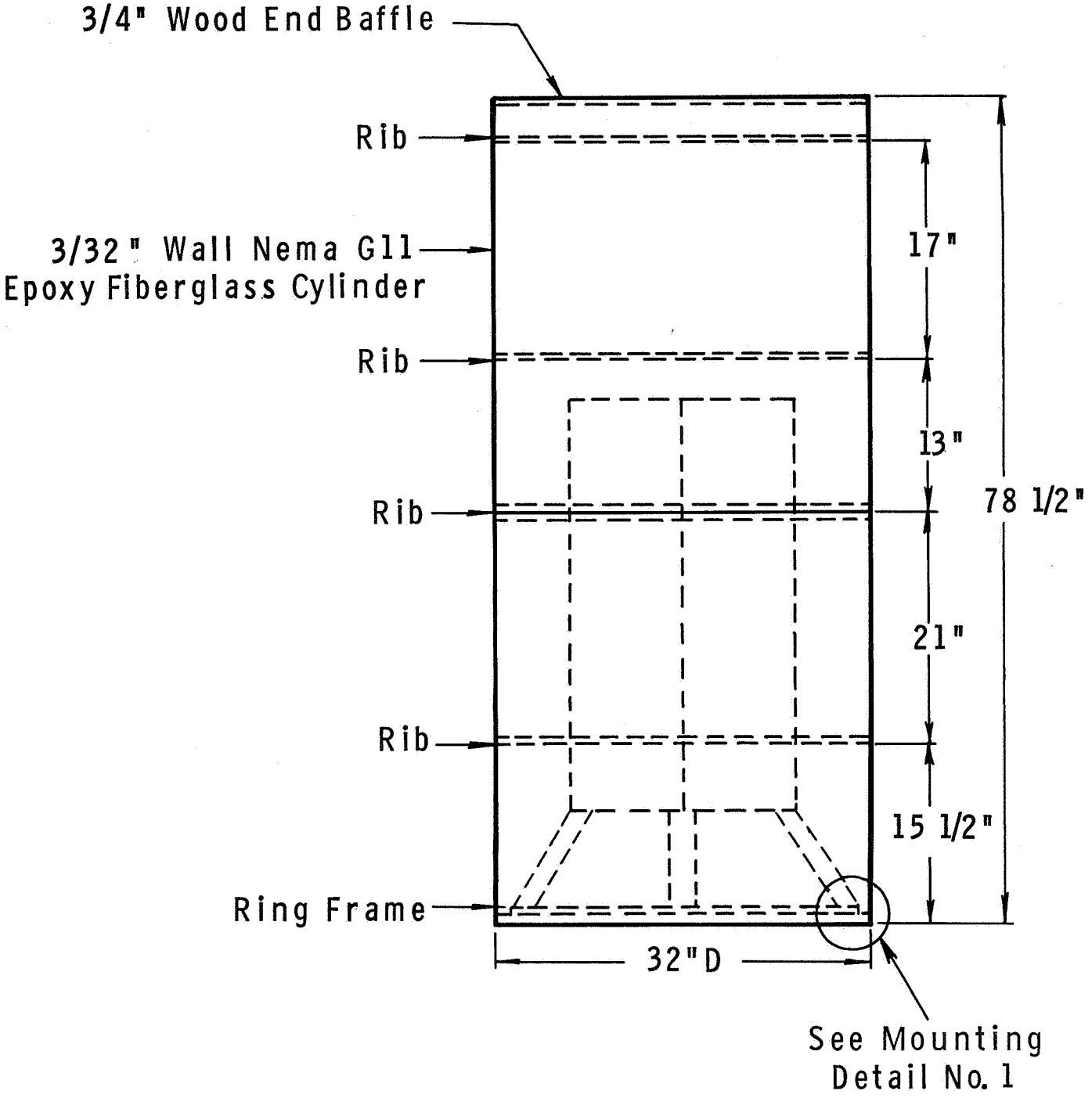

FIG. 8 MODEL-SPACECRAFT - SHROUD ASSEMBLY

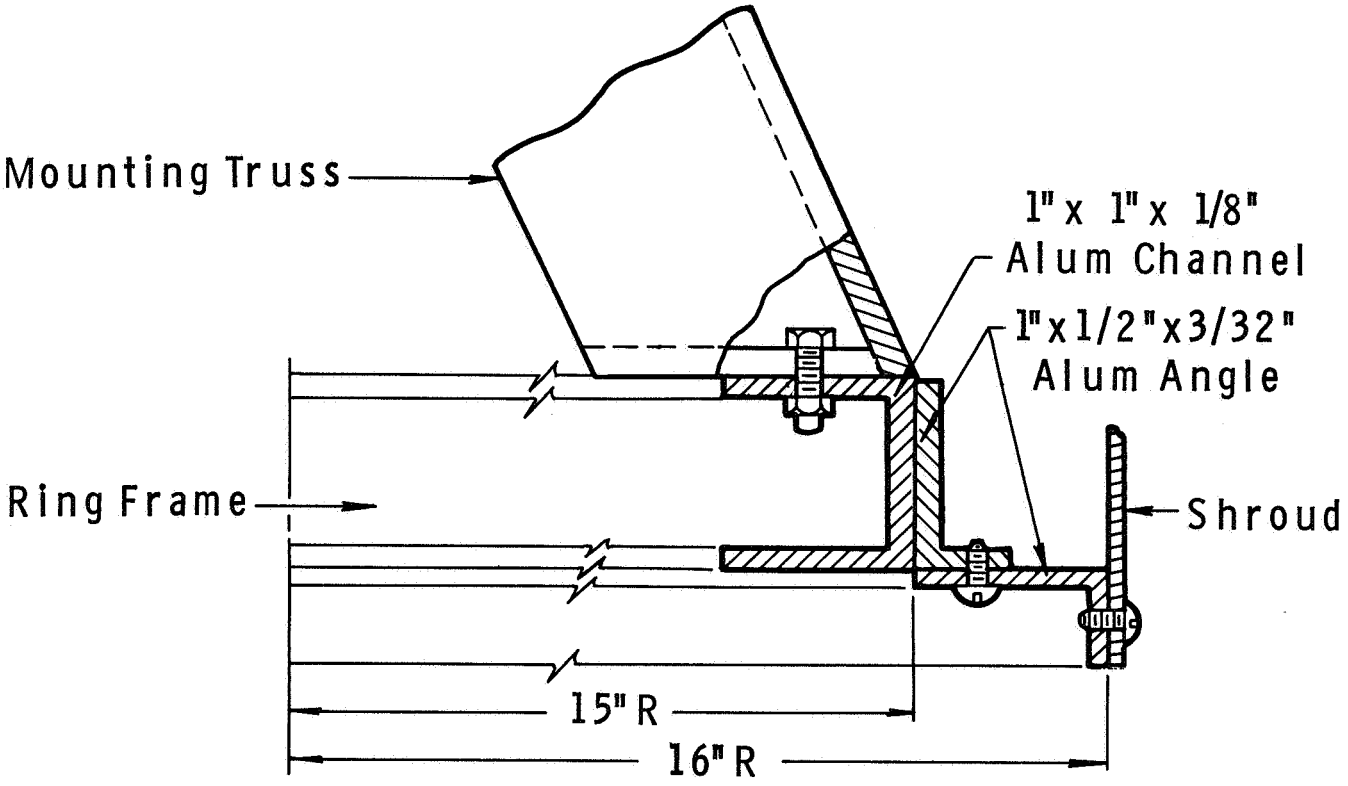

FIG.9 MOUNTING DETAIL NO.1 - RING FRAME

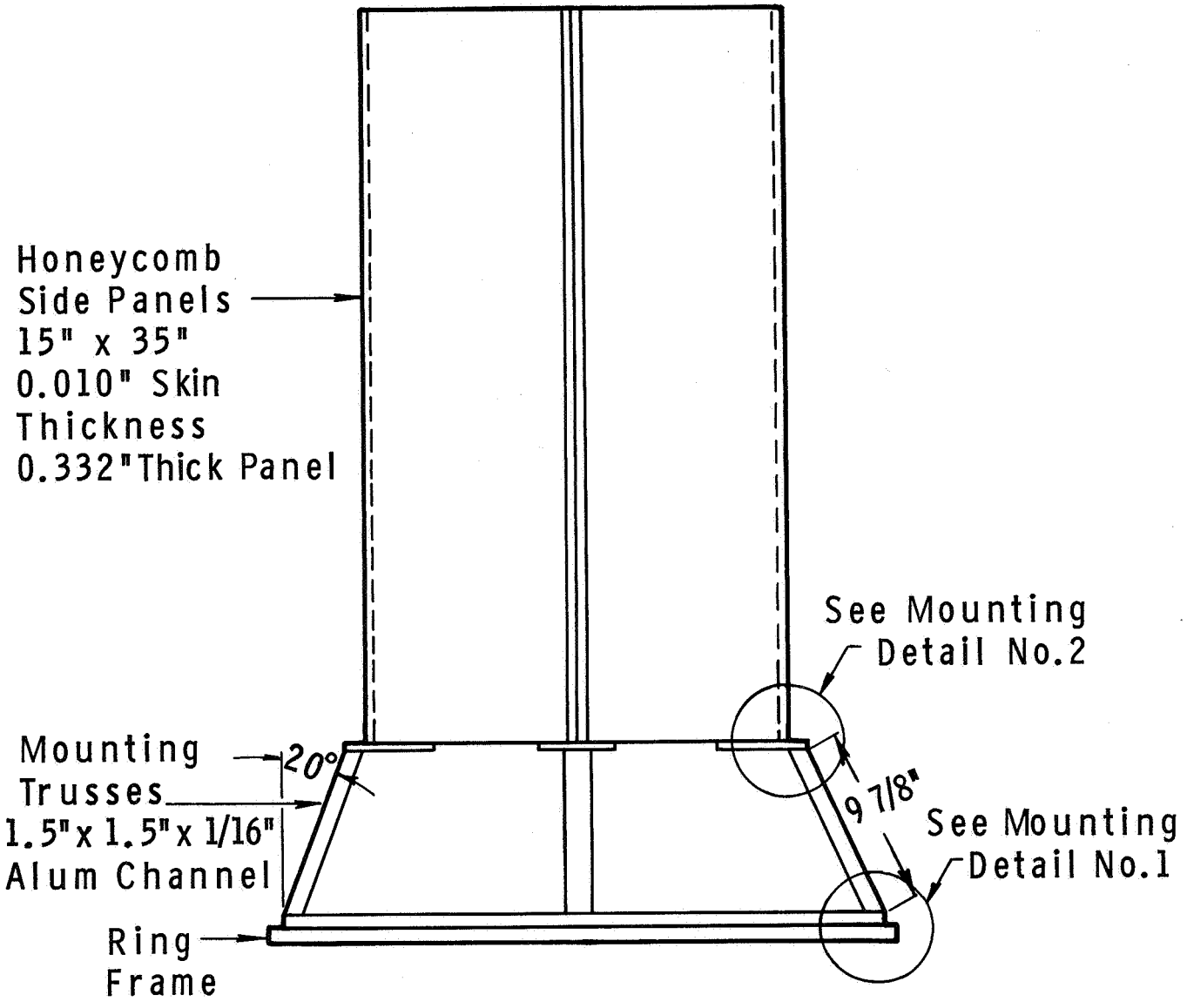

FIG. 10 MODEL SPACECRAFT

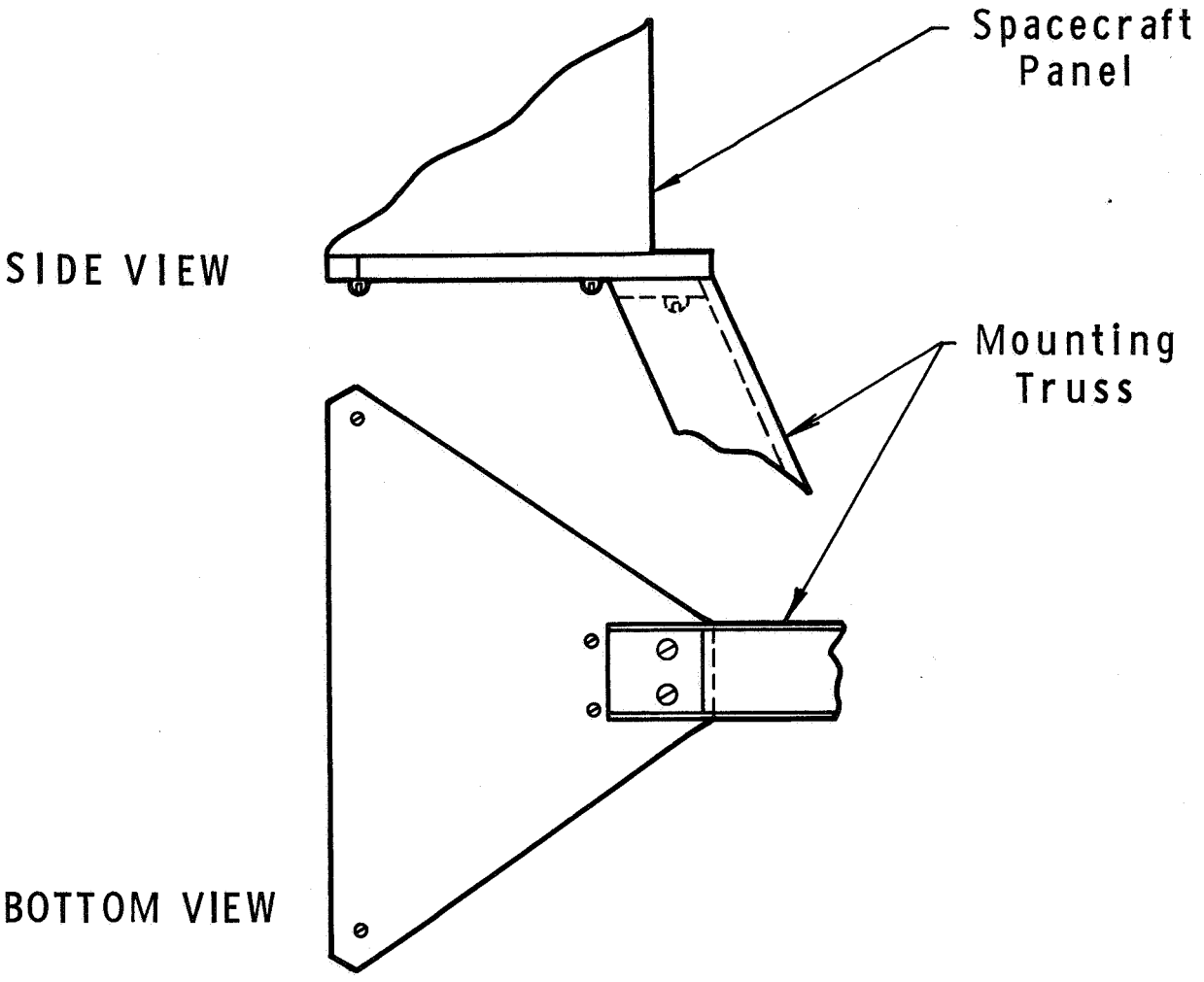

FIG. 11 MOUNTING DETAIL NO. 2

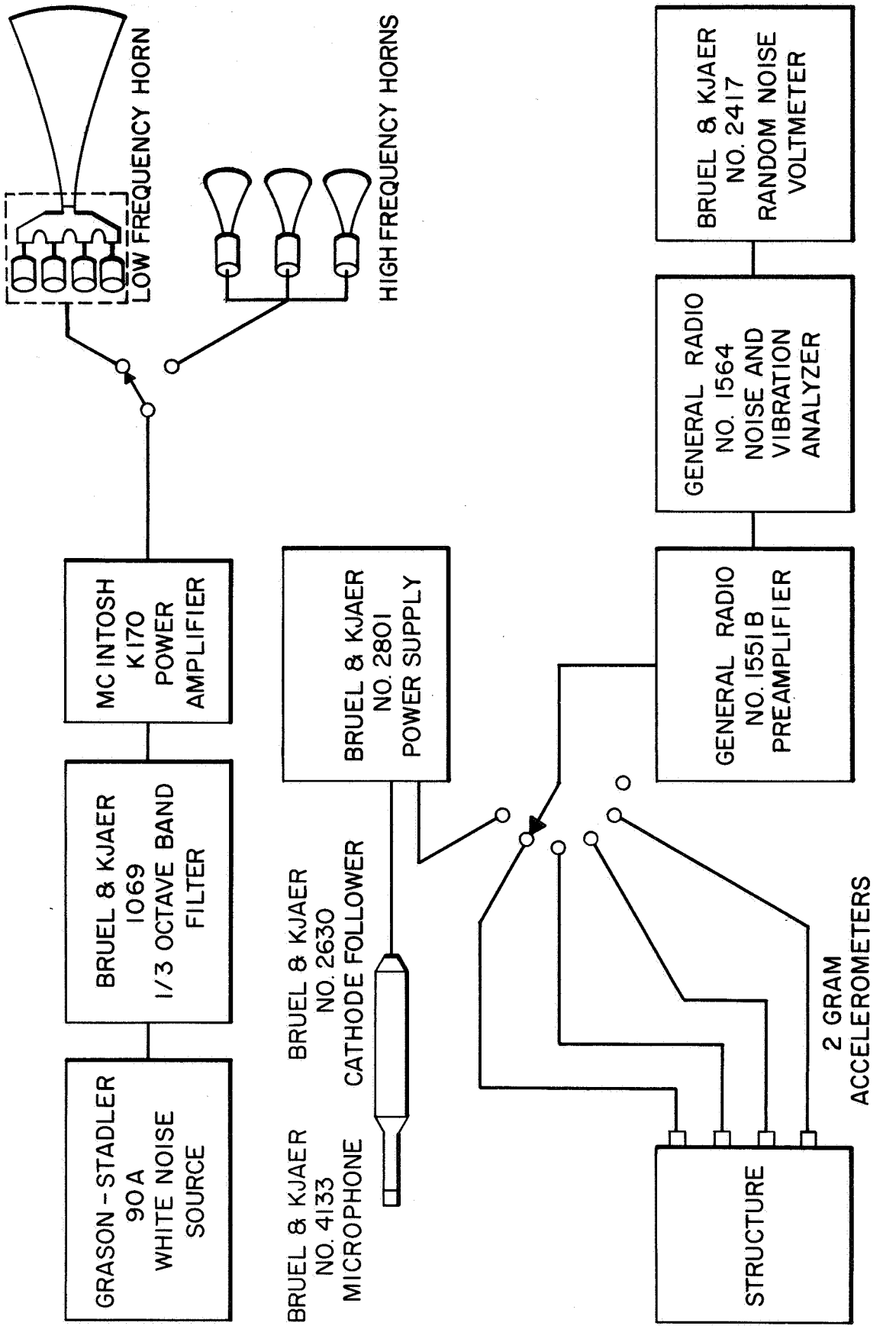

FIG. 12 EXPERIMENTAL SETUP FOR MEASURING RESPONSE

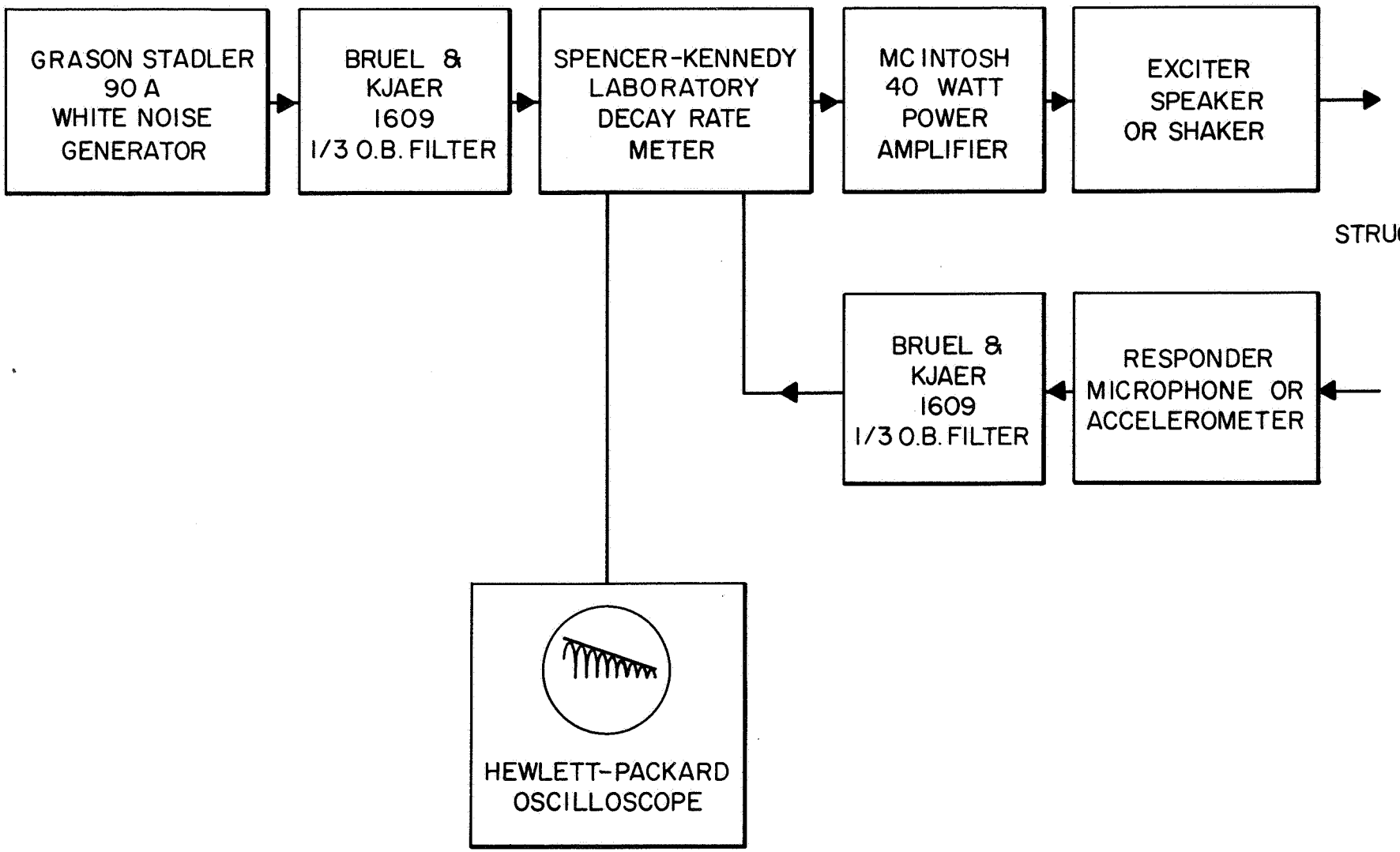

FIG. 13 EXPERIMENTAL SETUP FOR MEASURING DAMPING

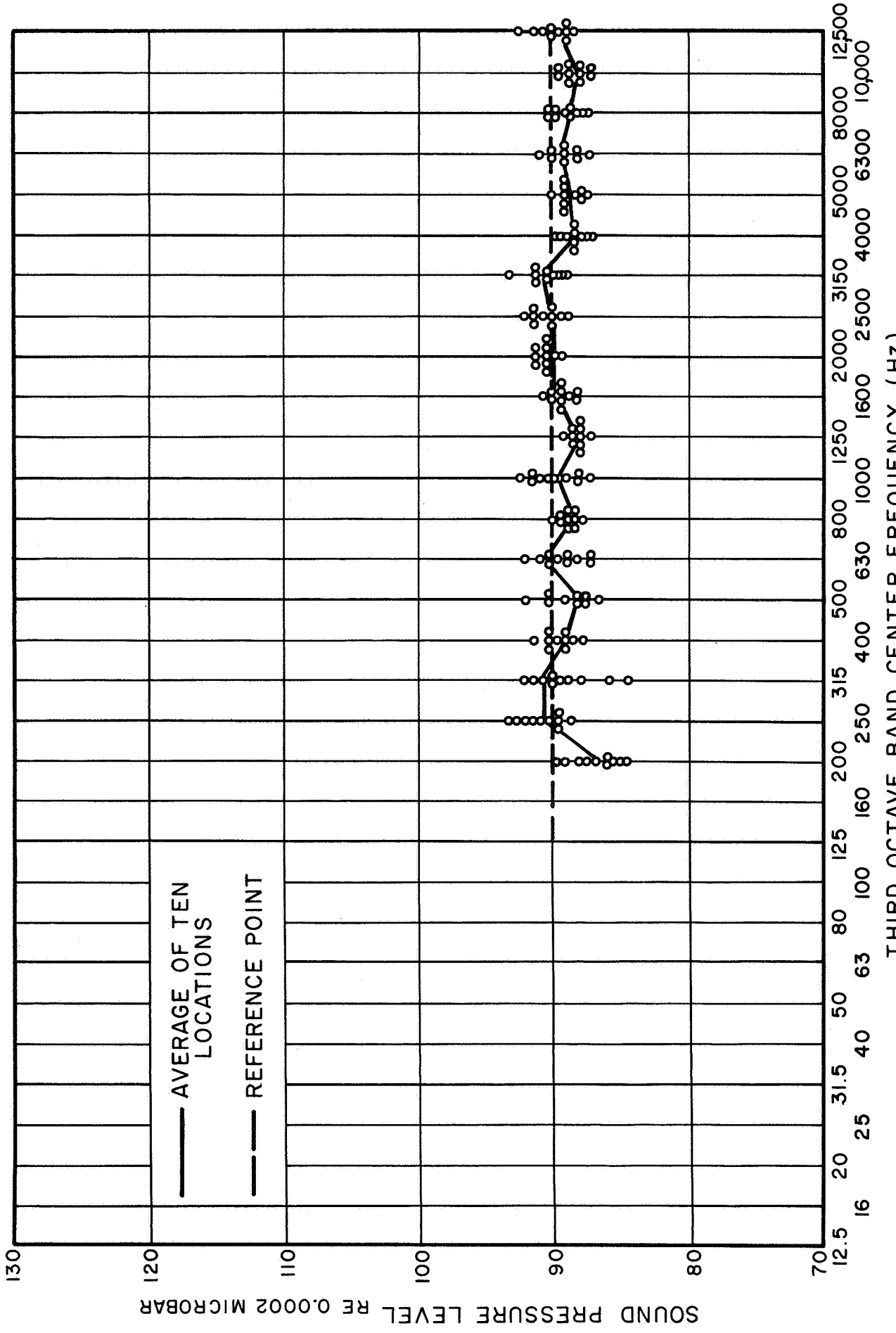

FIG. 14 VARIATION OF SOUND PRESSURE LEVEL IN TEST ROOM

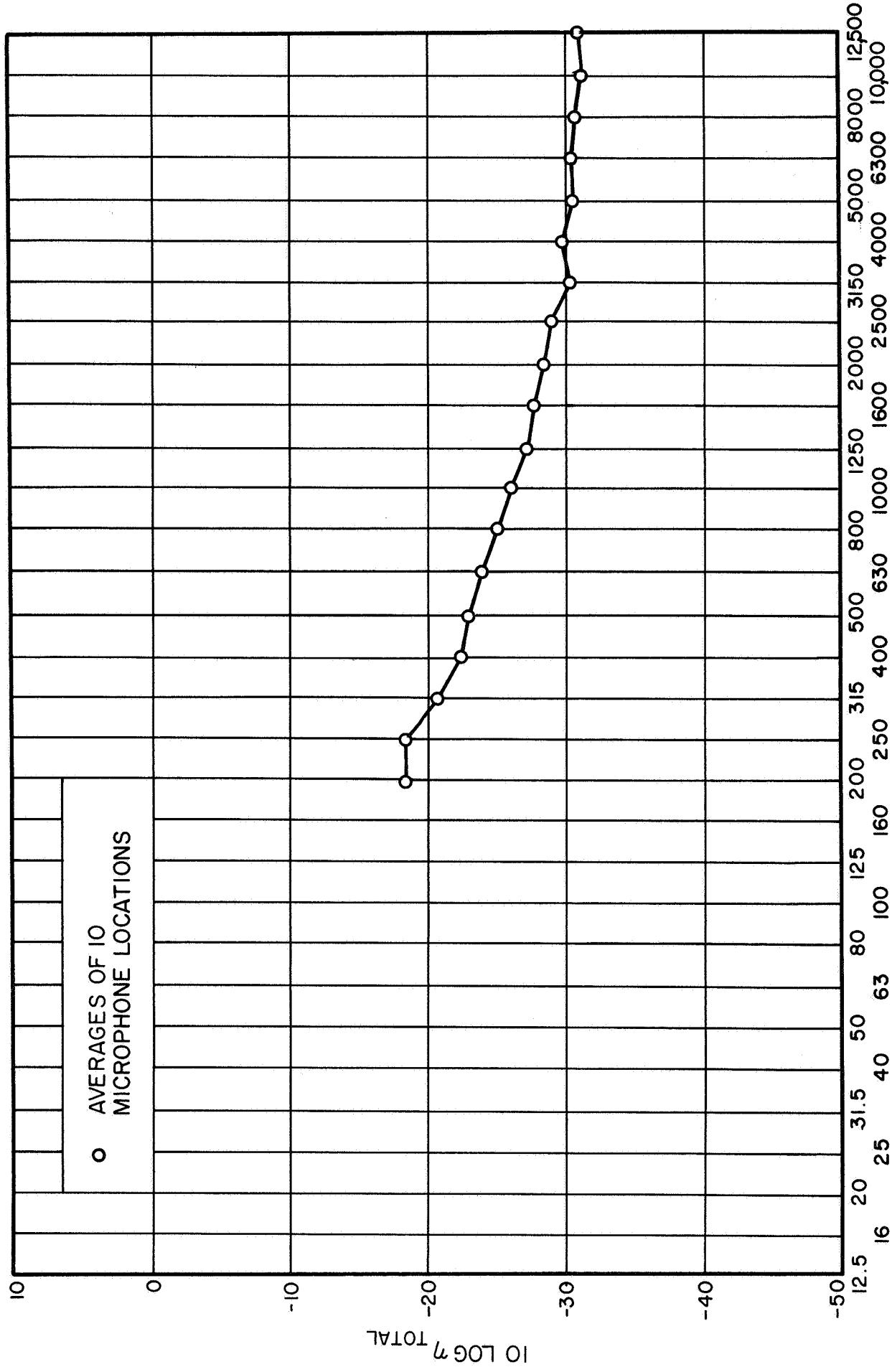

FIG. 15 TOTAL DISSIPATION LOSS FACTOR OF THE TEST ROOM

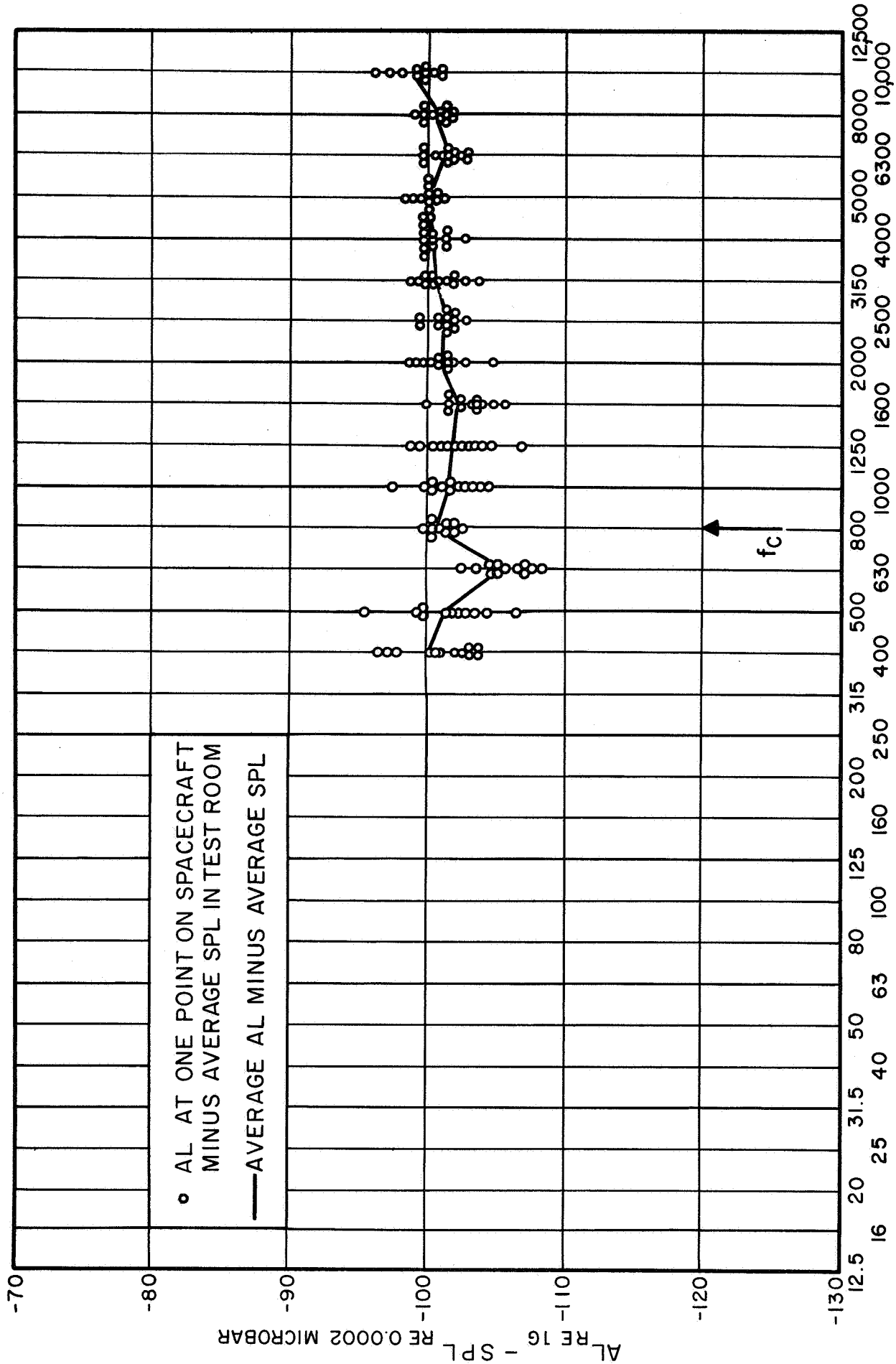

FIG. 16 RESPONSE OF MODEL SPACECRAFT TO ACOUSTIC EXCITATION

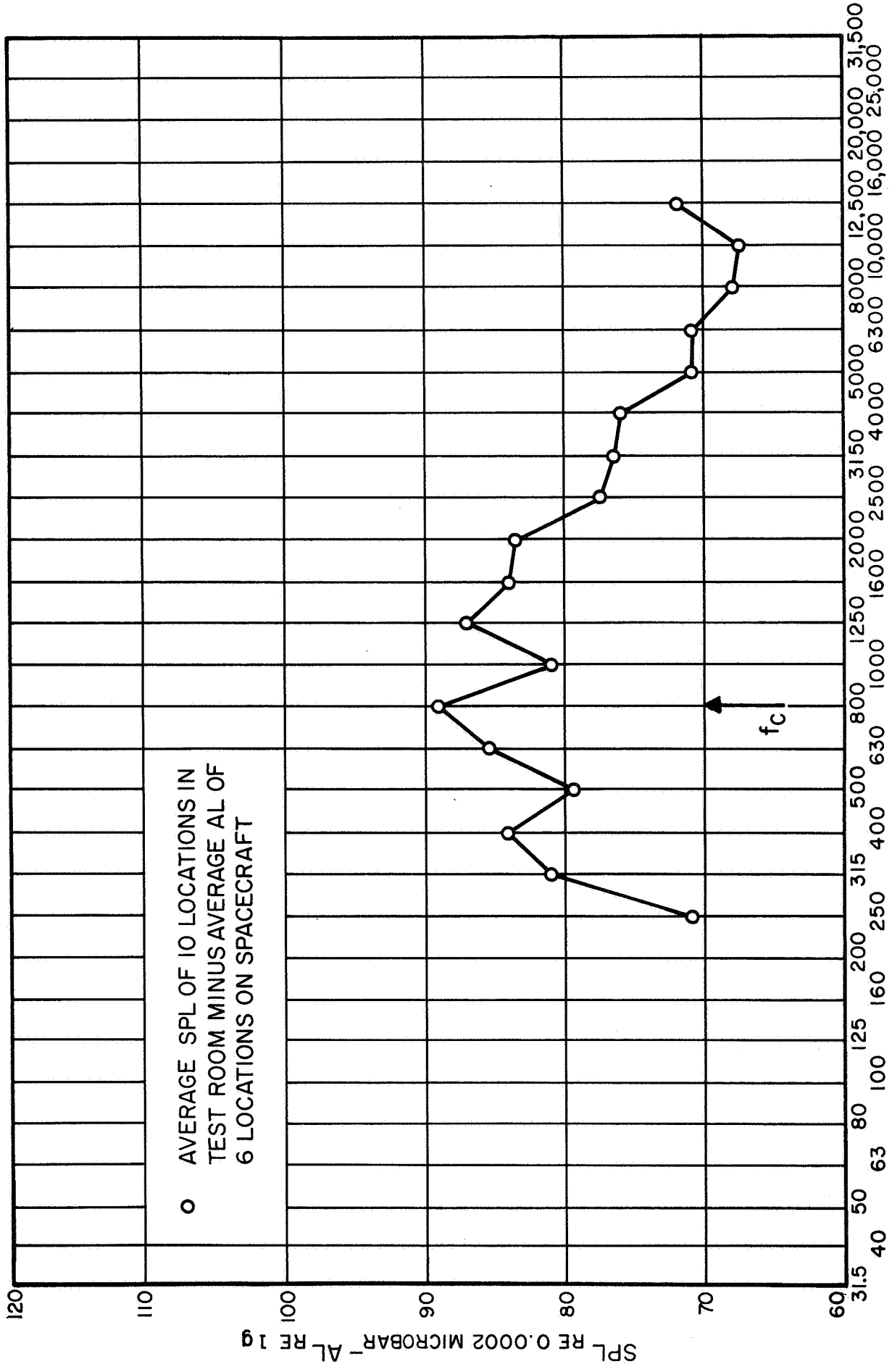

FIG. 17 RADIATION BY MODEL SPACECRAFT WHEN EXCITED MECHANICALLY

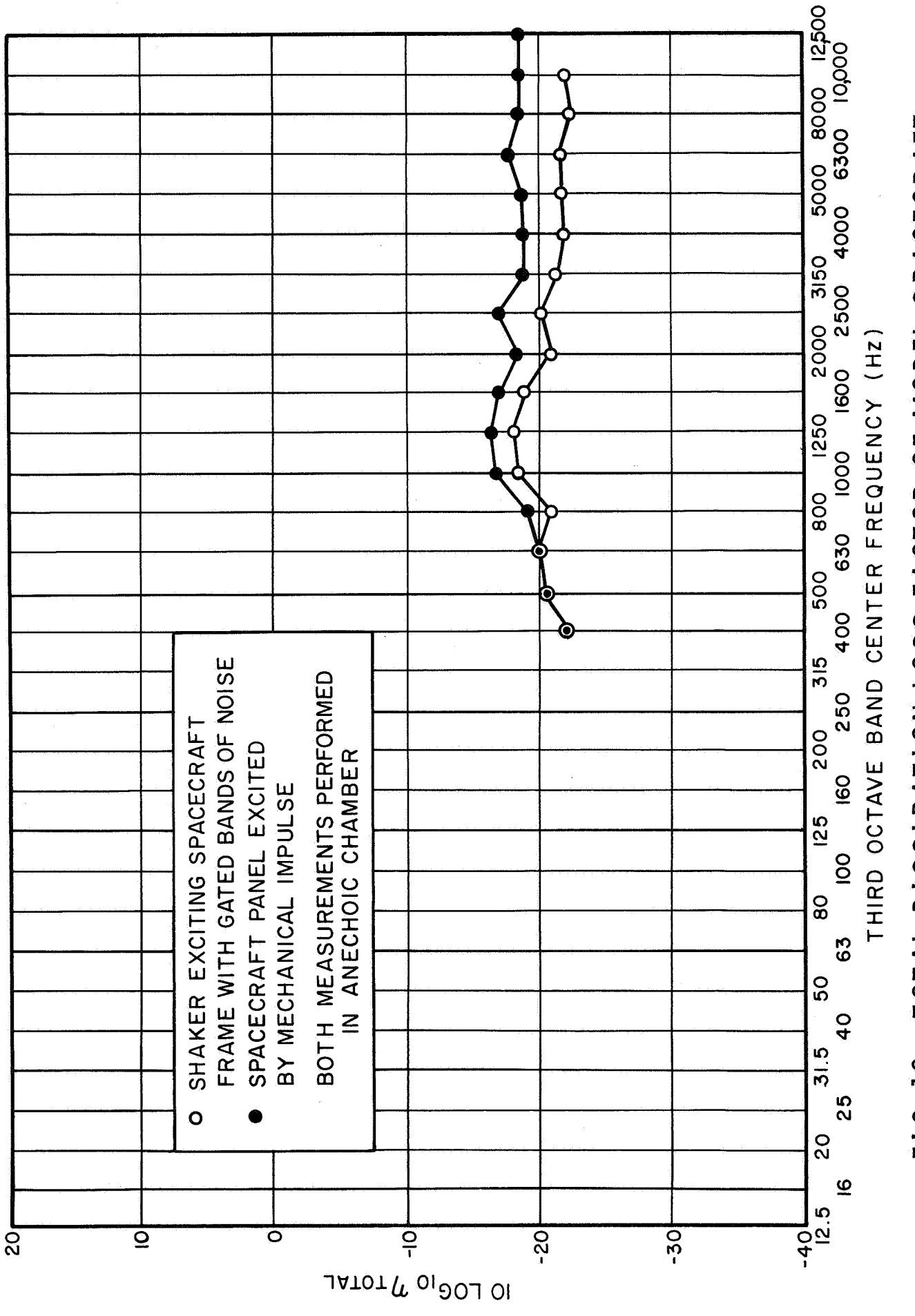

FIG. 18 TOTAL DISSIPATION LOSS FACTOR OF MODEL SPACECRAFT

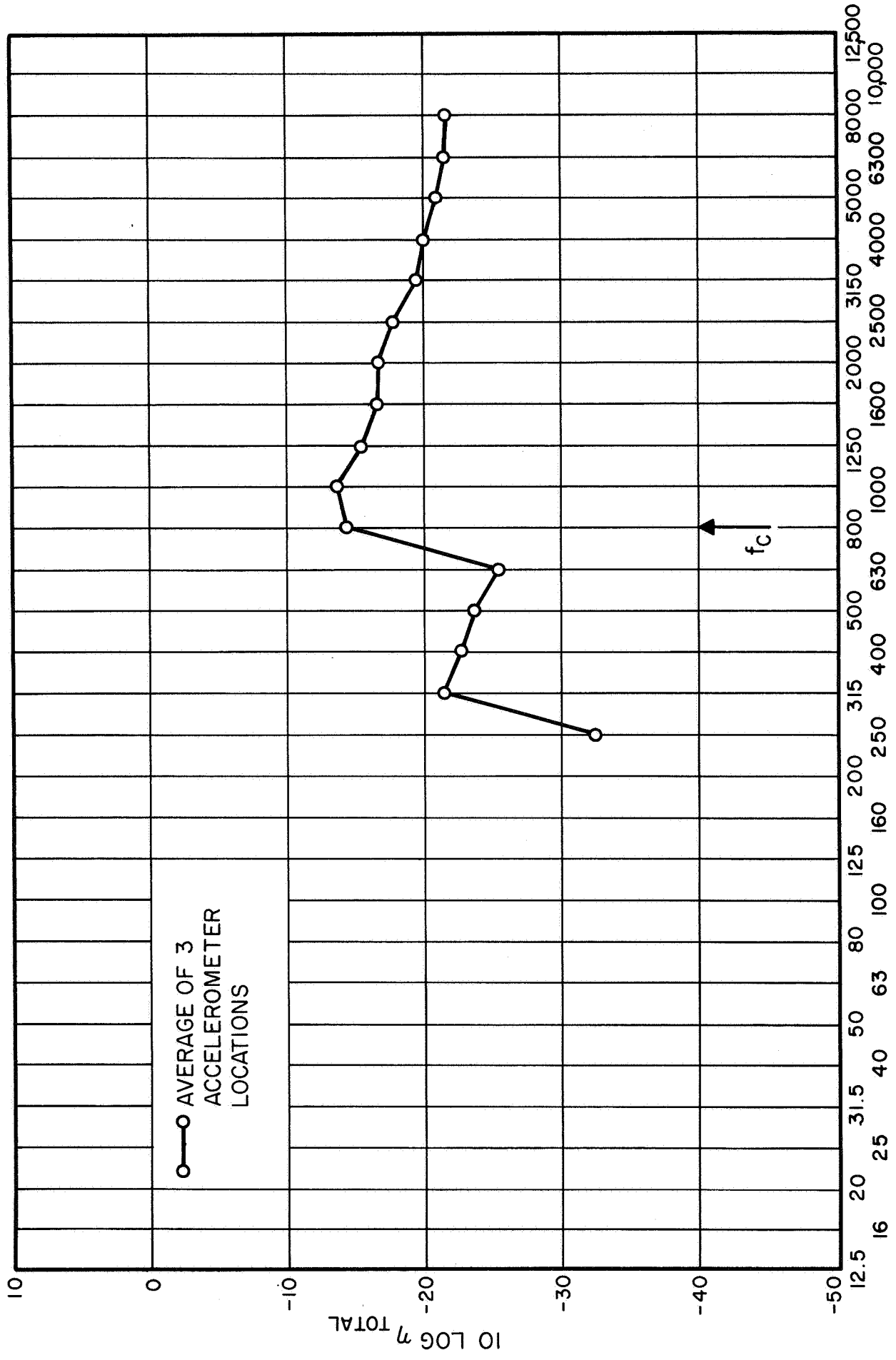

FIG. 19 TOTAL LOSS FACTOR OF SINGLE UNBAFFLED PANEL

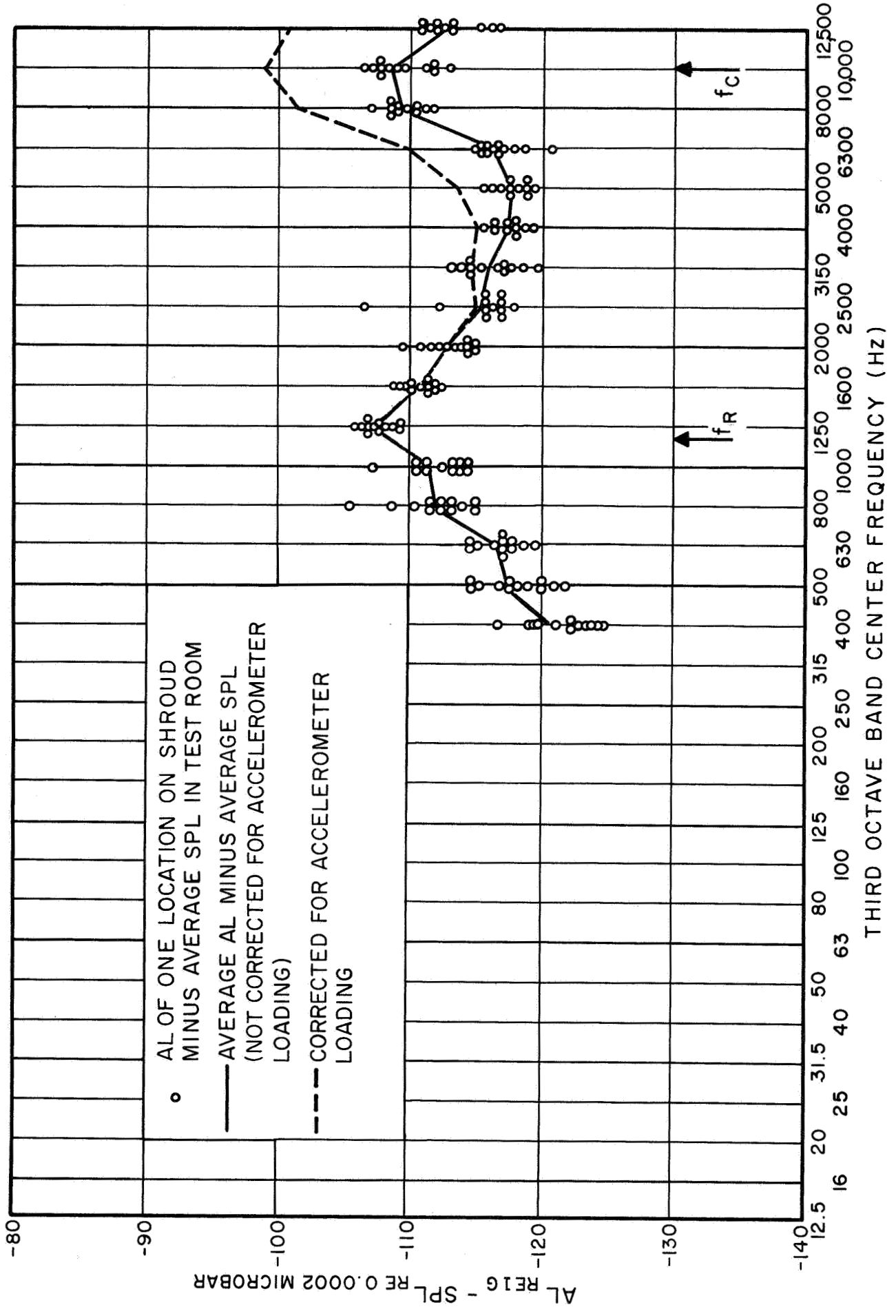

FIG. 20 RESPONSE OF MODEL SHROUD TO ACOUSTIC EXCITATION

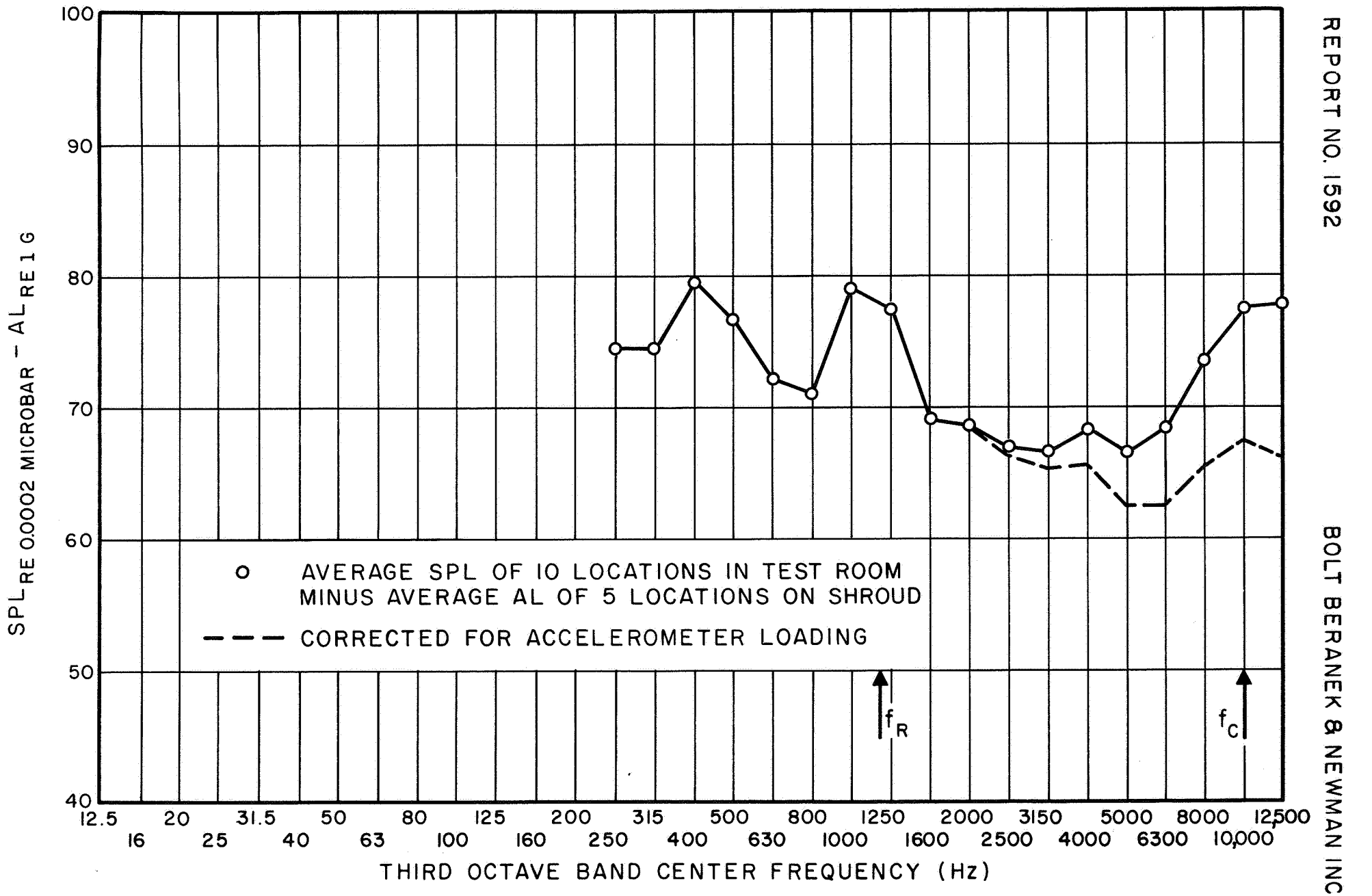

FIG. 21 RADIATION BY MODEL SHROUD WHEN EXCITED MECHANICALLY

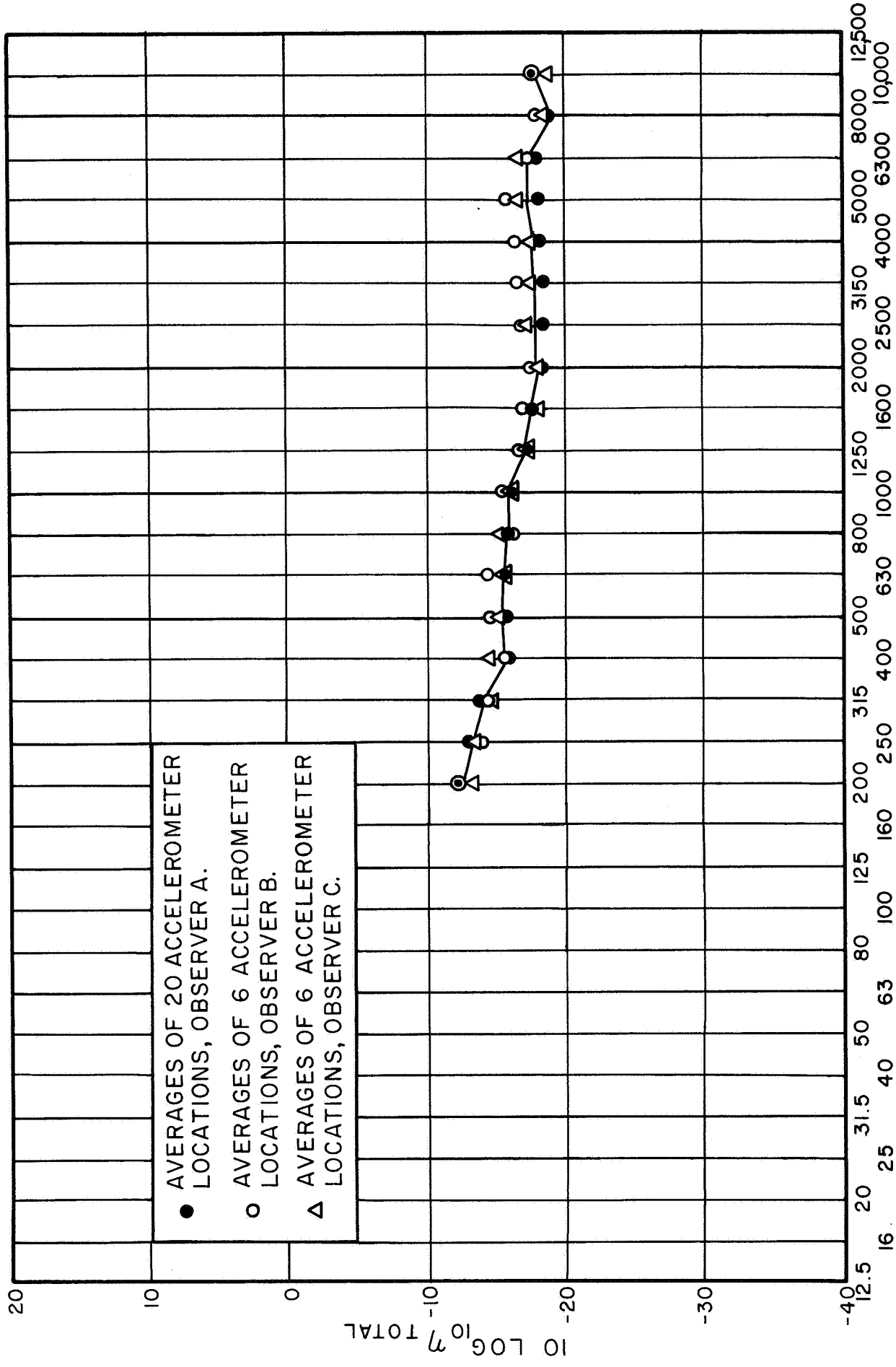

FIG. 22 TOTAL DISSIPATION LOSS FACTOR OF MODEL SHROUD

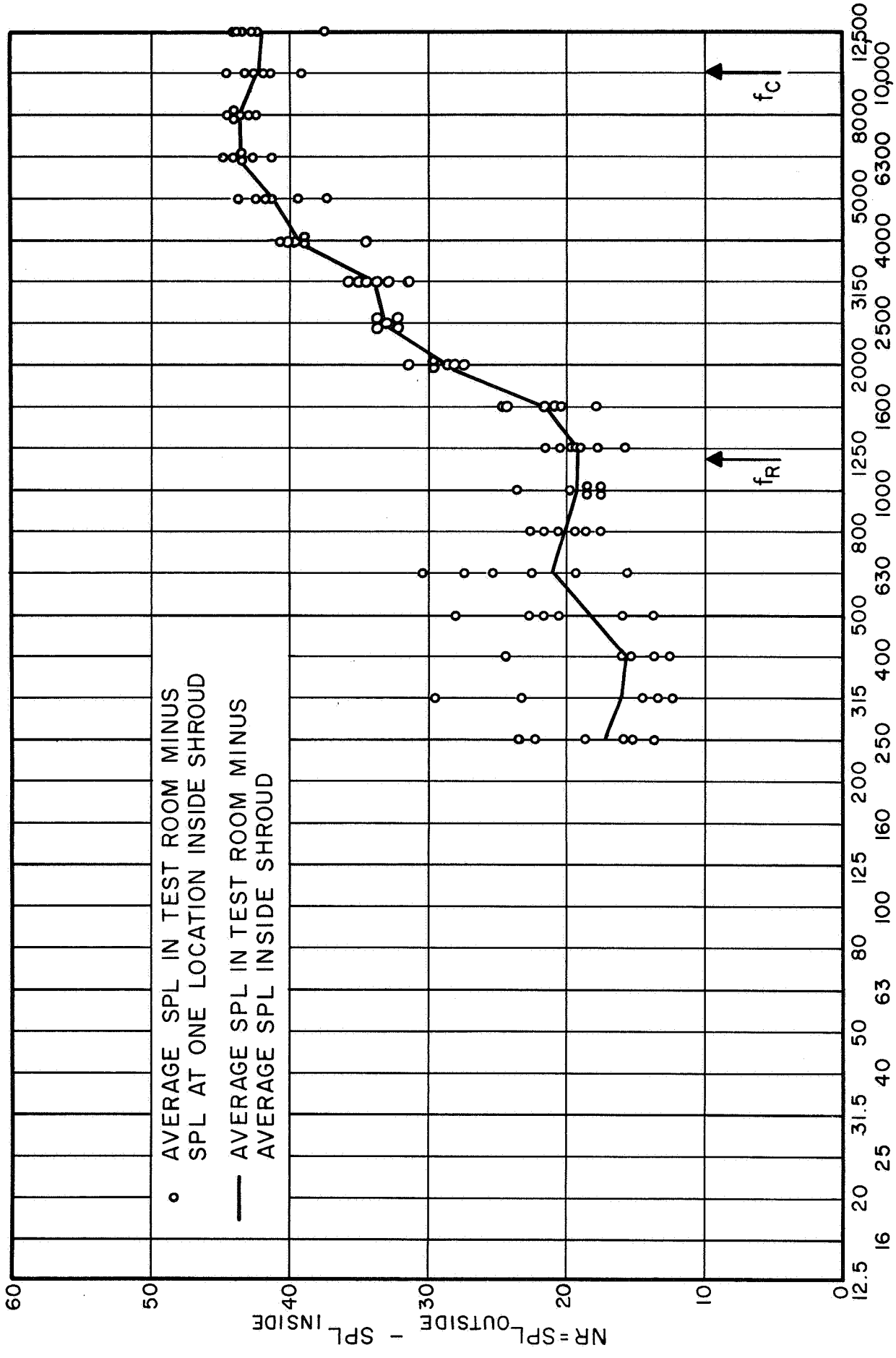

FIG. 23 NOISE REDUCTION BY MODEL SHROUD

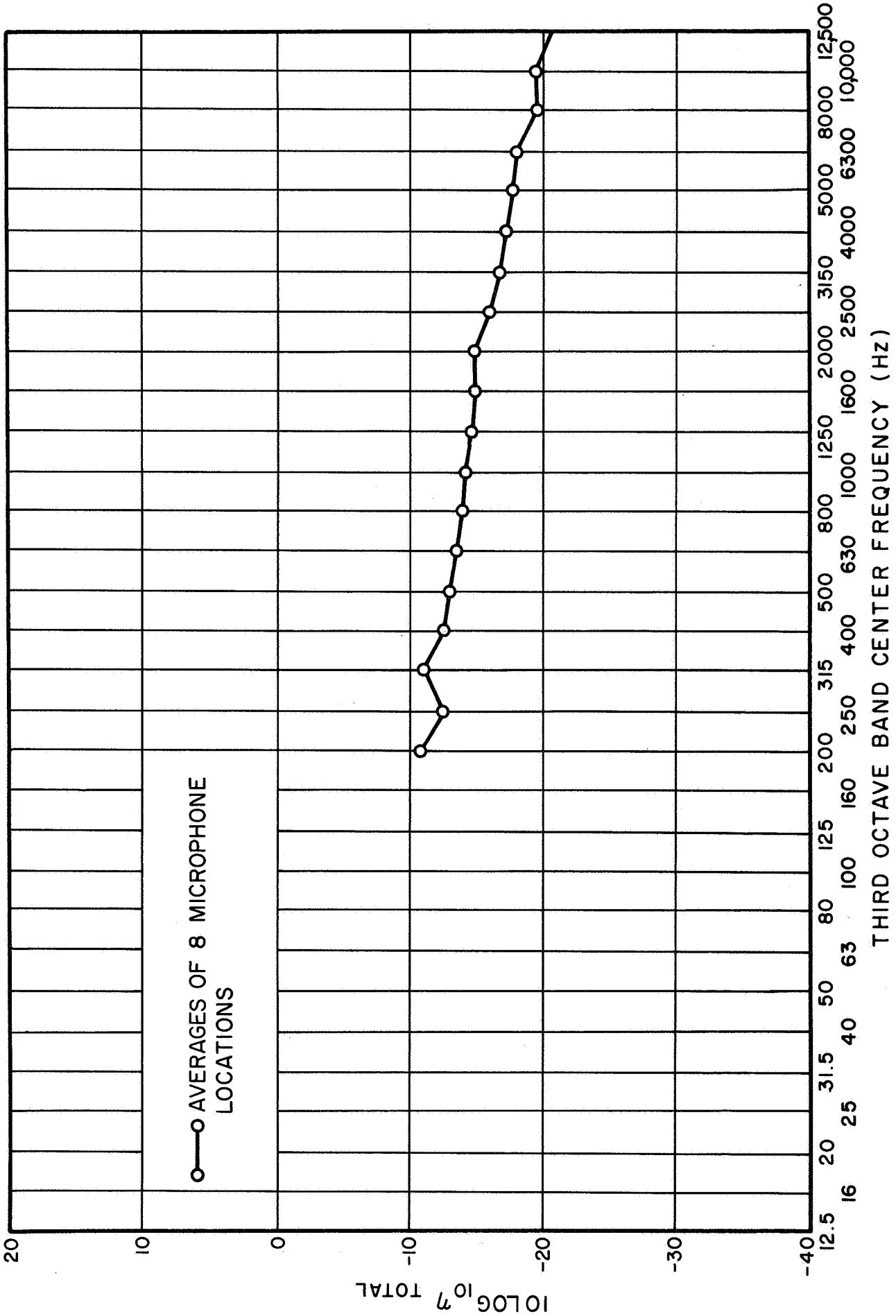

FIG. 24 TOTAL DISSIPATION LOSS FACTOR OF INTERNAL ACOUSTIC SPACE

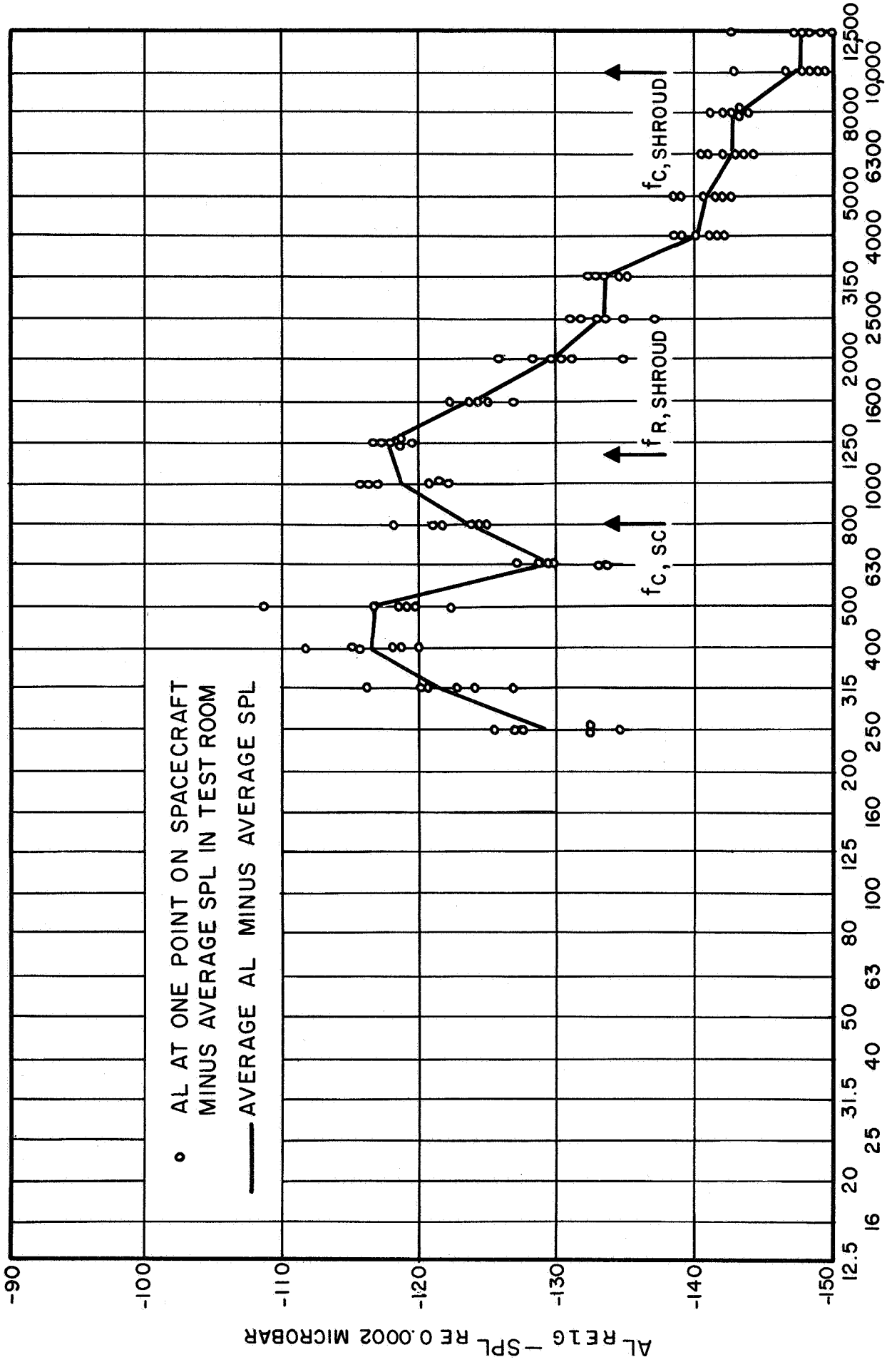

FIG. 25 RESPONSE OF MODEL SPACECRAFT WHEN ENCLOSED IN MODEL-SHROUD - MOUNTING TRUSSES NOT CONNECTED

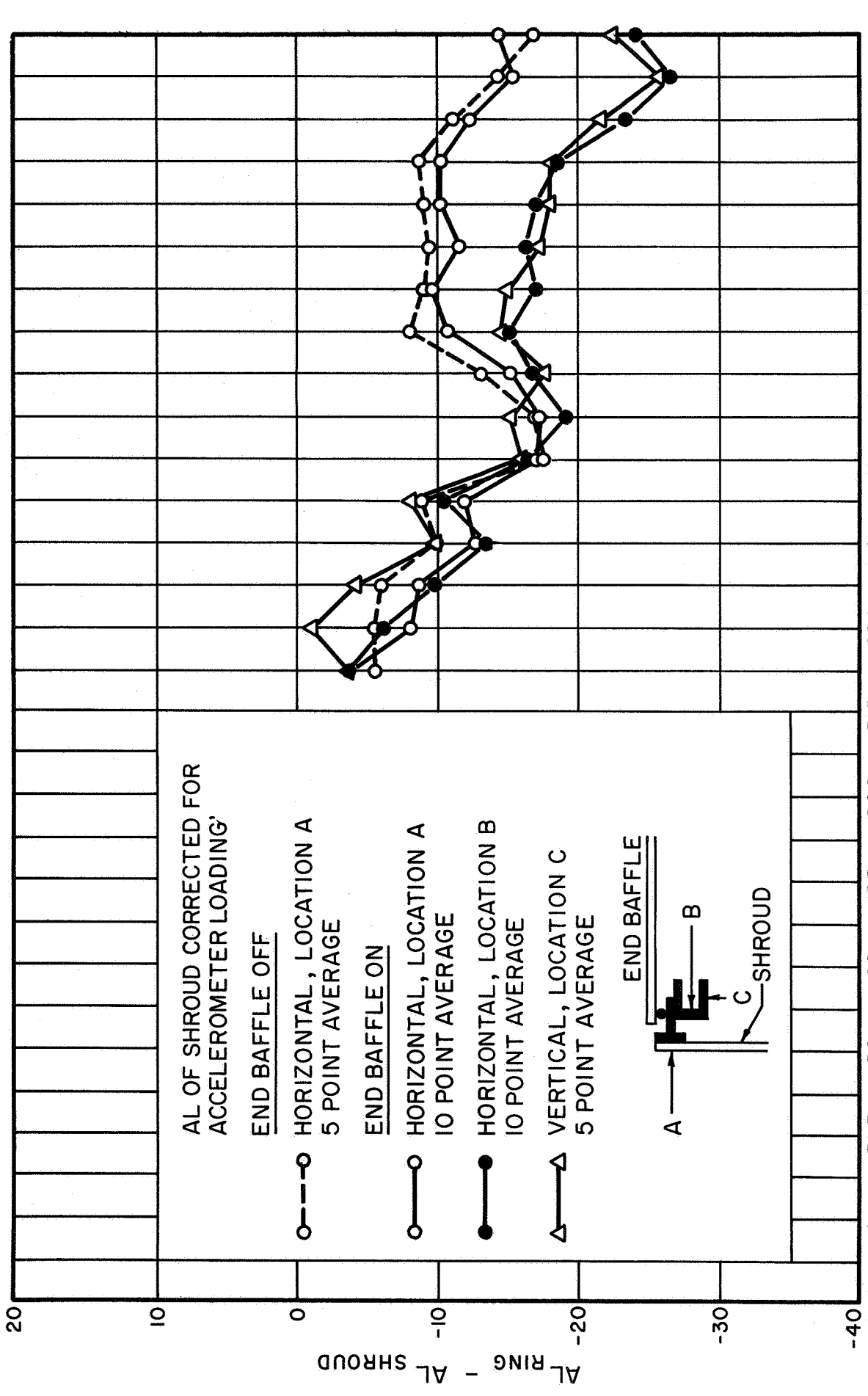

FIG. 26 MODEL-RING-FRAME RESPONSE - SPACECR AFT NOT CONNECTED TO TO MOUNTING TRUSSES

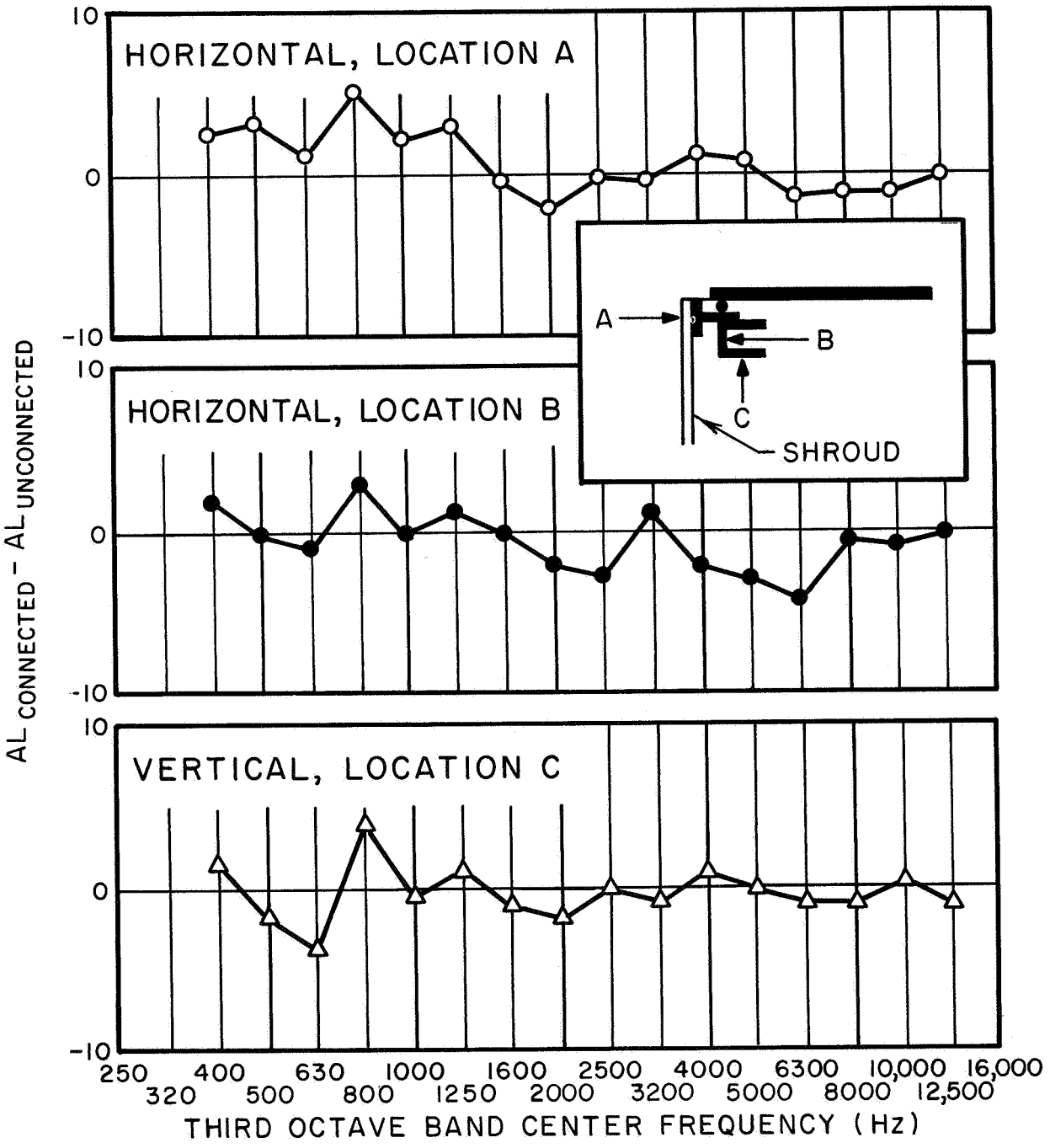

FIG. 27 COMPARISON OF RING FRAME RESPONSES - SPACECRAFT CONNECTED VERSUS SPACECRAFT UNCONNECTED

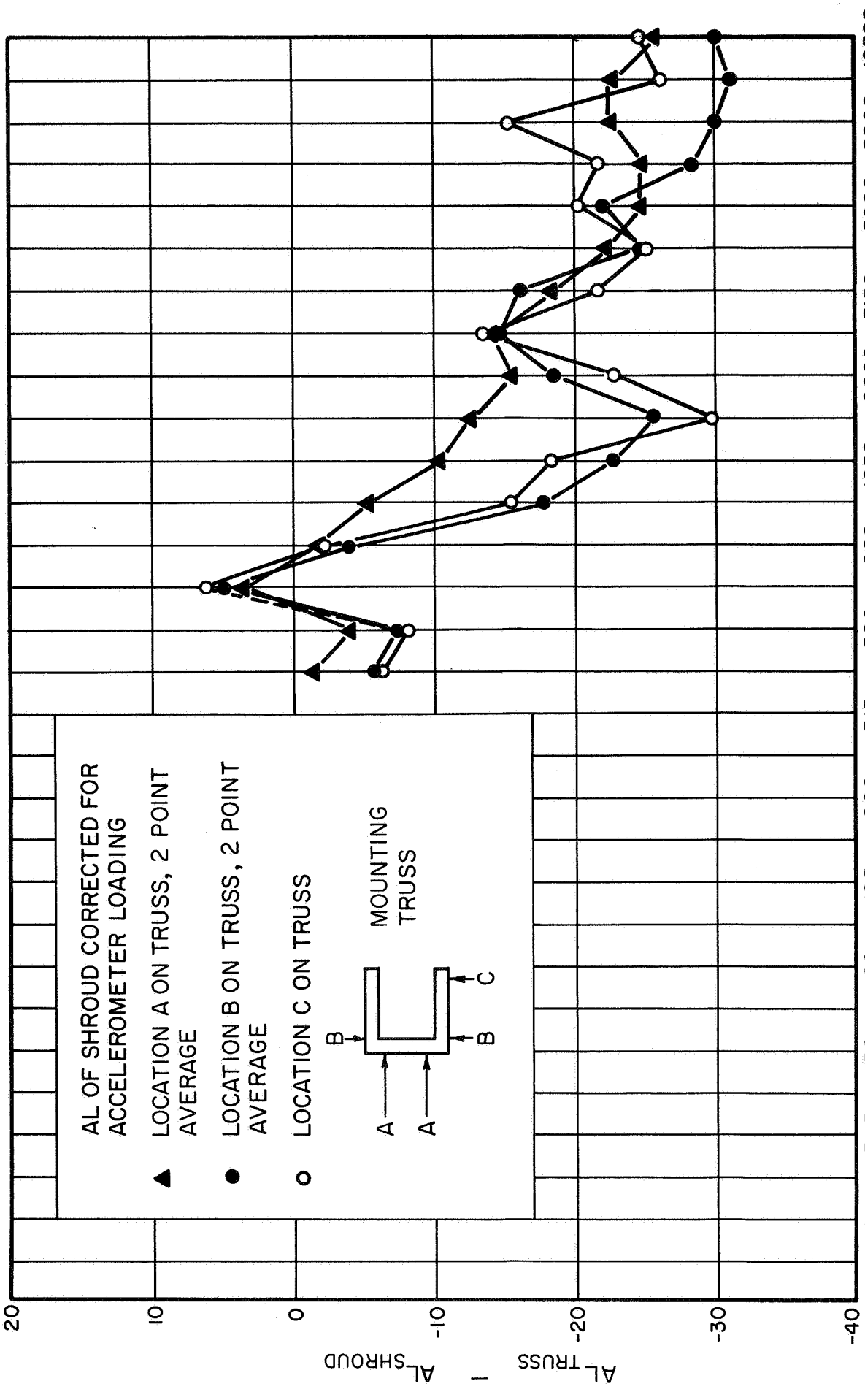

FIG. 28 RESPONSE OF MODEL-MOUNTING-TRUSS NO. 1 - SPACECRAFT CONNECTED

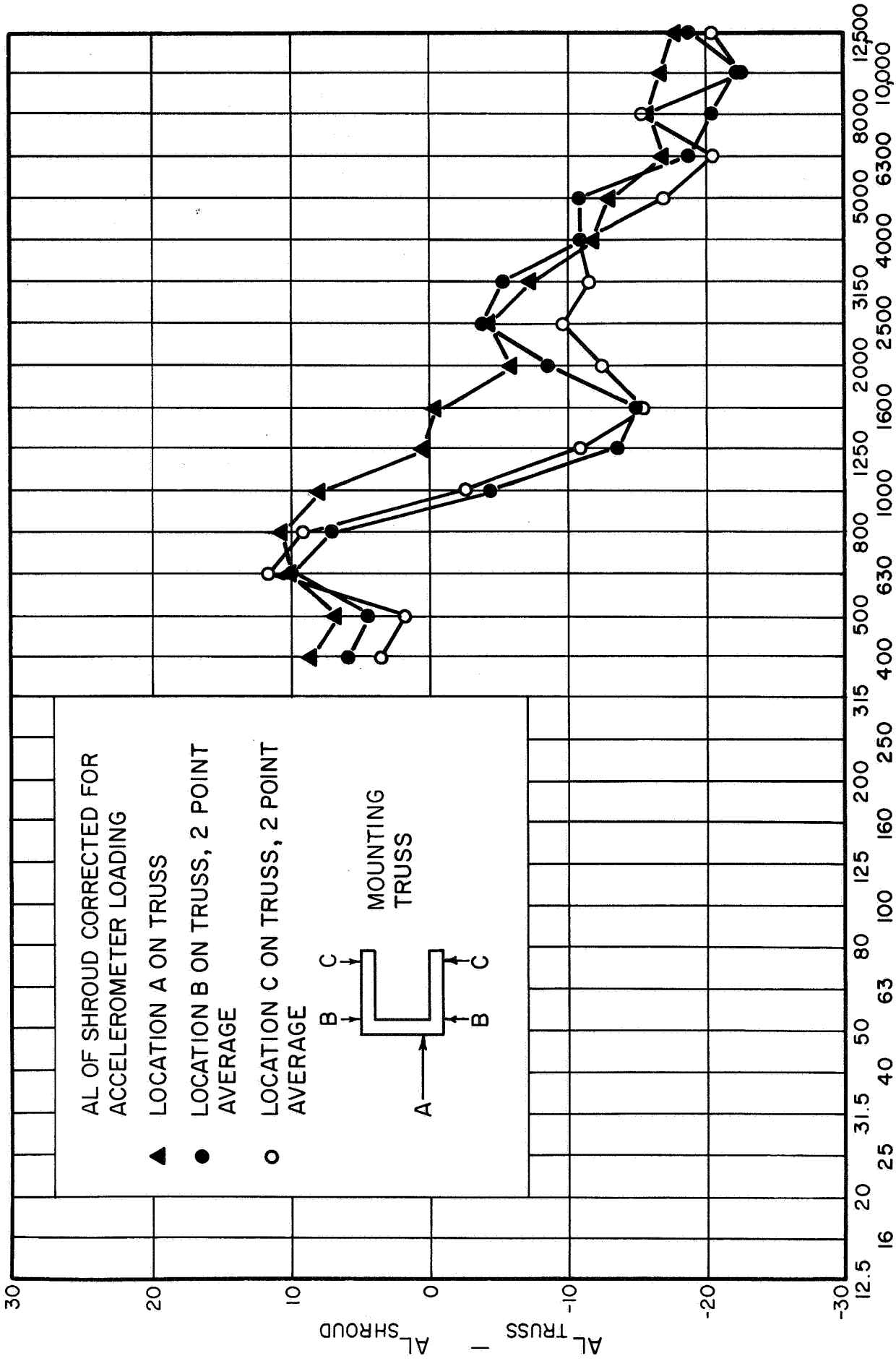

FIG. 29 RESPONSE OF MODEL MOUNTING TRUSS NO. 2 - SPACECRAFT CONNECTED

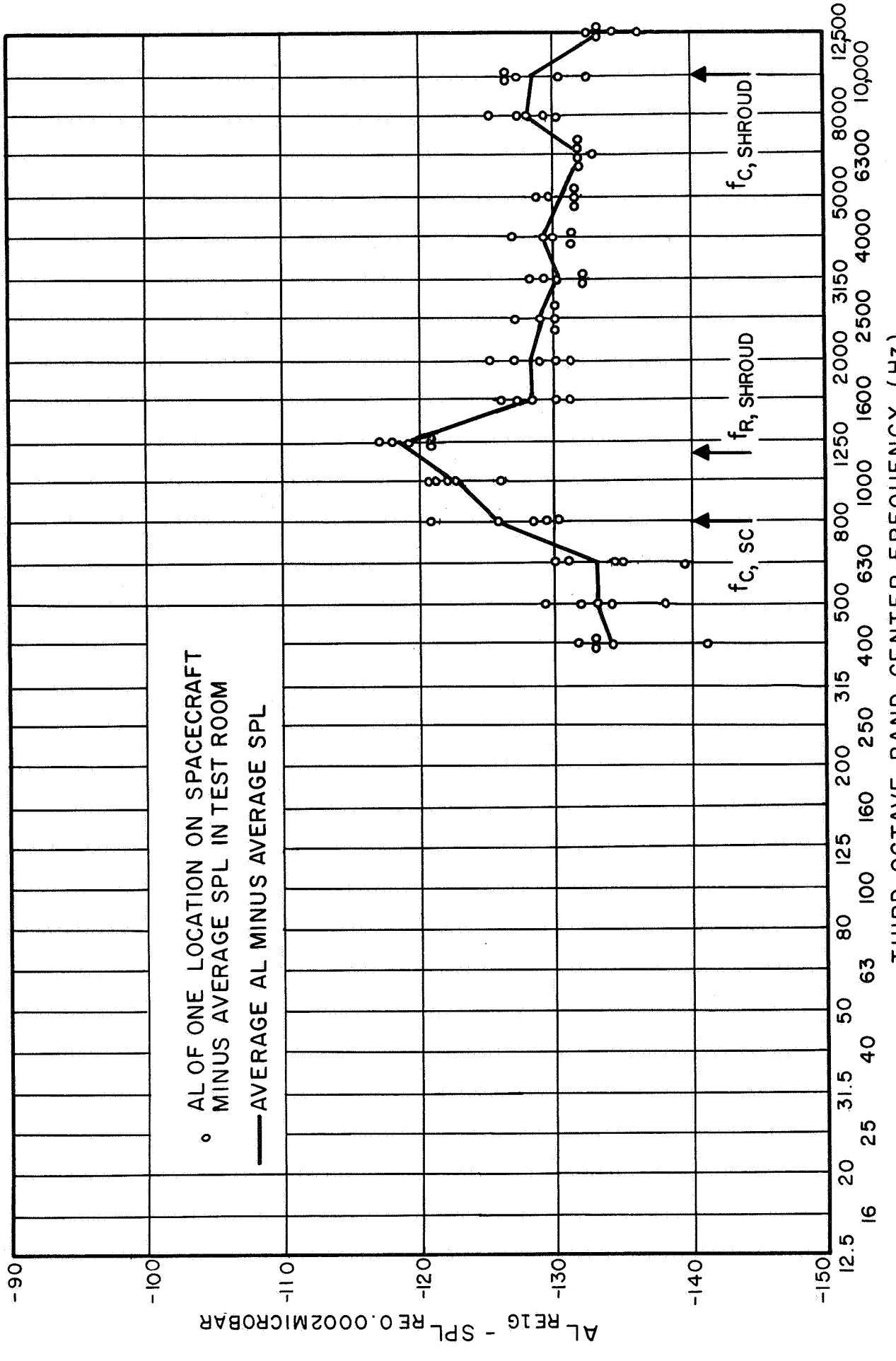

FIG. 30 RESPONSE OF MODEL SPACECRAFT WHEN ENCLOSED IN SHROUD-MECHANICAL PATH TRANSMISSION ONLY

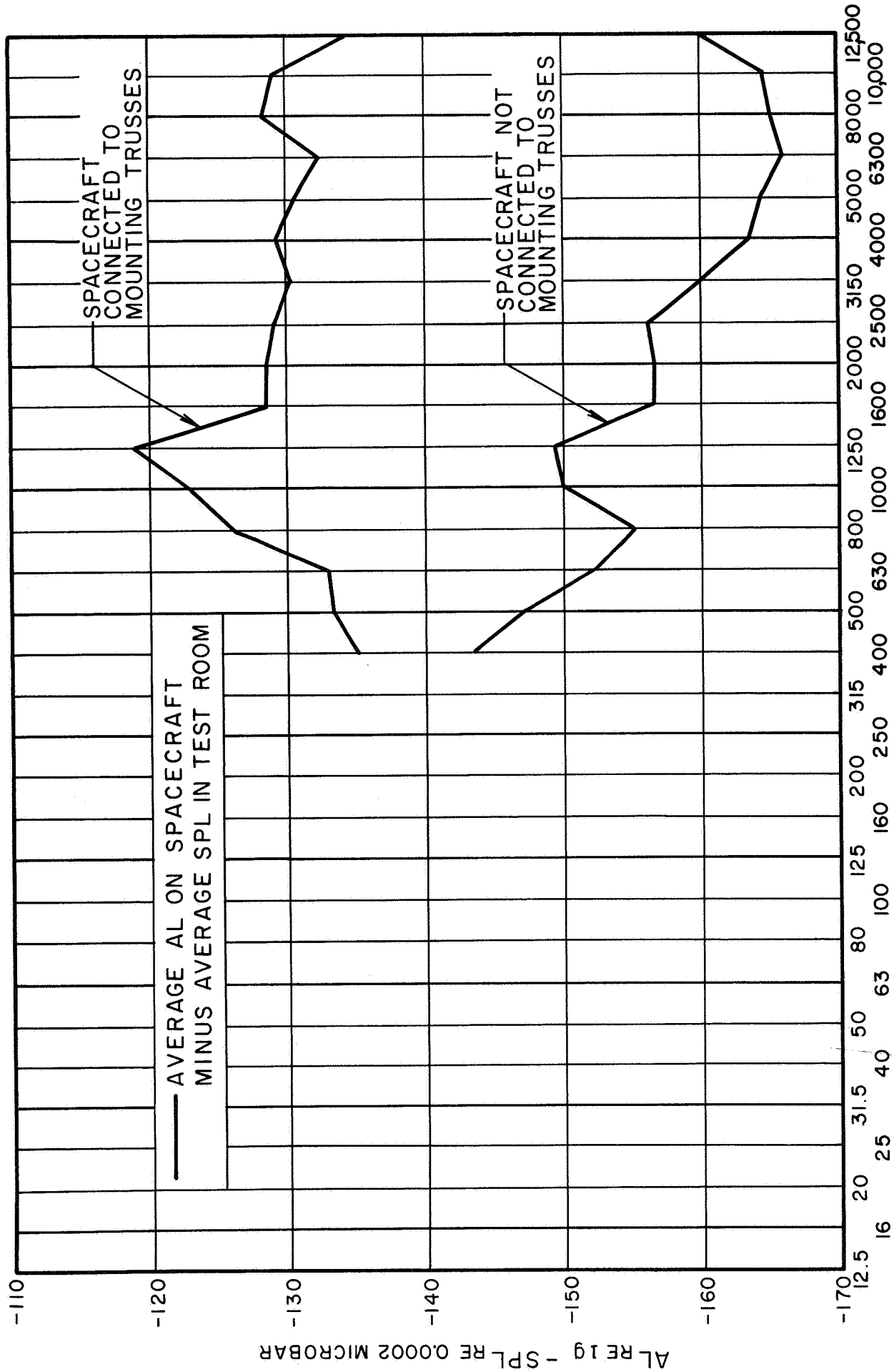

FIG.31 RESPONSE OF MODEL SPACECRAFT WHEN ENCLOSED IN SOUNDPROOF BOX AND SHROUD

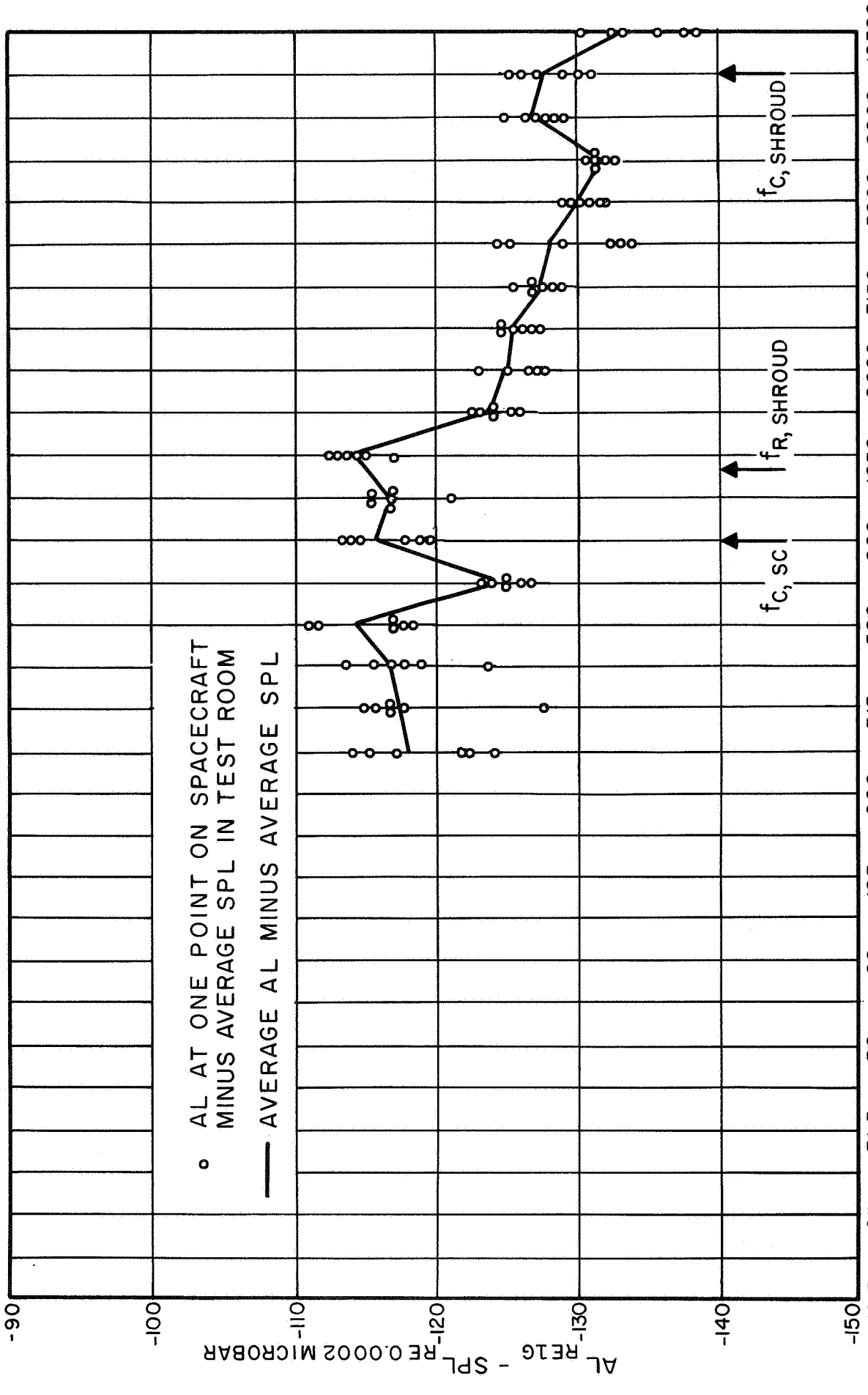

FIG. 32 RESPONSE OF MODEL SPACECRAFT WHEN ENCLOSED IN SHROUD - MOUNTING TRUSSES CONNECTED

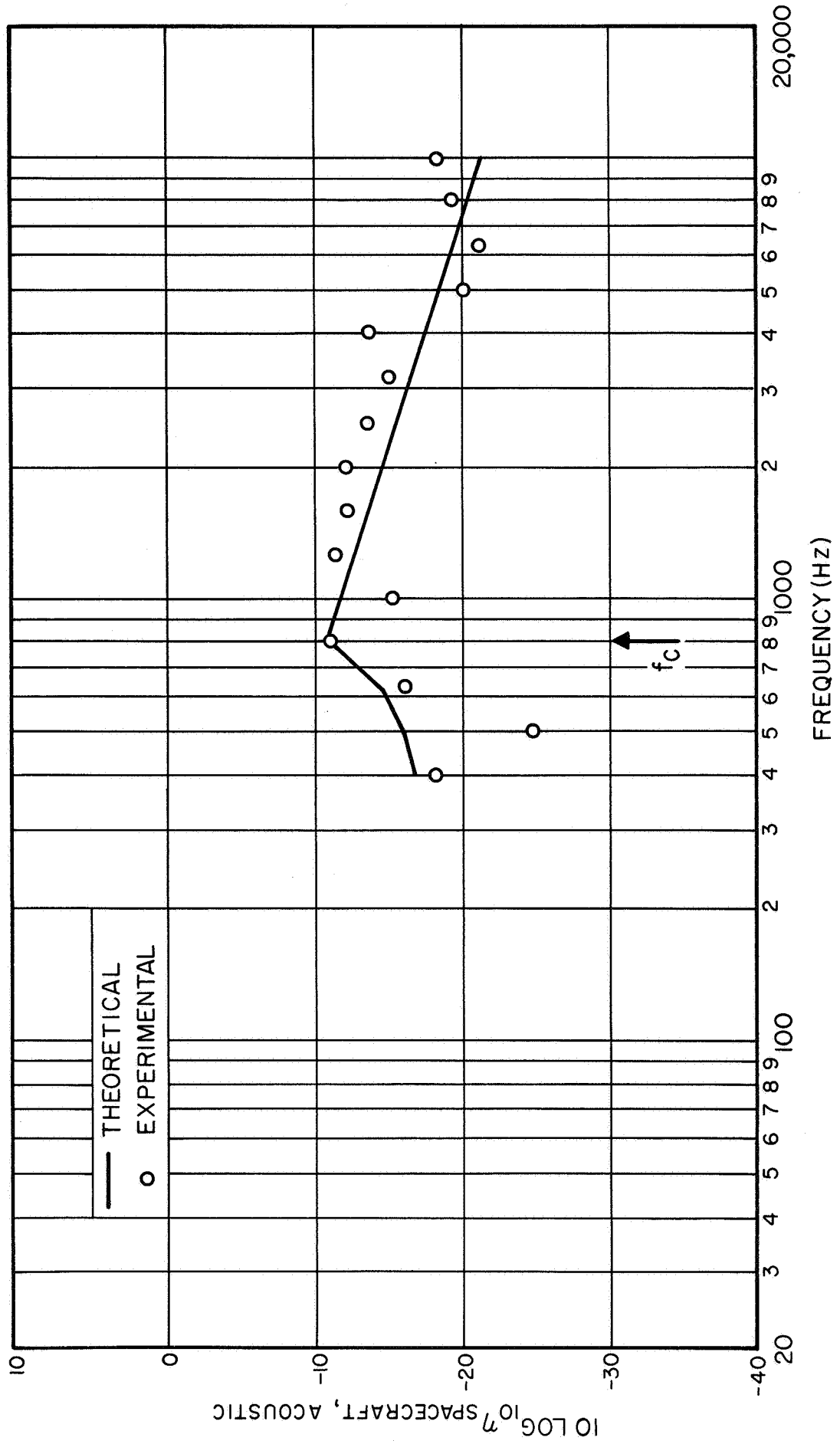

FIG. 33 COUPLING LOSS FACTOR BETWEEN MODEL SPACECRAFT AND ACOUSTIC SPACE

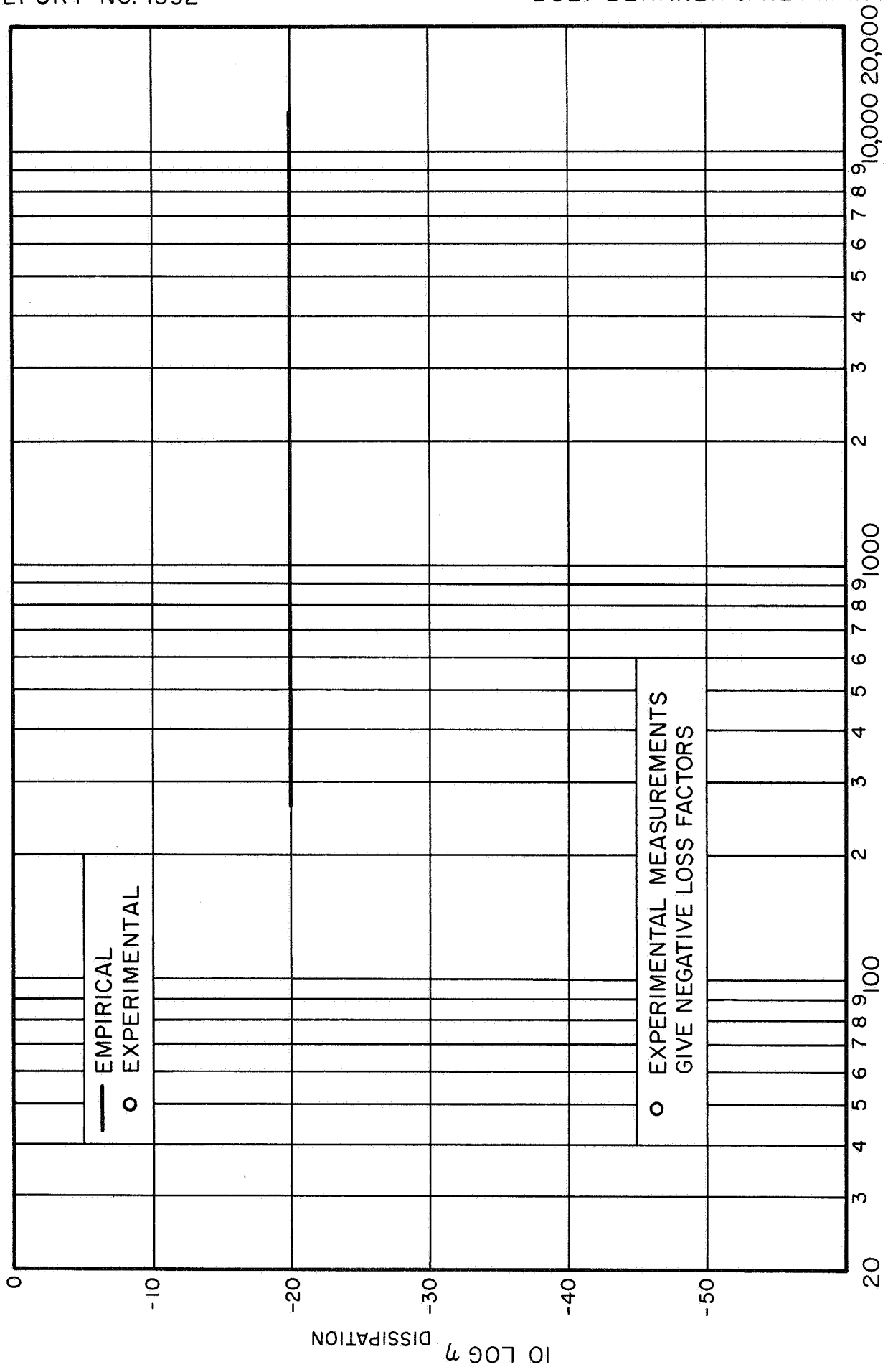

FIG. 34 DISSIPATION LOSS FACTOR OF MODEL SPACECRAFT

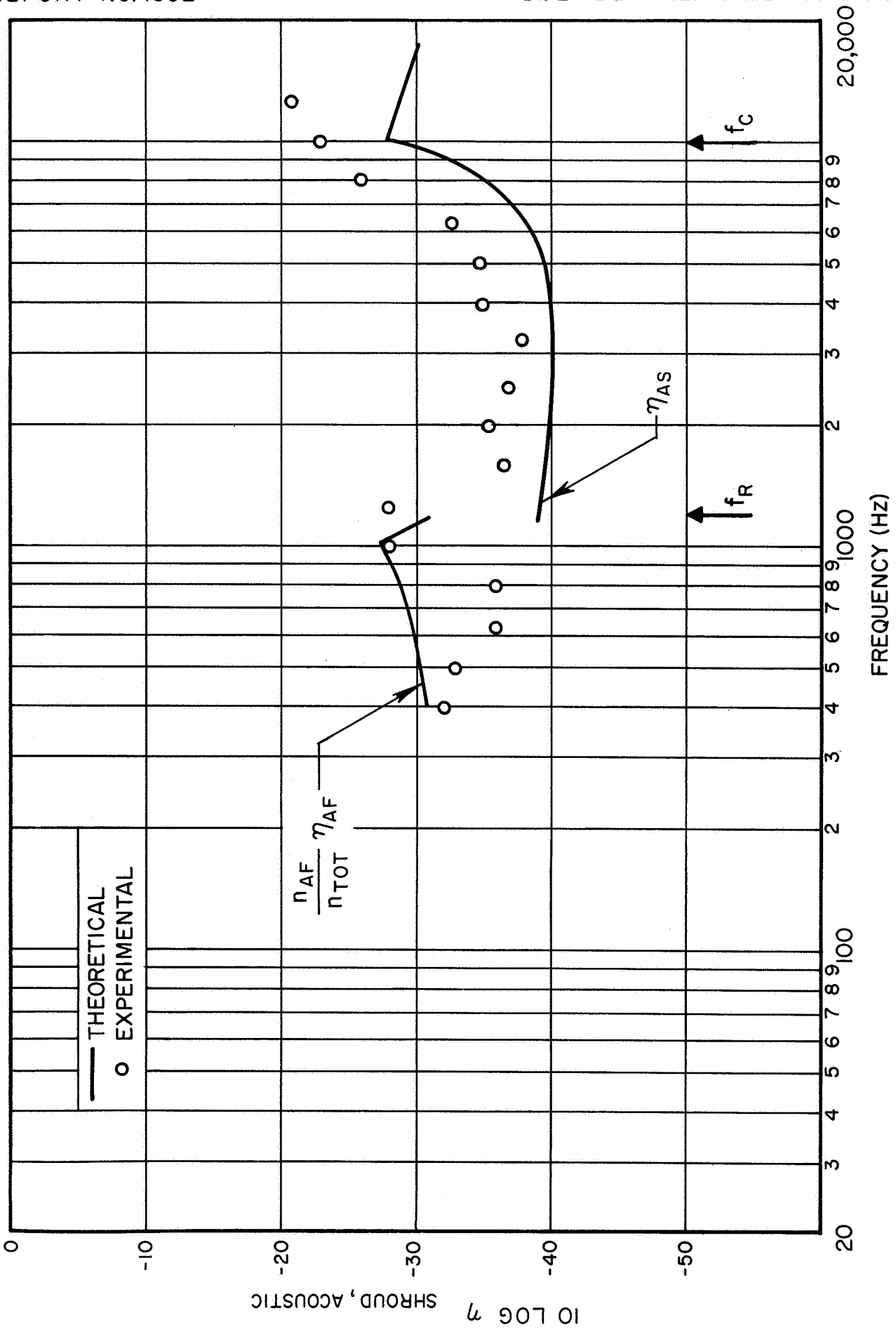

FIG. 35 COUPLING LOSS FACTOR BETWEEN MODEL SHROUD AND ACOUSTIC SPACE

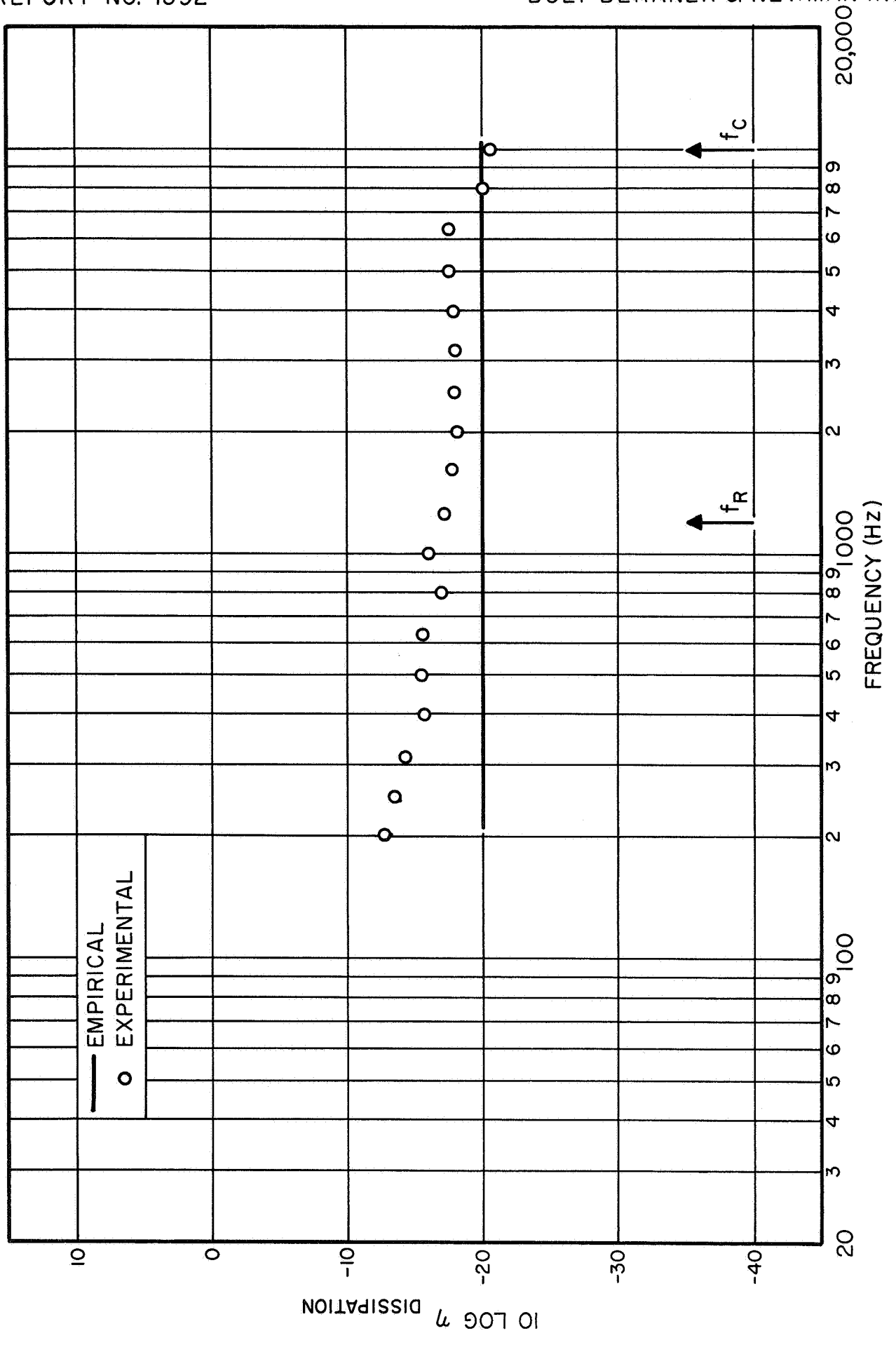

FIG. 36 DISSIPATION LOSS FACTOR OF MODEL SHROUD

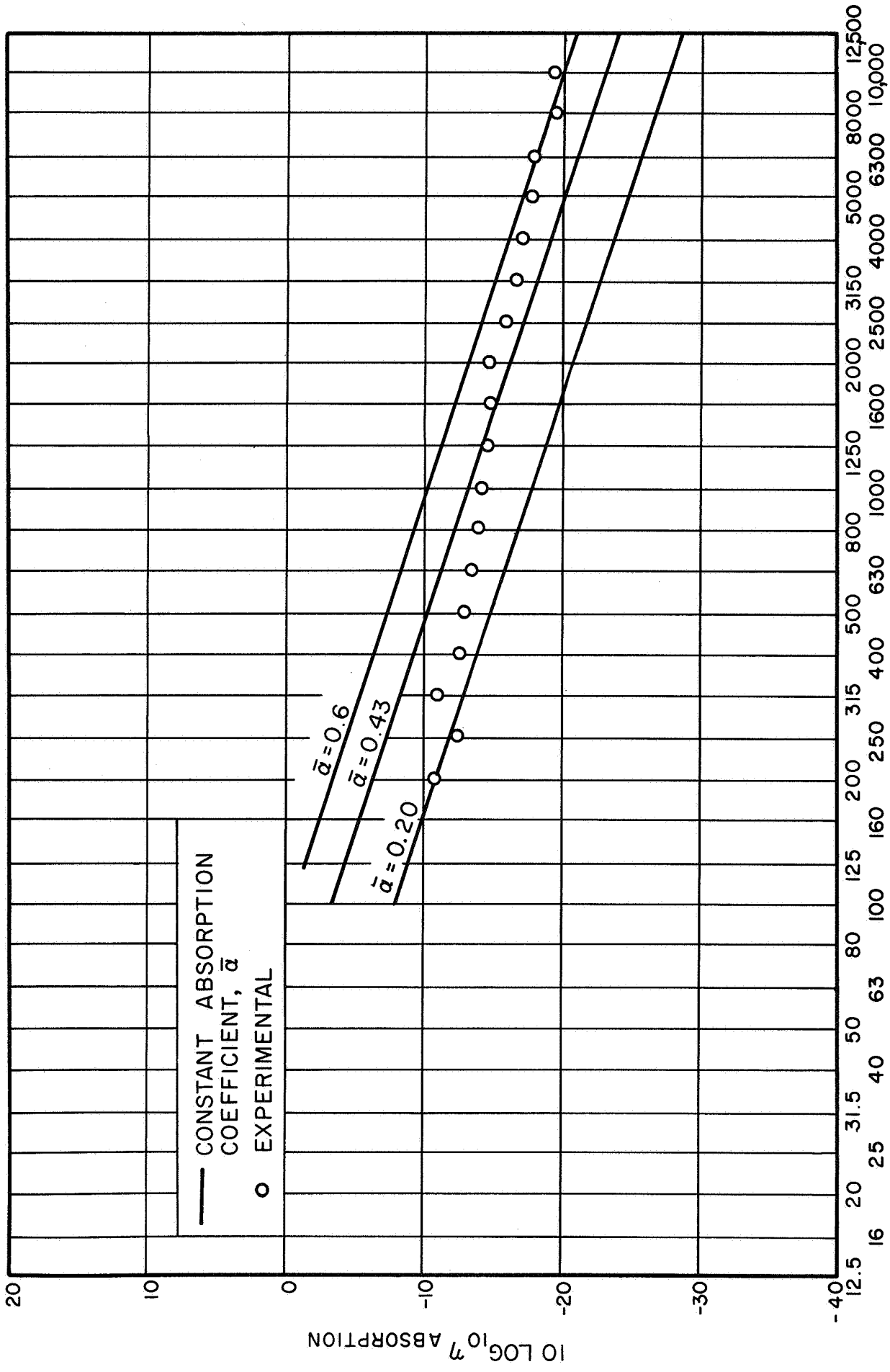

FIG. 37 DISSIPATION LOSS FACTOR OF INTERNAL ACOUSTIC SPACE

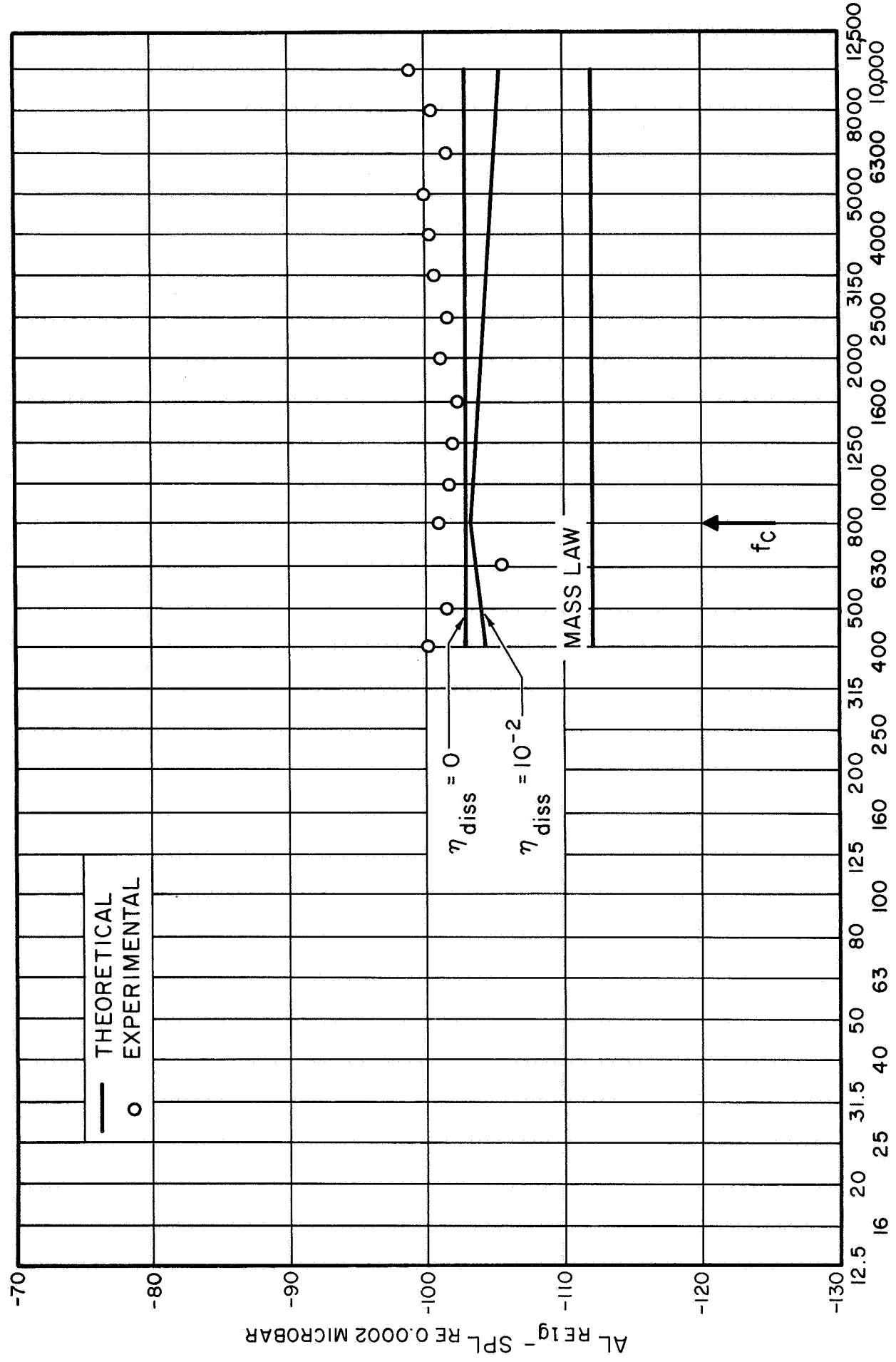

FIG. 38 MODEL SPACECRAFT RESPONSE - COMPARISON OF EXPERIMENT WITH THEORY

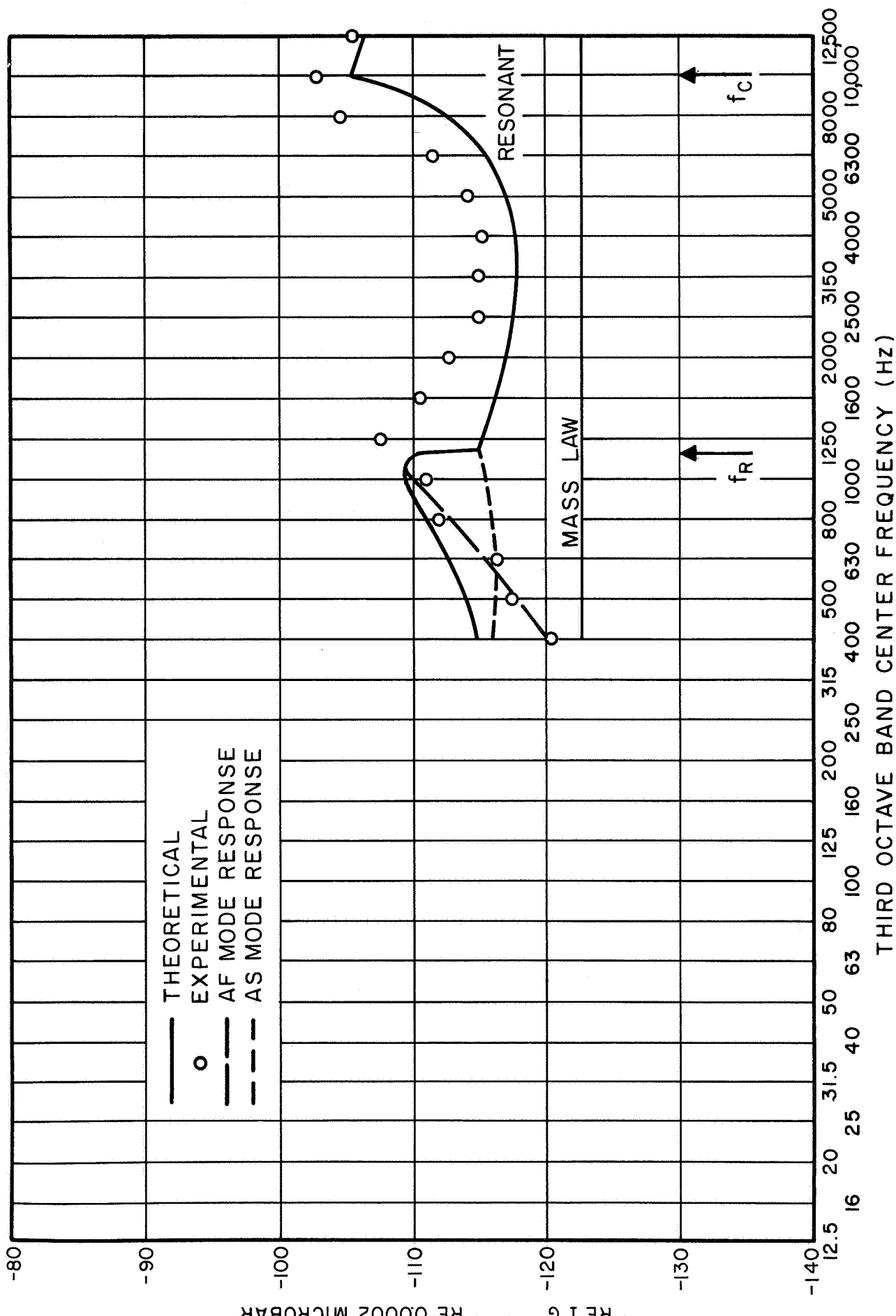

FIG. 39 MODEL SHROUD RESPONSE - COMPARISON OF EXPERIMENT WITH THEORY

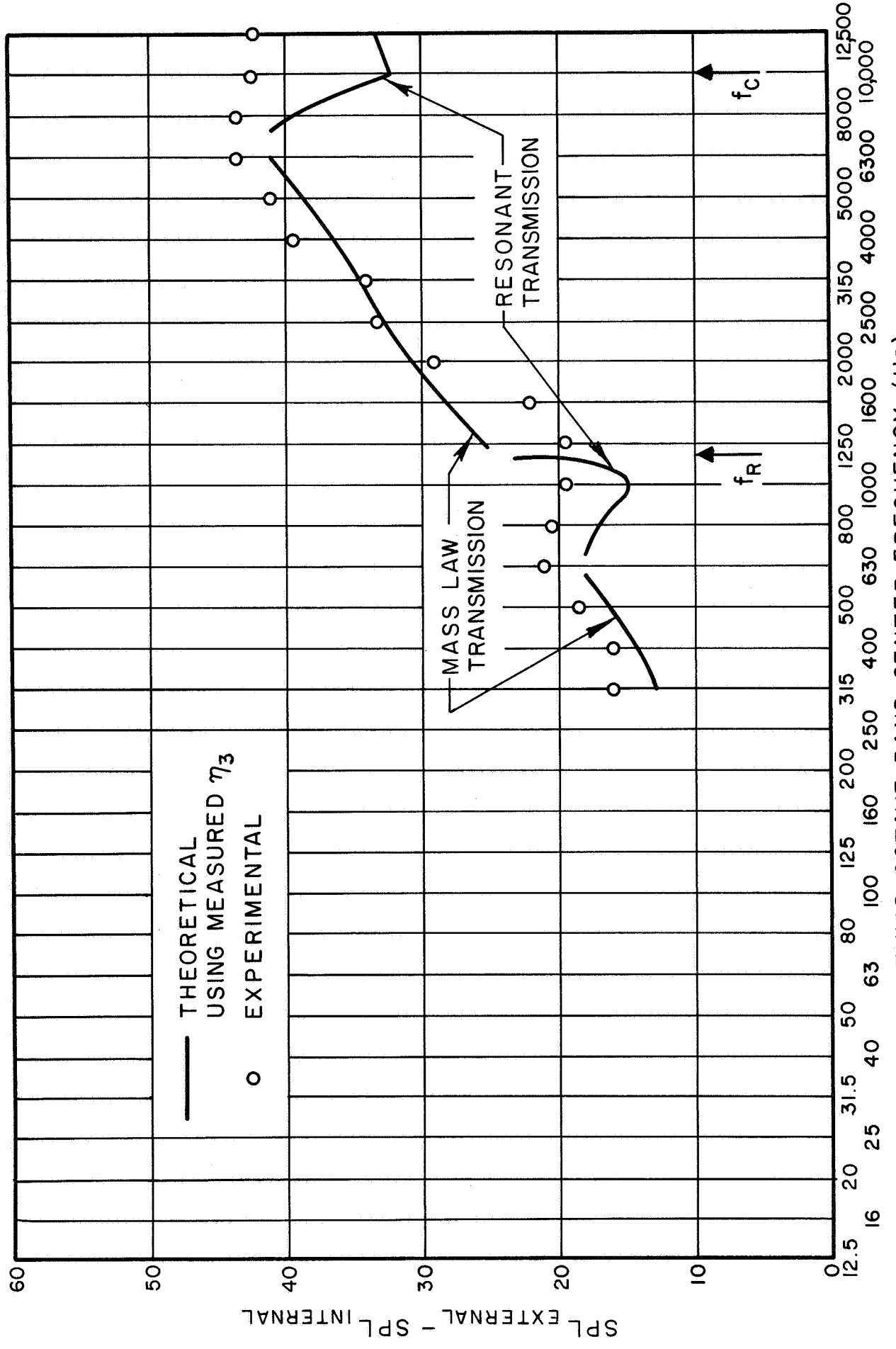

FIG. 40 NOISE REDUCTION BY MODEL SHROUD - COMPARISON OF EXPERIMENT WITH THEORY

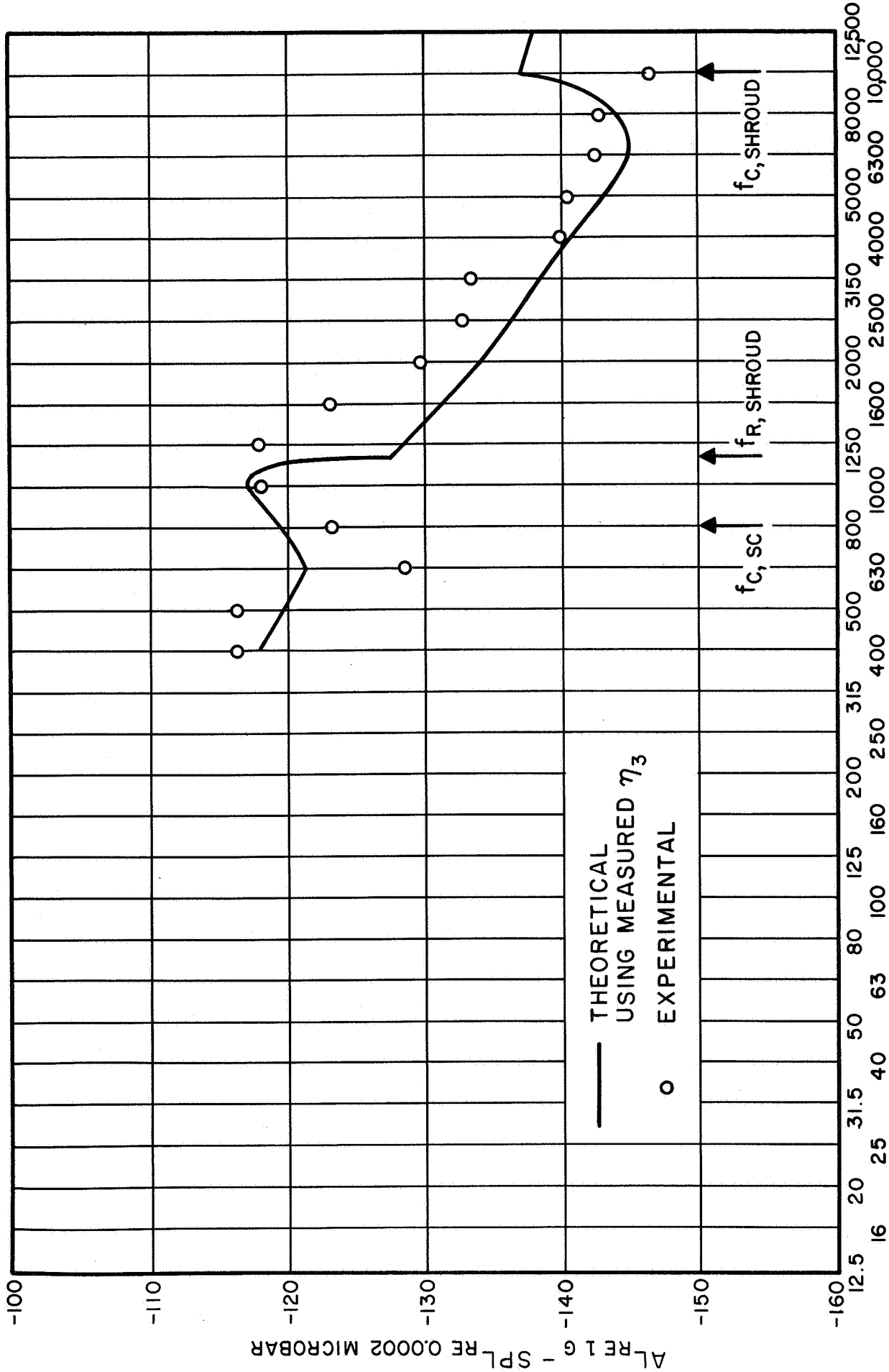

FIG. 41 MODEL SPACECRAFT RESPONSE DUE TO ACOUSTIC TRANSMISSION - COMPARISON OF EXPERIMENT WITH THEORY

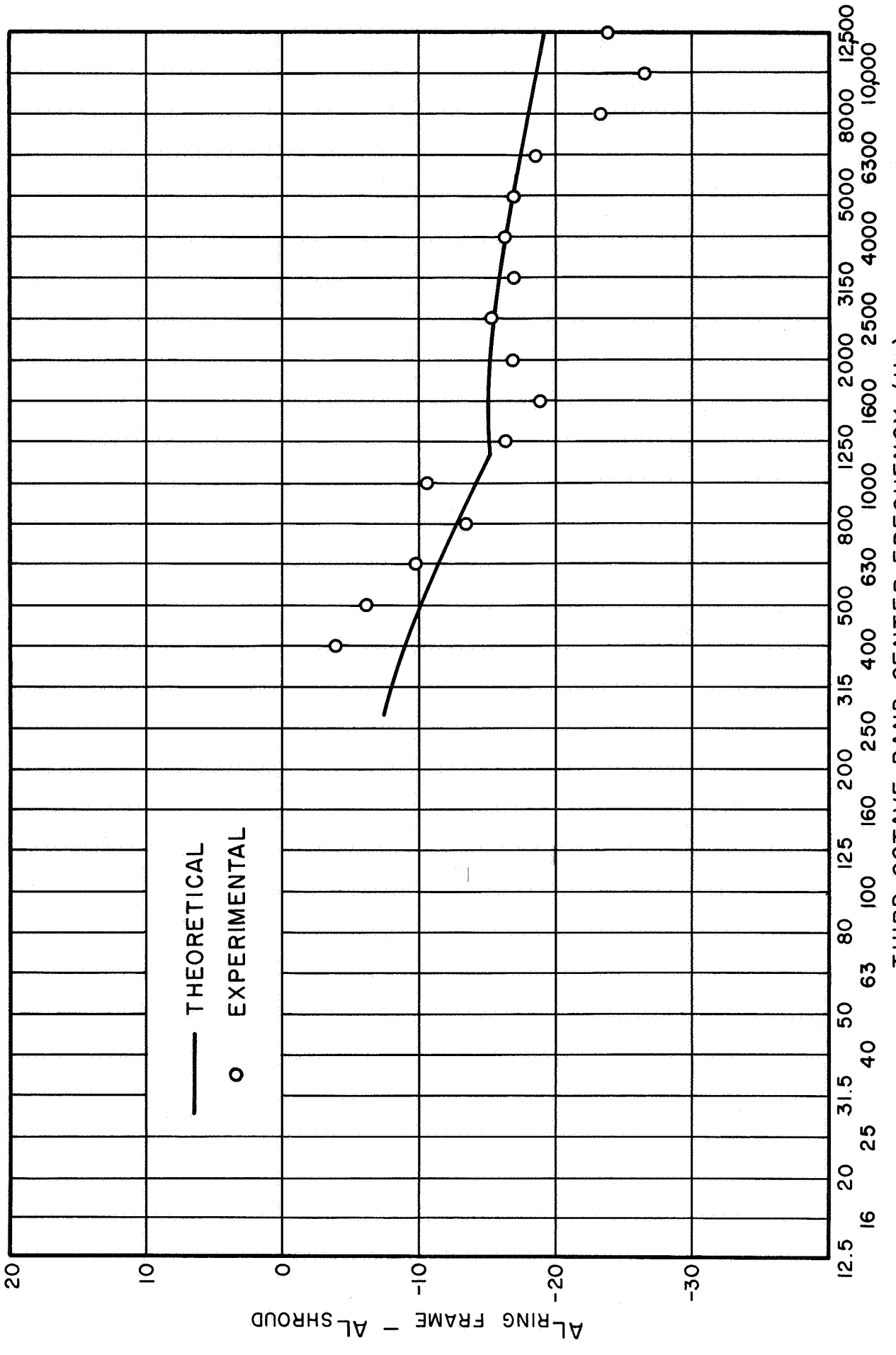

FIG. 42 MODEL RING FRAME RESPONSE — COMPARISON OF EXPERIMENT WITH THEORY

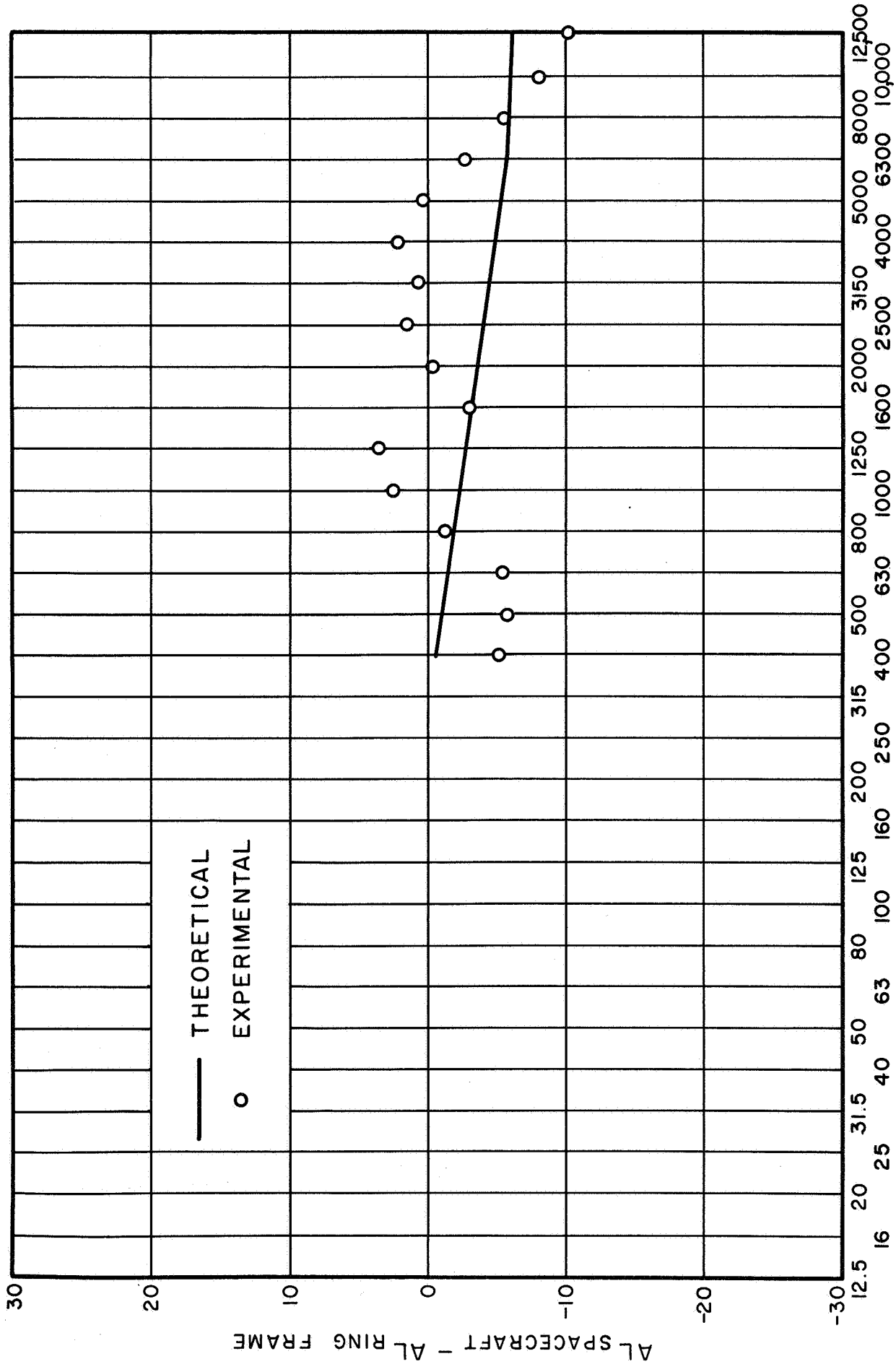

FIG. 43 MODEL SPACECRAFT RESPONSE TO EXCITATION BY RING FRAME – COMPARISON OF EXPERIMENT WITH THEORY

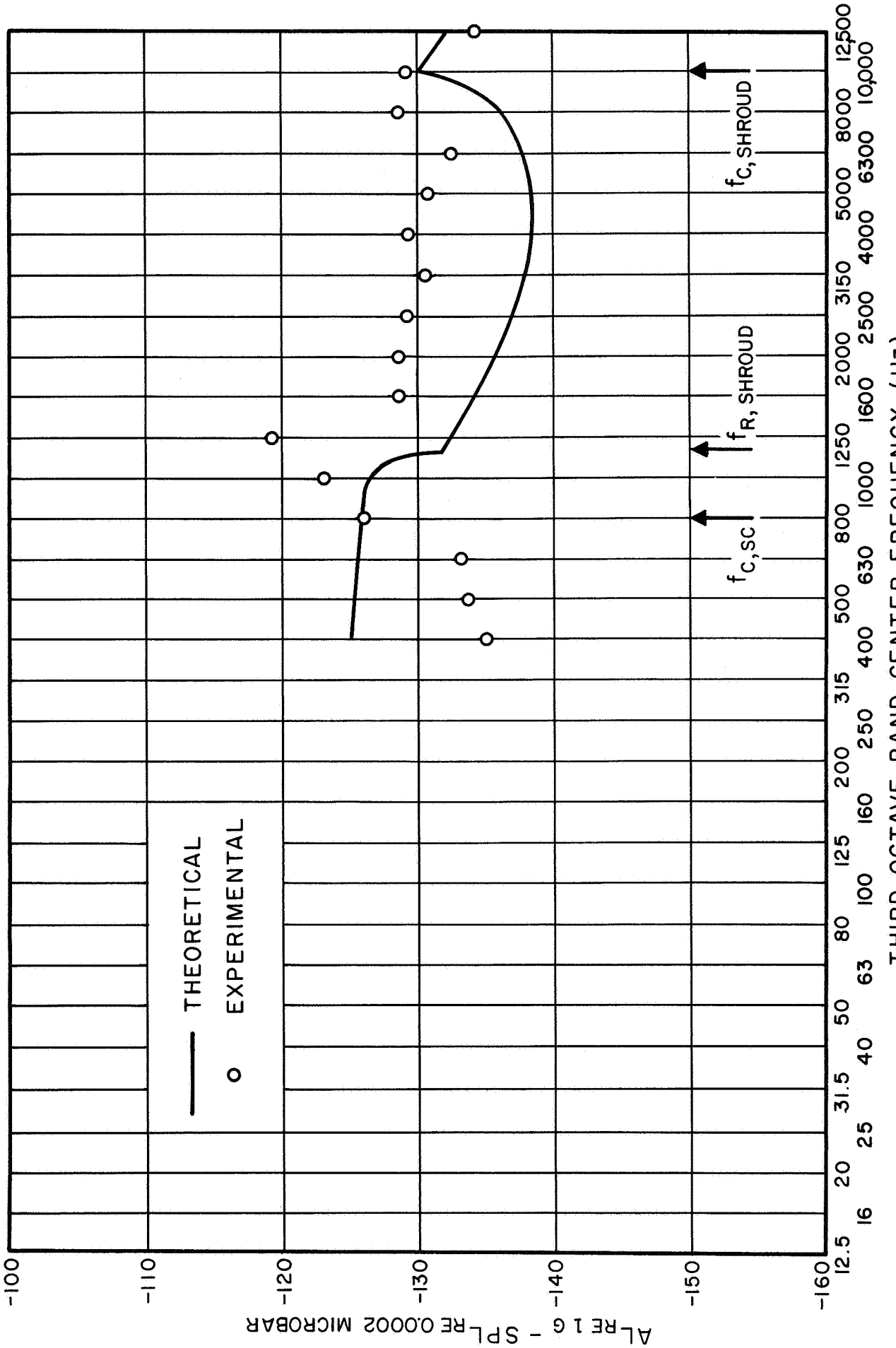

FIG. 44 MODEL SPACECRAFT RESPONSE DUE TO MECHANICAL PATH TRANSMISSION - COMPARISON OF EXPERIMENT WITH THEORY

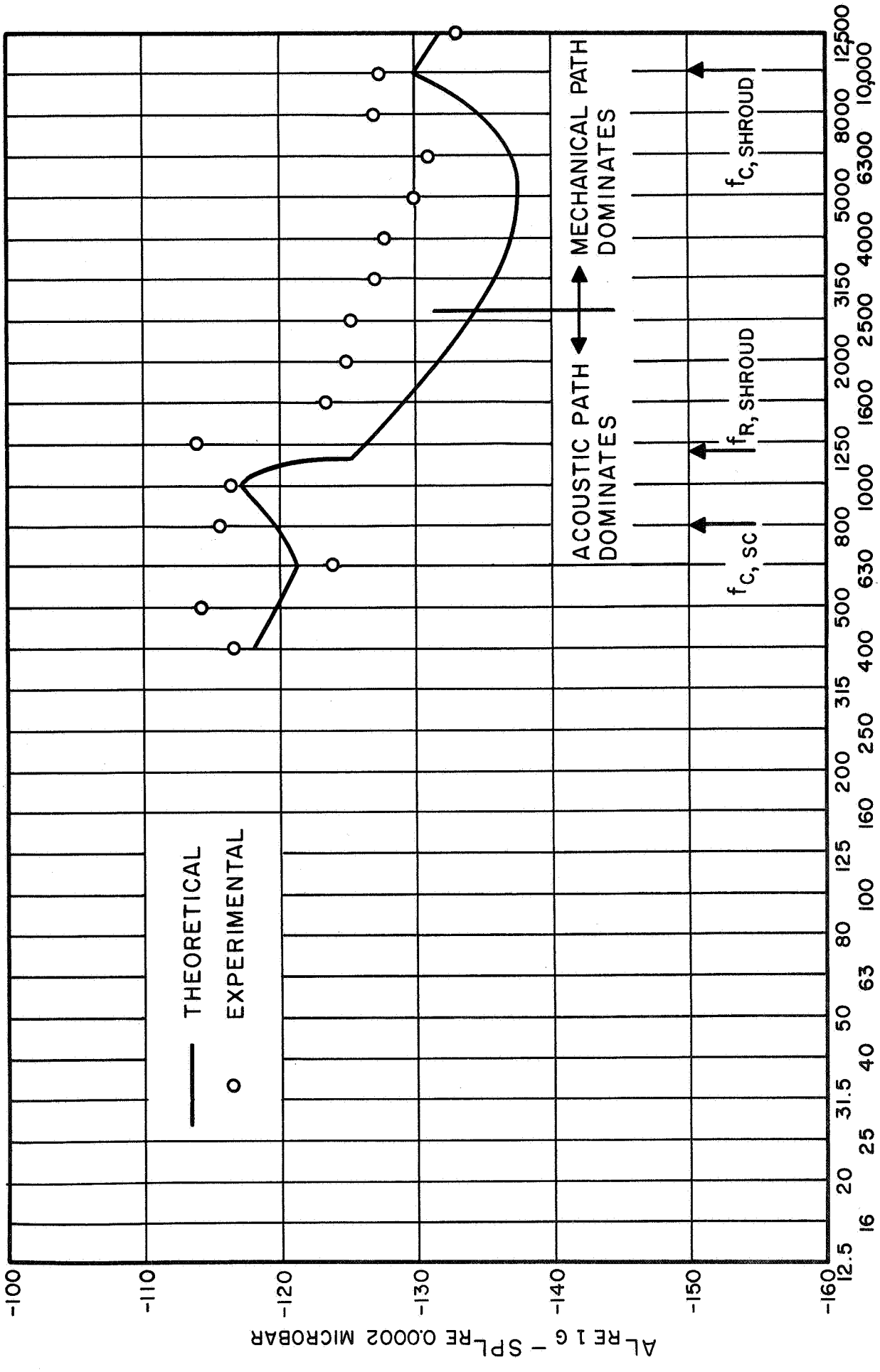

FIG. 45 MODEL SPACECRAFT RESPONSE DUE TO TRANSMISSION BY BOTH PATHS - COMPARISON OF EXPERIMENT WITH THEORY

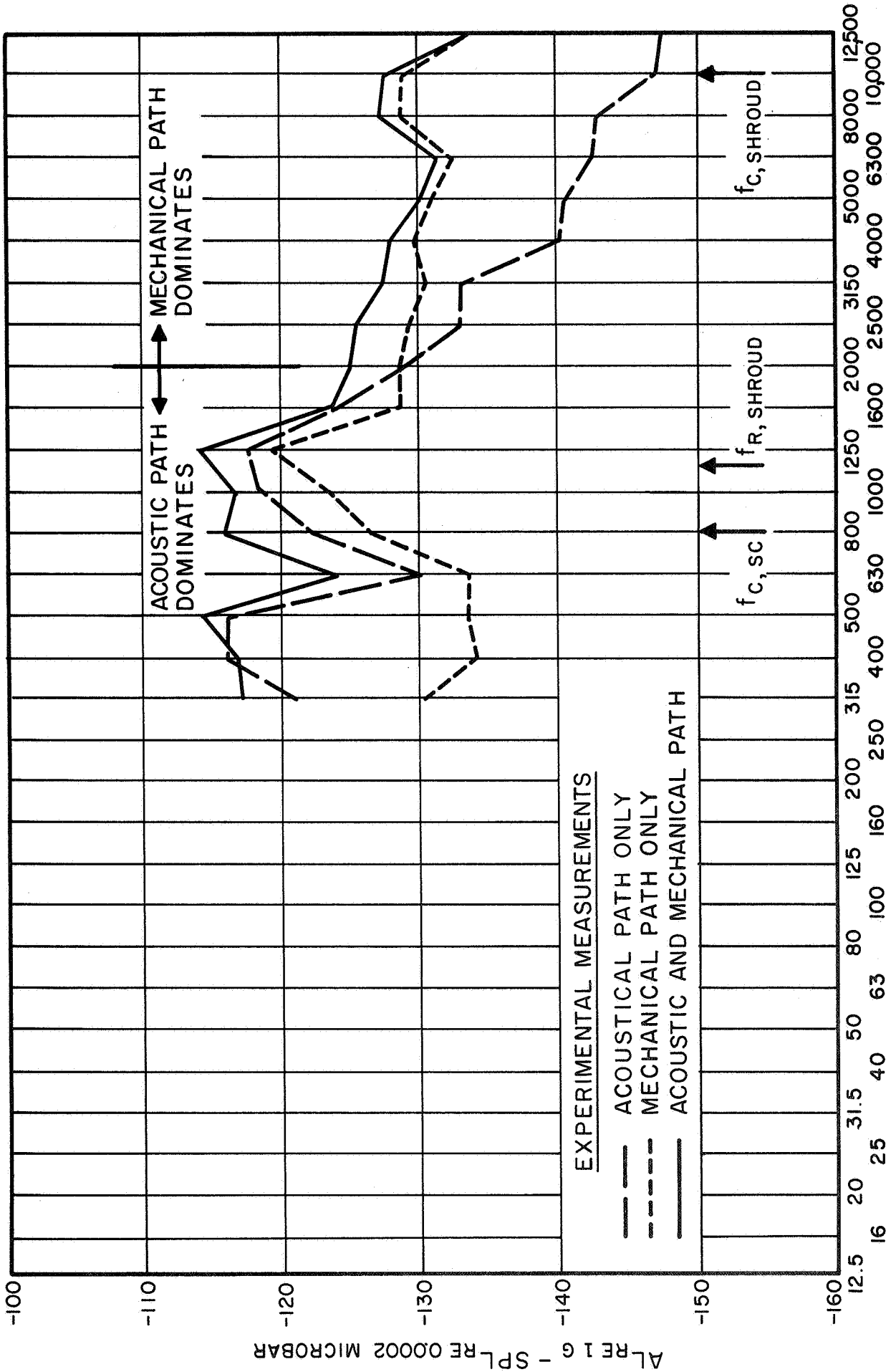

FIG. 46 MODEL-SPACECRAFT RESPONSE WHEN ENCLOSED IN MODEL SHROUD

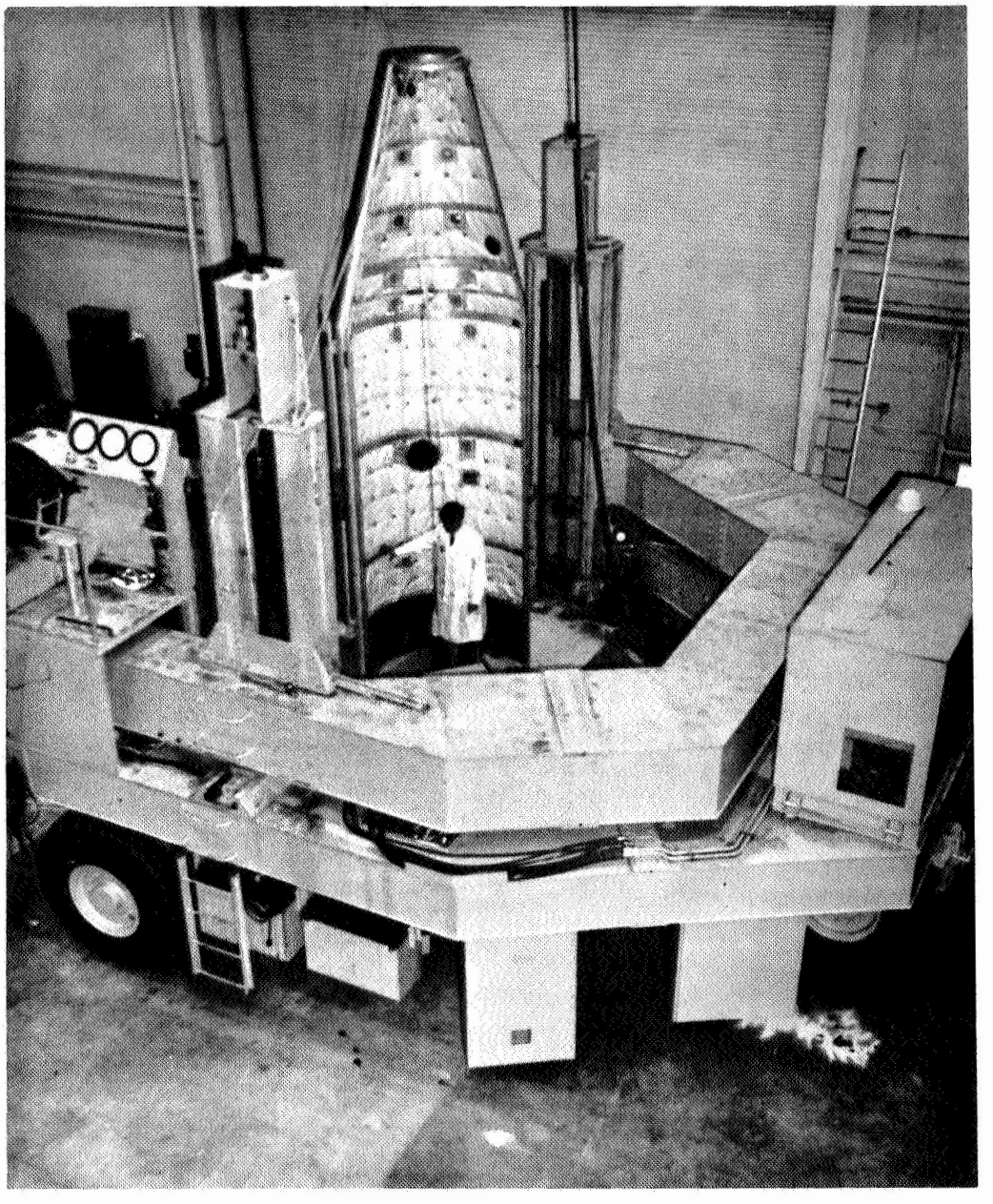

FIG. A-1 THE LPS CARRIER AND NIMBUS-OGO SHROUD

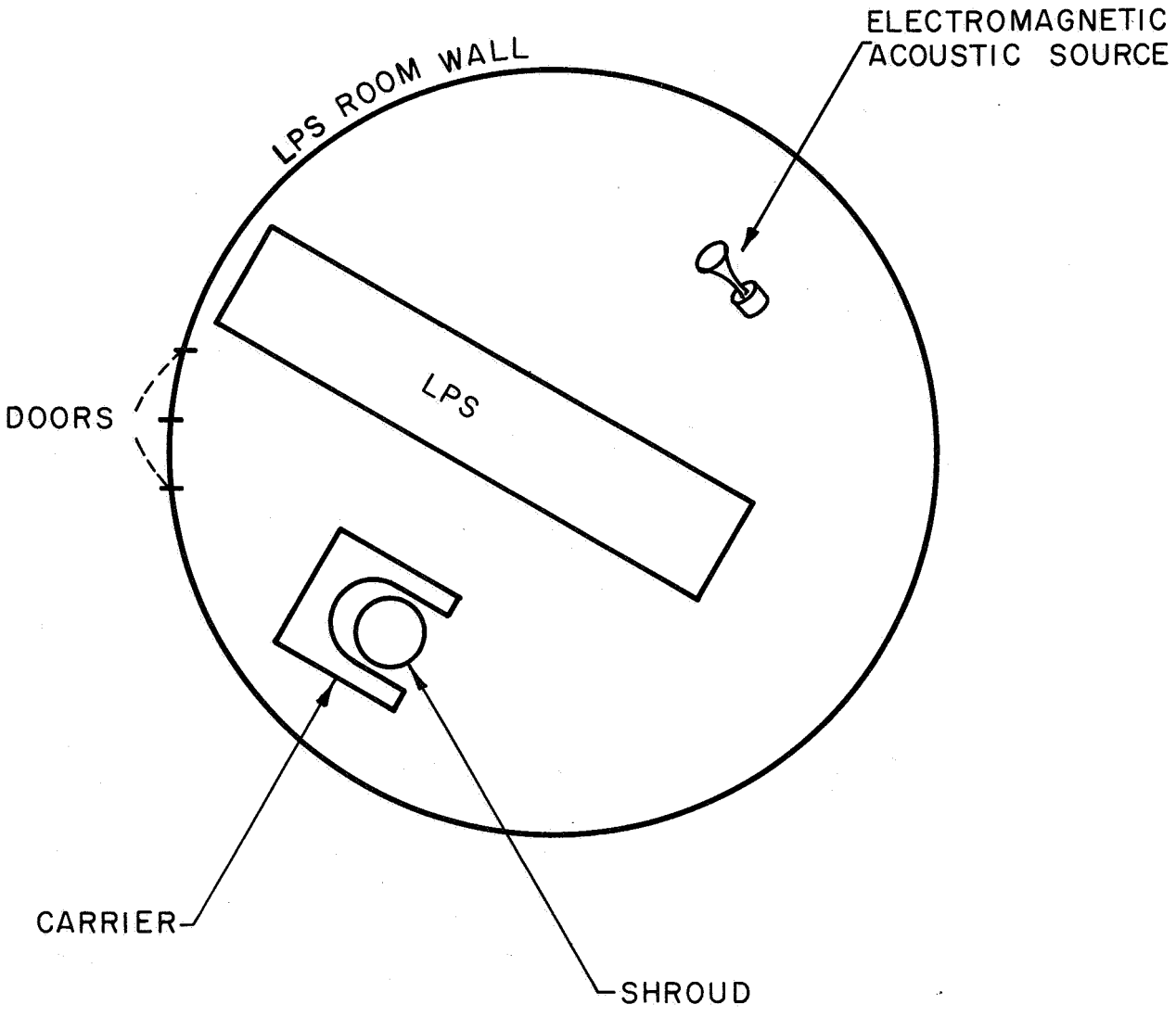

FIG. A-2 LOCATION OF THE SHROUD IN THE LPS ROOM

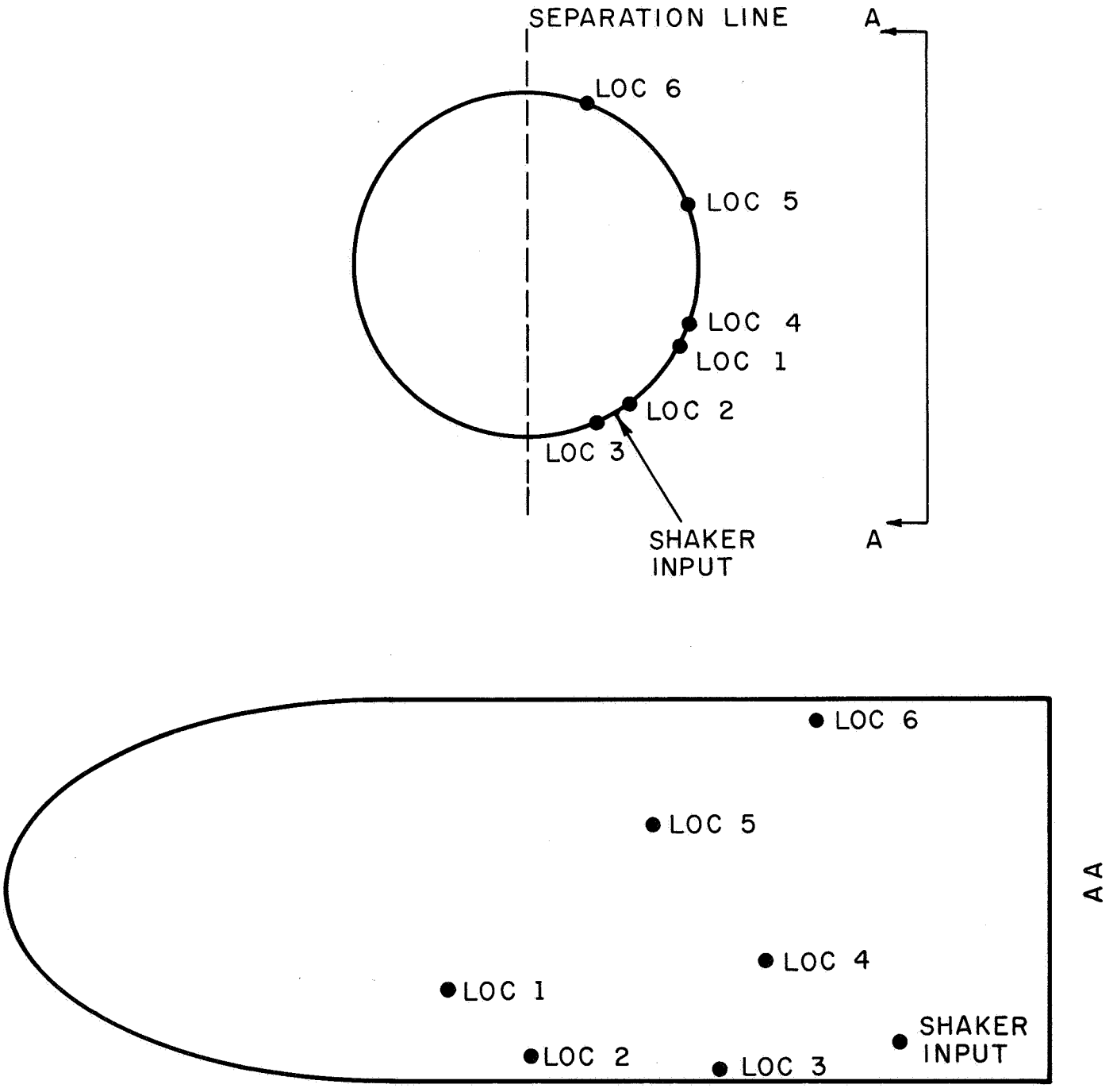

FIG. A-3 ACCELEROMETER LOCATIONS

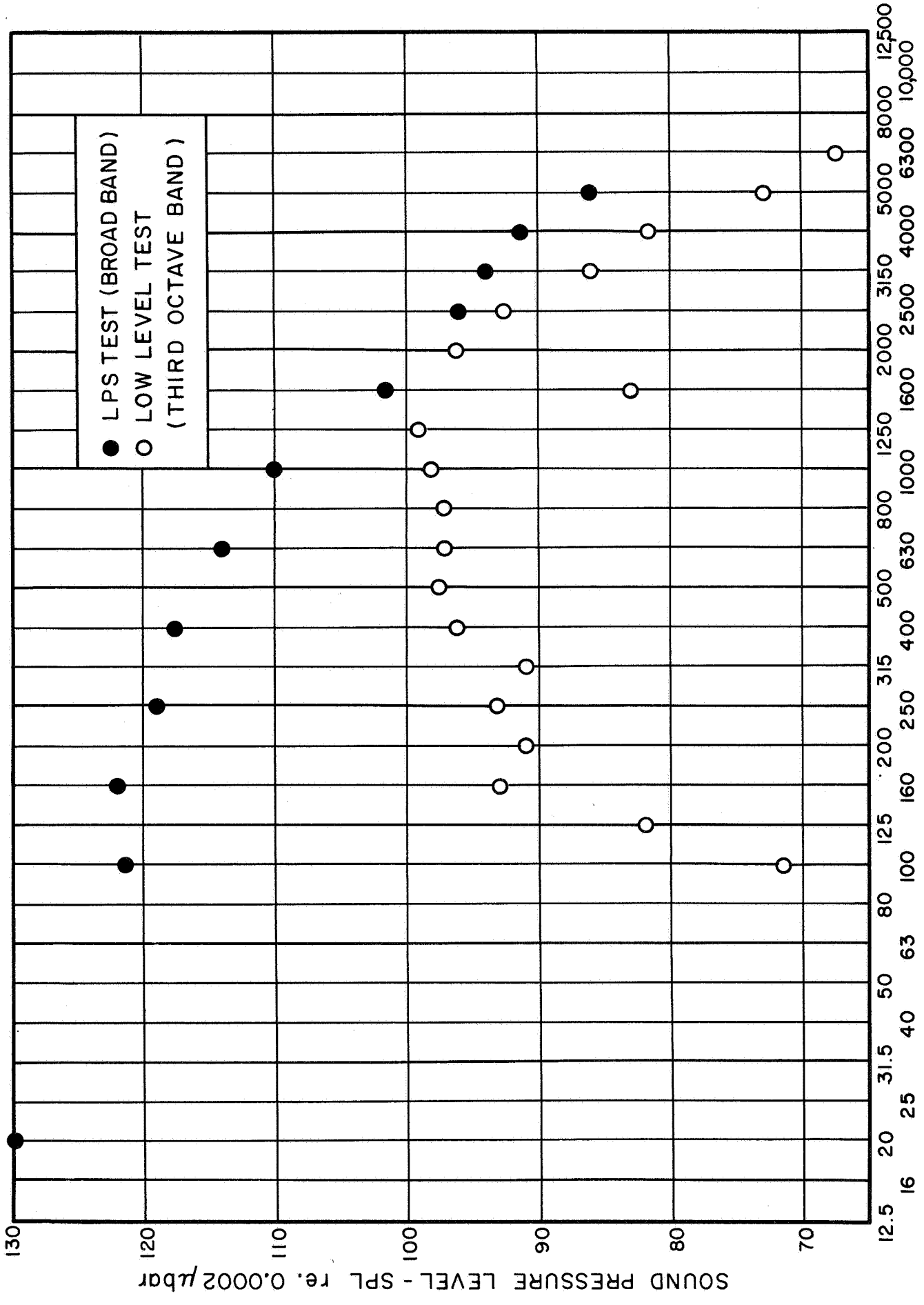

FIG. A-4 SOUND PRESSURE LEVEL USED TO EXCITE THE SHROUD

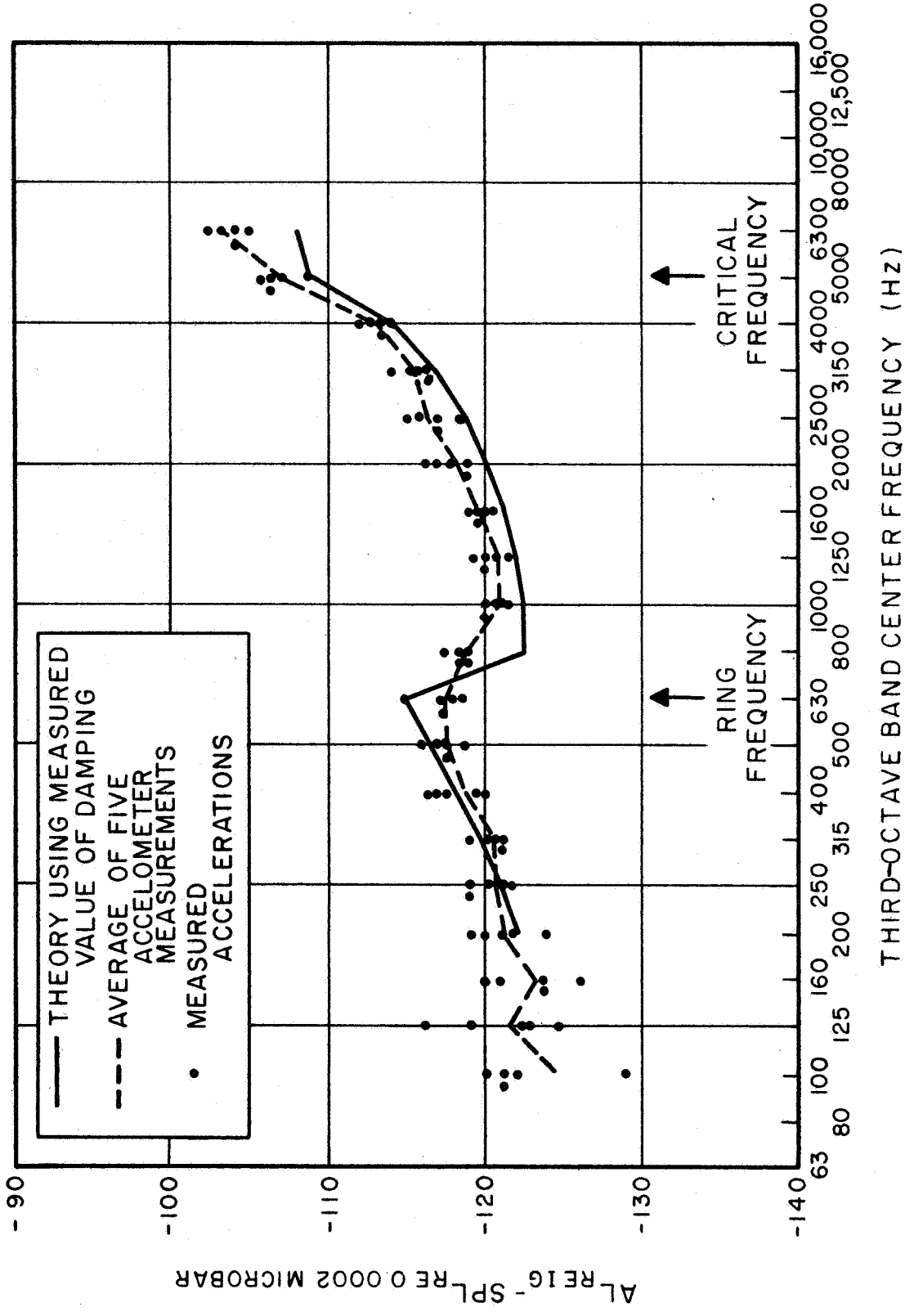

FIG. A-5 SOUND-INDUCED VIBRATION OF NIMBUS-OGO SHROUD

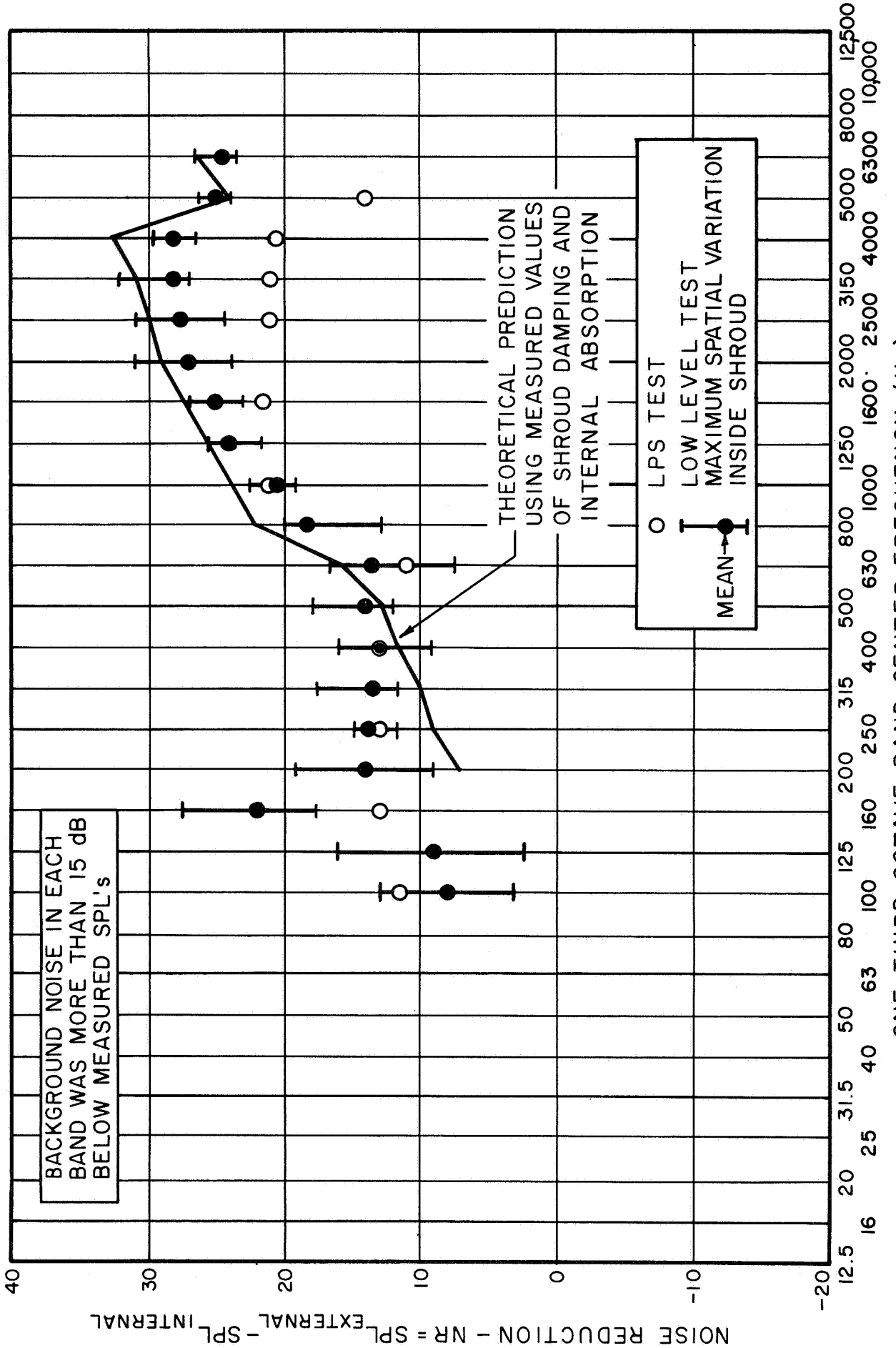

FIG. A-6 NOISE REDUCTION BY THE NIMBUS-OGO SHROUD

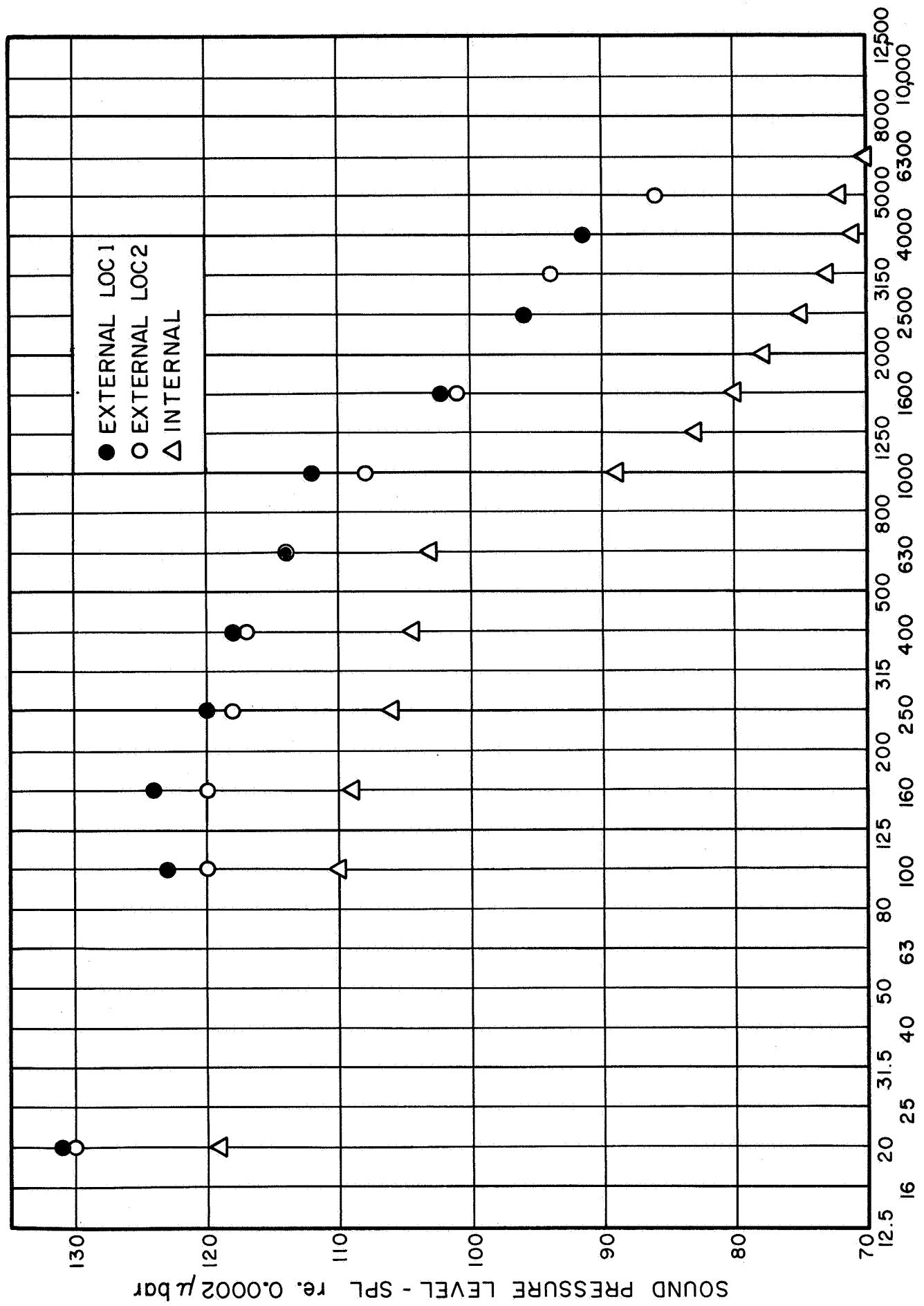

FIG. A-7 SOUND PRESSURE LEVELS MEASURED DURING LPS TEST

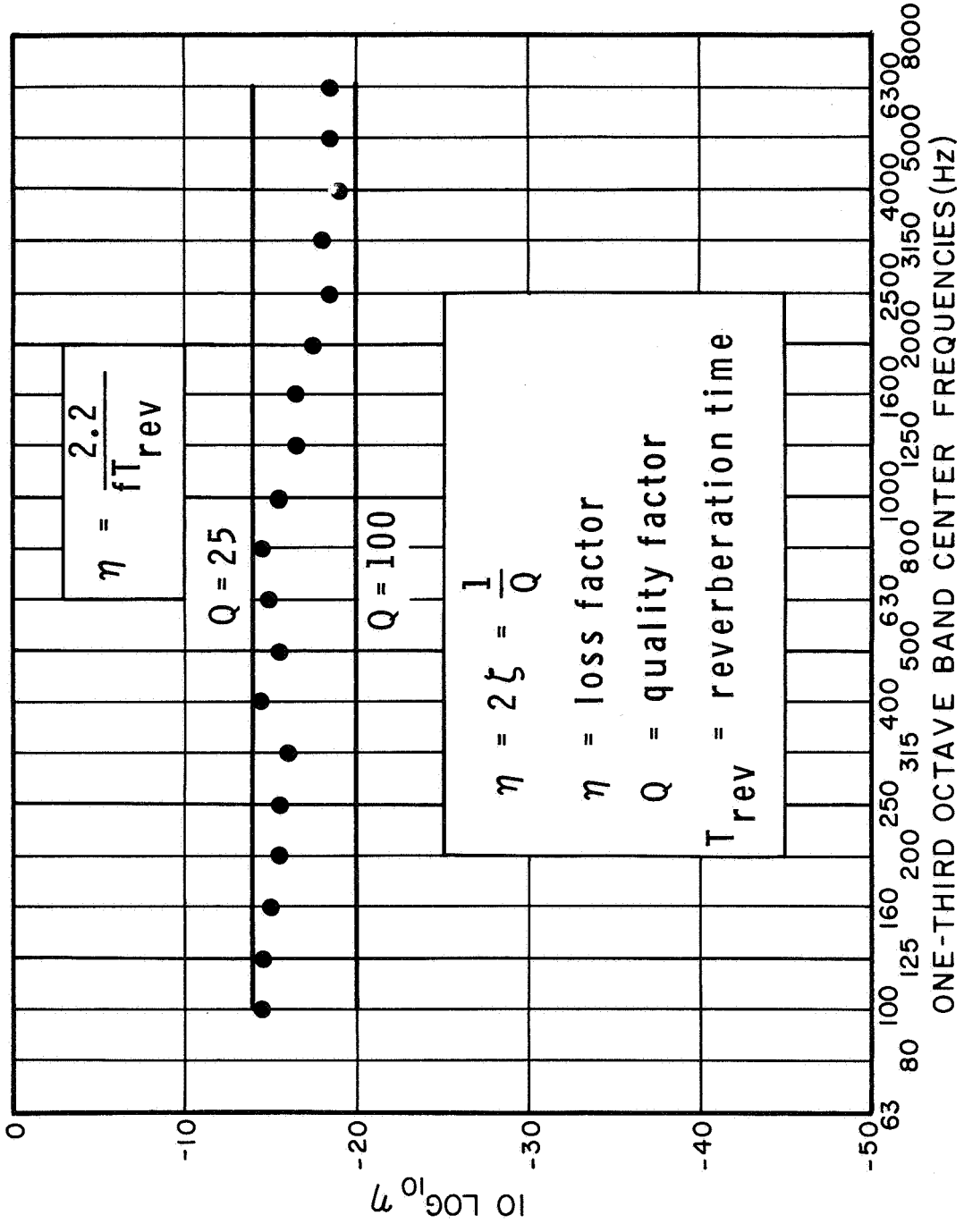

FIG. A-8 DISSIPATION LOSS FACTOR FOR THE NIMBUS-OGO SHROUD

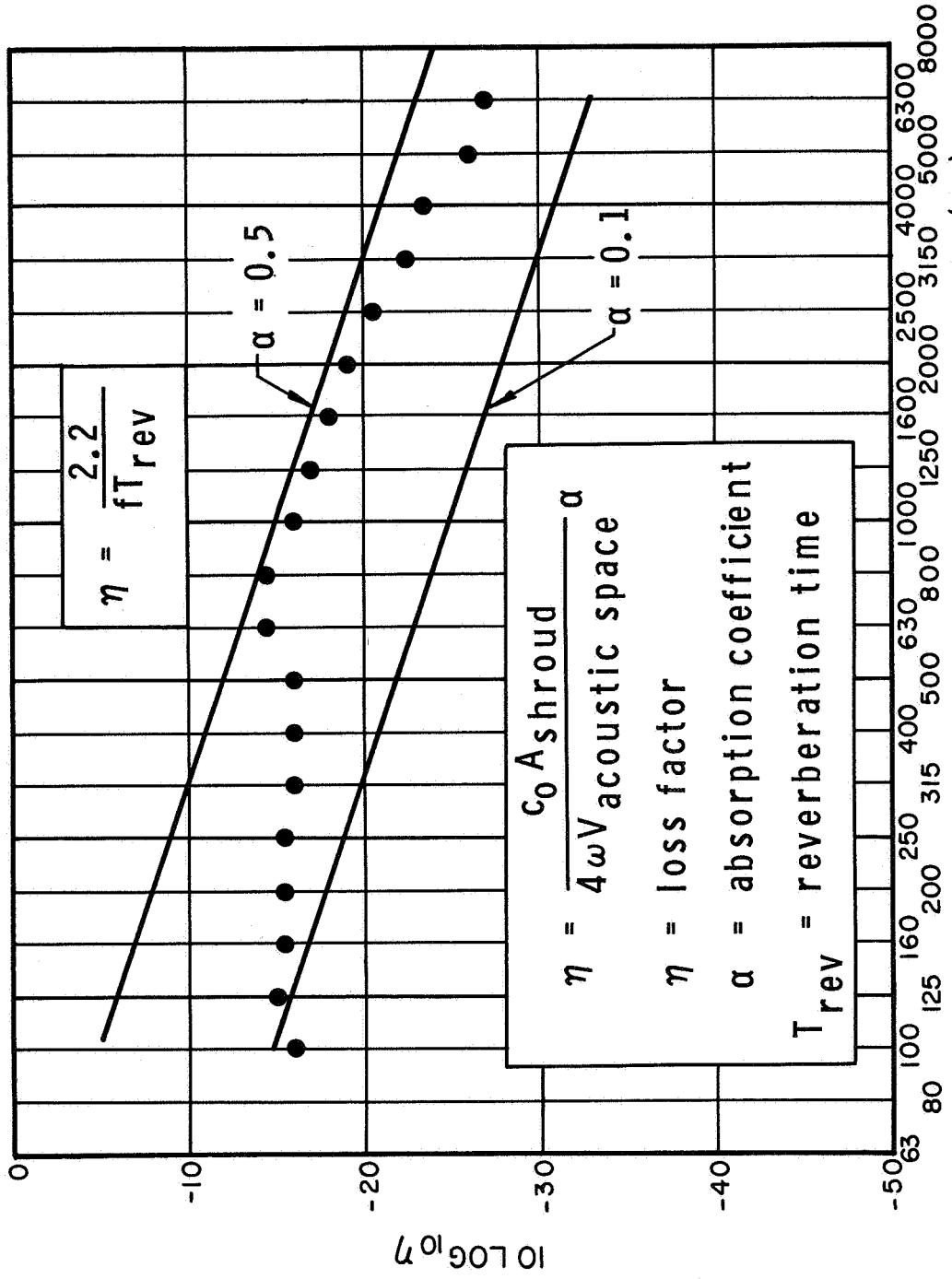

FIG. A-9 DISSIPATION LOSS FACTOR FOR THE INTERNAL ACOUSTIC SPACE OF THE NIMBUS-OGO SHROUD

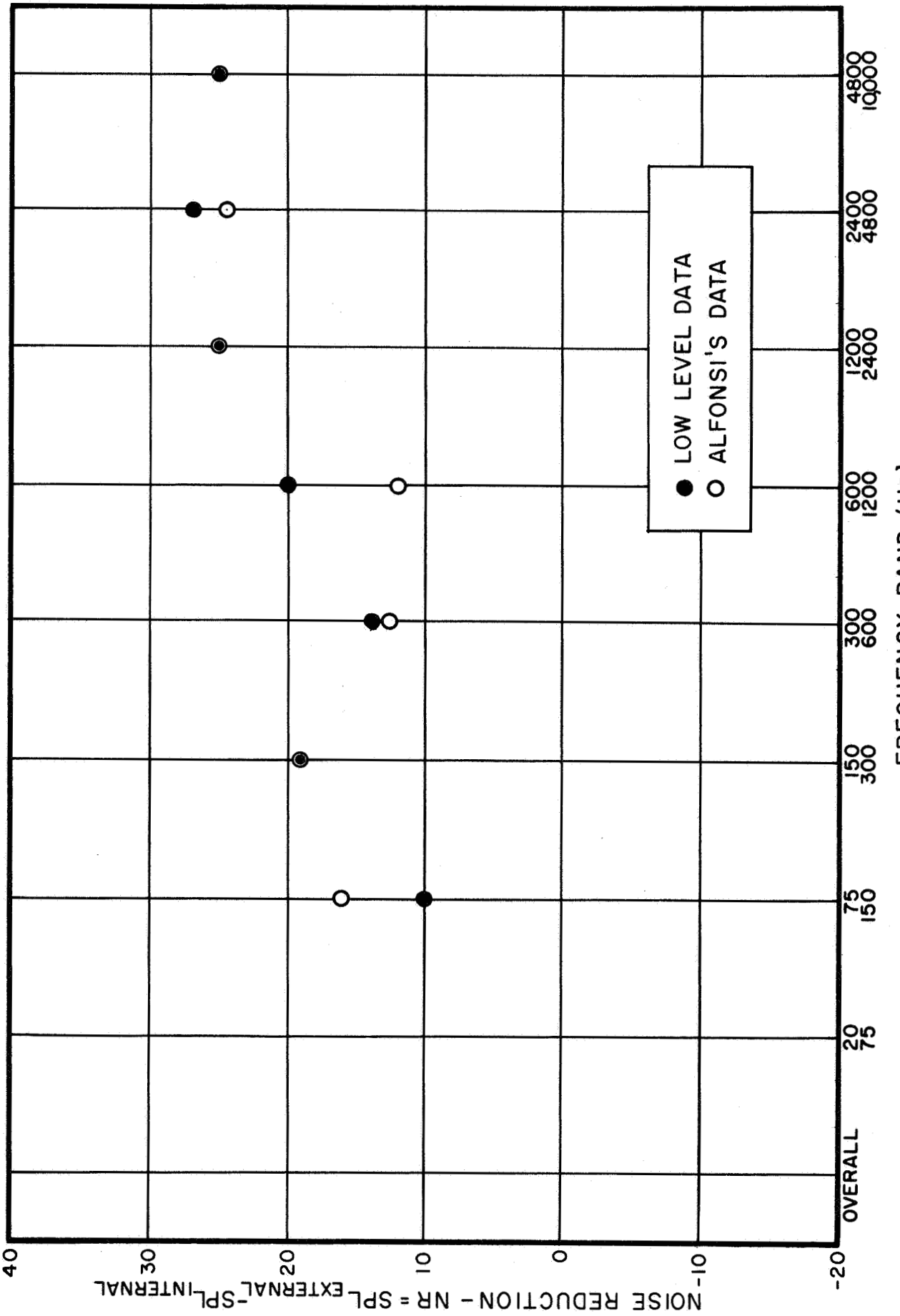

FIG. A-10 COMPARISON OF EXPERIMENTAL RESULTS

Unclassified

Security Classification

DOCUMENT CONTROL DATA - R & D

(Security classification of title, body of abstract and indexing annotation must be entered when the overall report is classified)

1. ORIGINATING ACTIVITY *(Corporate author)*
BOLT BERANEK AND NEWMAN INC
50 Moulton Street
Cambridge, Massachusetts 02138

2a. REPORT SECURITY CLASSIFICATION
Unclassified

2b. GROUP

3. REPORT TITLE
EXPERIMENTAL STUDY OF SOUND AND VIBRATION TRANSMISSION TO A SHROUD-ENCLOSED SPACECRAFT

4. DESCRIPTIVE NOTES *(Type of report and inclusive dates)*
Annual: 20 January 1967 – 20 January 1968

5. AUTHOR(S) *(First name, middle initial, last name)*
Jerome E. Manning and Nicholas Koronaios

6. REPORT DATE	7a. TOTAL NO. OF PAGES	7b. NO. OF REFS
1 July 1968	108	8

8a. CONTRACT OR GRANT NO.
NAS5-10302

b. PROJECT NO.

c.

d.

9a. ORIGINATOR'S REPORT NUMBER(S)
BBN Report 1592

9b. OTHER REPORT NO(S) *(Any other numbers that may be assigned this report)*

10. DISTRIBUTION STATEMENT
Distribution of this report is provided in the interest of information exchange. Responsibility for the contents resides in the authors or organization that prepared it.

11. SUPPLEMENTARY NOTES

12. SPONSORING MILITARY ACTIVITY
National Aeronautics and Space Administration
Goddard Space Flight Center
Greenbelt, Maryland 20771

13. ABSTRACT

An experimental study of the vibration transmission in a 1/2-scale-model spacecraft-shroud assembly is described. The role of acoustic and mechanical vibration-transmission paths is studied. The individual elements of the assembly are studied as well as the complete assembly in order to better understand the vibration-transmission mechanisms. Data obtained in the program are compared with predictions obtained by using statistical energy analysis. An Appendix describes vibration measurements made on an actual OGO-Nimbus shroud.

14. KEY WORDS	LINK A		LINK B		LINK C	
	ROLE	WT	ROLE	WT	ROLE	WT
Vibration						
Noise						
Spacecraft						